UNIVERSITÀ
DEGLI STUDI
DI PADOVA

Sede Amministrativa: Università degli Studi di Padova

Sede Amministrativa della Scuola: Dipartimento di Scienze Cardiologiche, Toraciche e Vascolari

SCUOLA DI DOTTORATO DI RICERCA IN SCIENZE MEDICHE, CLINICHE E SPERIMENTALI

INDIRIZZO "SCIENZE CARDIOVASCOLARI"

CICLO: 26°

Exploring the Clinical Feasibility and Reliability of Three-Dimensional Echocardiography for Advanced Quantitative Analysis of Left Ventricular Myocardial Deformation

Direttore della Scuola: Ch.mo Prof. Gaetano Thiene

Coordinatore d'indirizzo: Ch.mo Prof. Gaetano Thiene

Supervisore: Ch.mo Prof. Sabino Iliceto

Dottorando: Dott.ssa Denisa Muraru

Publication: January 2014

Address for Correspondence:
Denisa Muraru, MD
Dpt of Cardiac, Thoracic and Vascular Sciences, University of Padua
Via Giustiniani 2, 35128, Padua, Italy
Tel. +39 049 8218640
Fax +39 049 8211802
Mobile +39 329 0491866
E-mail denisa.muraru@gmail.com

Table of Contents

Abbreviations **iii**

Extended Summary (English) **v**

Riassunto (Italian) **ix**

Chapter 1. Introduction **1**

1.1. Importance of quantitative assessment of LV function 1

1.2. Rationale and aims of thesis 2

Chapter 2. Myocardial Fiber Architecture and Function **5**

2.1. Architecture of cardiac myofibers 5

2.2. Myocardial mechanics and its link with cardiac myofiber arrangement 7

2.3. LV myocardial function and contractility 10

Chapter 3. Echocardiographic Assessement of LV Myocardial Deformation **13**

3.1. Importance and rationale 13

3.2. Definition of strain and strain-rate 14

3.3. Quantitative parameters 15

3.4. Timing of mechanical events 17

3.5. LV deformation analysis by echocardiography 17

3.5.1. One-dimensional strain by Doppler tissue imaging 18

3.5.2. Two-dimensional strain by speckle-tracking echocardiography 20

Chapter 4. LV Myocardial Strain Assessement by Three-dimensional Speckle-tracking echocardiography **27**

4.1. Principle 27

4.2. Advantages and limitations of 3D versus 2D speckle-tracking 29

4.3. Methodology 31

4.4. Validation 33

4.5. Clinical value of 3D speckle-tracking to date 34

4.6. Reproducibility 35

4.7. Feasibility 37

Chapter 5. Methodology **41**
5.1. Selection of subjects 41
5.2. LV analysis by conventional 2D echocardiography and 2DSTE 43
5.3. LV analysis by conventional 3D echocardiography and 3DSTE 44
Chapter 6. Measurement Variability of 3D Strain **49**
6.1. Introduction 49
6.1. Methods 50
6.2.1. 3D acquisition 50
6.2.2. 3D analysis 50
6.2.3. Reproducibility assessment 52
6.2.4. Analysis of sources of inter-vendor inconsistency 52
6.3. Results 54
6.3.1. Feasibility 54
6.3.2. Observer and test-retest variability 57
6.3.3. Inter-vendor variability 58
6.3.4. Sources of inter-vendor inconsistency 59
6.4. Discussion 62
Chapter 7. Normative Values of LV Myocardial Strain Measurements Using 3D Speckle-Tracking Echocardiography **69**
7.1. Introduction 69
7.2. Methods 70
7.3. Results 73
7.3.1. Reference vlaues of 3D strain parameters 75
7.3.2. Relationship with clinical, haemodynamical and technical factors 77
7.3.3. Relationship with LV echocardiographic parameters 80
7.3.4. Comparison with LV strain by 2DSTE 80
7.4. Discussion 80
Chapter 8. Value of LV Myocardial Strain by 3D Speckle-Tracking to Estimate Infarct Size and Transmurality after ST-Elevation Mycardial Infarction **87**
8.1. Introduction 87
8.2. Methods 88
8.2.1. Echocardiography 89
8.2.2. Cardiac magnetic resonance 91
8.3. Results 92
8.3.1. Feasibility 92
8.3.2. Relationship of global LV strain parameters with infarct size indices 95
8.3.3. Relationship of LV segmental strain with infarct transmurality 96
8.4. Discussion 98
Chapter 9. LV Geometry and Myocardial Function Analysis by 3D Echocardiography in Hypertrophic Cardiomyopathy **103**
9.1. Introduction 103
9.2. Methods 104
9.3. Results 105
9.4. Discussion 108
References **111**
List of Publications **127**
Acknowledgements **141**

Abbreviations

2DE	Two-dimensional echocardiography
2DSTE	Two-dimensional speckle-tracking echocardiography
3DE	Three-dimensional echocardiography
3DSTE	Three-dimensional speckle-tracking echocardiography
Aε	Area strain
BSA	Body surface area
CMR	Cardiac magnetic resonance
Cε	Circumferential strain
DTI	Doppler Tissue Imaging
ECG	Electrocardiogram
EDV	End-diastolic volume
ESV	End-systolic volume
EF	Ejection fraction
fps	Frames per second
HCM	Hypertrophic cardiomyopathy
HF	Heart failure
HR	Heart rate
ISI	Infarct size index
LV	Left ventricle/left ventricular
LVOT	Left ventricular outflow tract
LGE	Late gadolinium enhancement
Lε	Longitudinal strain
PW	Pulsed wave
ROI	Region of interest
Rε	Radial strain
STEMI	ST-elevation myocardial infarction
WMSI	Wall motion score index
vps	volumes per second

Extended Summary

Background. Assessment of left ventricular (LV) function is a fundamental part of clinical cardiology, holding important diagnostic, prognostic and management implications. The most important advance in LV quantification over the last decade was the development of techniques aimed to quantify tissue motion and deformation from ultrasound images, such as tissue Doppler imaging (DTI) and two-dimensional speckle-tracking echocardiography (2DSTE). More recently, speckle-tracking algorithms have been applied to three-dimensional (3D) volumetric acquisitions of the LV (i.e. referred to as 3D speckle-tracking echocardiography, 3DSTE), making possible to analyze all LV myocardial strain components from the same dataset. At present, 3DSTE technology is a research tool in its infancy of development, and its potential clinical value still remains to be demonstrated. With respect to prior technologies (DTI and 2DSTE), 3DSTE comes with several advantages, but also with new challenges. It is currently unknown if the theoretical benefits of an additional third dimension to study the complex LV mechanics (no more "out-of-plane" motion of speckles, only a single acquisition needed etc) are not actually outweighted by the new technical challenges derived from using a volumetric acquisition of the LV (i.e. lower spatial and temporal resolution of speckles than with 2DSTE).

A major concern of 2DSTE strain is the large intervendor variability of strain measurements provided by various commercially-available software packages. At present, it is unclear if a similar problem may affect also 3DSTE, and to what extent. Furthermore, despite researchers are increasingly employing 3DSTE to study various pathologic conditions, the reference values and normal pattern of LV myocardial strain in healthy adults by 3DSTE, as well as the possible influence of various clinical and technical factors on LV strain values are currently unknown. Finally, the validation process of 3DSTE is difficult due to the lack of adequate three-

dimensional gold standard that can be applied noninvasively in human subjects to validate regional LV function in 3D. Therefore, there is a great need for rigorous validation work, methodological and intervendor standardization to be undertaken before its application in clinical settings.

Methods and Results. Project design: single-centre, prospective, observational clinical study, aiming to explore the clinical feasibility and usefulness of LV 3D strain analysis using state-of-the-art commercially available 3DE equipment. The project involves a series of 4 clinical studies.

The aim of the **Study #1** was to assess the intervendor consistency and variability of LV 3D strain values between the two 3DSTE equipments commercially available: VividE9 (GE, Vingmed, Horten, Norway) and Artida (Toshiba Medical Systems Corporation, Tokyo, Japan) ultrasound systems. Sixty patients (38 ± 12 years, 64% males) with a wide range of LV end-diastolic volumes and ejection fractions were enrolled. Global longitudinal (3DLε), radial (3DRε), circumferential (3DCε) and area (3DAε) strain values were obtained offline using the corresponding proprietary software package. Overall, the intervendor agreement of 3DRε, 3DCε and 3DAε measured with Artida and VividE9 was poor. 3DLε showed the closest values between the two platforms (bias = 1.5%, limits of agreement (LOA) from −2.9 to −5.9%, $P < 0.05$). Artida provided significantly higher values of both 3DCε and 3DAε than VividE9 (bias = 6.6% for 3DCε, 6.0% for 3DAε and -24% for 3DRε respectively, $P < 0.001$). All 3D strain components showed good reproducibility (intraclass correlation coefficients: 0.82–0.98), except for 3DRε by Artida, which showed only a moderate reproducibility. Therefore, reference values should be identified for each system, and baseline and follow-up data in longitudinal studies should be obtained using the same 3DSTE equipment.

The aim of the **Study #2** was to assess the normative values for LV 3D strain in 218 healthy volunteers (age range 18-76, 57% women) by vendor-specific 3DSTE equipment (Vivid E9, 4D AutoLVQ software,). For comparison LV strain was also measured by vendor-

specific 2DSTE software and by a vendor-independent 3DSTE software. Feasibility of global 3D strain analysis by 4D AutoLVQ was 89%, lower than 2DLε (95%) and similar to 2DCε (92%). Feasibility of segmental 3DSTE analysis ranged from 46% to 100%. Reference values of 3D strain parameters were identified according to gender and age group. 3DLε decreased, while 3DCε increased with ageing ($p<0.001$). Men had lower 3DLε, 3DRε, 3DAε and 2DLε than women ($p<0.02$). At stepwise multivariable linear regression analysis, demographic (age and gender), cardiac (LV size and mass) and technical (image quality and temporal resolution) factors accounted for the variance of LV 3D strain measurements. Since major inter-software differences in LV strain measurements were identified ($p<0.001$ for all), limits of normality for LV strain analysis by vendor-specific 3DSTE software should not be used interchangeably with those by 2DSTE or vendor-independent 3DSTE softwares.

The aim of the **Study #3** was to assess if LV deformation by 3D STE in patients after ST-elevation myocardial infarction (STEMI) could provide an accurate and objective assessment of infarct size and transmurality, in comparison with magnetic resonance with late gadolinium enhancement (LGE-CMR). A total of 77 STEMI patients were enrolled by 2D and 3D echo, and in 46 patients LGE-CMR studies were performed within 24 hours. The relative amount of DE tissue per segment was used to define transmural necrosis (51-100% DE). LV function was assessed from three apical LV 2D views by measuring 2DLε, and from 3D LV full-volume datasets, assessing visual wall motion score (WMS) and measuring 3DLε, 3DCε, 3DAε and 3DRε. Strain parameters were correlated with conventional indices of LV systolic function (LVEF) and infarct size (troponin I, WMSI, infarct size index at LGE-CMR). Despite a good accuracy for 2DLε and 3D strain parameters (AUC=0.81-0.73), visual wall motion assessment by experienced reader on good-quality 3D data sets (AUC=0.87) was found to be superior than strain quantification to predict transmural necrosis at LGE-CMR.

The aims of the **Study #4** to describe the LV myocardial mechanics in patients with hypertrophic cardiomyopathy (HCM) using 2DSTE and 3DSTE, and to compare it with the normal

deformation pattern in healthy subjects. In 32 HCM pts and 32 age- and gender-matched controls, we analyzed peak global 2DLε and 3DLε, 3DCε, 3DRε, 3DAε. LV ejection fraction (LVEF), LV mass and outflow tract area (LVOTA) were measured by 3D echo. Symptomatic status was defined by NYHA class (II-IV). Although LVEF was similar in pts and controls (64±6% vs 62±4%, p=0.29), LV systolic strain was significantly impaired in pts (p<0.0001), except for 3DCε, which was only marginally lower. In HCM patients, all strain parameters were correlated with LV end-systolic volume (r=0.55 to 0.67), LVEF (r=-0.82 to -0.88) and mass (r=0.33 to 0.56). Symptomatic patients had more impaired 3DAε, 3DRε and 3DCε, but also had more LVOT obstruction and concentric remodelling, and higher E/e'. At ROC curve analysis, 3DAε, 3DRε and 3DCε had a good accuracy to identify symptomatic pts (AUCs 0.72-0.73). 3D LV mass had an inverse correlation with LV longitudinal deformation: r=-0.74 for 2DLε and -0.70 for 3DLε (p<0.001 for both). In HCM with preserved LVEF, the longitudinal strain was significantly reduced, however symptom development is multifactorial and related to the additional impairment of LV deformation in circumferential-radial direction.

Conclusions. This project addressed several issues of of pivotal importance for 3DSTE. It provided a comprehensive analysis of 3DSTE measurement variability (intra- and inter-observer, at test-retest, inter-vendor and inter-software), and reported on the feasibility of 3DSTE in clinical setting and on the comparison with LV strain by 2DSTE. In addition, it is the first to report normal ranges of 3D strain parameters by 3DSTE using both vendor-specific and vendor-independent software packages. Finally, this project presents the added value of 3DSTE in comparison with previous methods for assessing LV function in 2 common pathologic conditions (acute STEMI, as the prototype of regional necrotic transmural injury; and HCM, as the prototype of myocardial disease with impaired longitudinal systolic mechanics despite preserved LVEF). This series of studies contributes with original data to the current scientific evidence-based knowledge on 3DSTE, which is essential for the development and appropriate use of this novel technology.

Riassunto

Introduzione. La valutazione della funzione ventricolare sinistra (VS) rappresenta una parte fondamentale della cardiologia clinica, per le sue notevoli implicazioni diagnostiche, prognostiche e di gestione dei pazienti.

Il progresso più importante nell'analisi quantitative della funzione VS negli ultimi dieci anni è stato lo sviluppo di tecniche finalizzate a quantificare il movimento e la deformazione del tessuto miocardico con tecniche ecografiche, come il Doppler tissutale (DTI) e l'ecocardiografia speckle-tracking bidimensionale (2DSTE). Più di recente, gli algoritmi speckle-tracking sono stati applicati alle acquisizioni tridimensionali (3D) del VS (cioè ecocardiografia 3D speckle-tracking, 3DSTE), rendendo possibile l'analisi di tutte le componenti della deformazione miocardica del VS su un unico dataset. Oggi, la tecnologia 3DSTE è agli albori del suo sviluppo, ed il suo potenziale valore clinico resta ancora da dimostrare. Rispetto alle tecnologie precedenti (DTI e 2DSTE), il 3DSTE gode di diversi vantaggi, ma comporta anche nuove sfide. Al momento, non è ancora noto se i benefici teorici di una supplementare terza dimensione per studiare la complessa meccanica del VS (non più movimento "fuori-piano" degli speckles, un'unica acquisizione necessaria, ecc) non siano in realtà controbilanciate dalle nuove sfide tecniche derivanti dall'utilizzo di un acquisizione volumetrica del VS (cioè minor risoluzione spaziale e temporale del 3DSTE rispetto al 2DSTE).

Una delle principali preoccupazioni con il 2DSTE è la grande variabilità delle misure di deformazione fra i vari software disponibili in commercio. Allo stato attuale, non è chiaro se un problema simile possa influire anche 3DSTE e, se sì, in quale misura. Inoltre, nonostante i ricercatori utilizzino sempre più frequentemente il 3DSTE per studiare varie condizioni patologiche, sono attualmente sconosciuti i valori di riferimento per la deformazione miocardica

del VS mediante 3DSTE, così come la possibile influenza di vari fattori clinici e tecnici sui valori di deformazione VS ottenibili con 3DSTE. Infine, il processo di validazione del 3DSTE è difficile a causa della mancanza di un'adeguata metodica di riferimento tridimensionale che possa essere applicata in maniera non invasiva in soggetti umani per validare la funzione VS regionale in 3D. Pertanto, c'è bisogno di un grande e rigoroso lavoro di validazione, di standardizzazione metodologica e intervendor da iportare a termine prima della sua applicazione in ambito clinico.

Metodi e Risultati. Progettazione: studio clinico mono-centrico, prospettico, osservazionale, con l'obiettivo di esplorare la fattibilità clinica e l'utilità dell'analisi della deformazone miocardica del VS utilizzando attrezzature 3DE allo stato dell'arte. Il progetto prevede una serie di 4 studi clinici.

L'obiettivo dello **Studio # 1** è stato quello di valutare la variabilità e la coerenza dei valori di deformazione VS tra le due apparecchiature 3DSTE disponibili in commercio: Vivid E9 (GE Vingmed, Horten, Norvegia) e Artida (Toshiba Medical Systems Corporation, Tokyo, Giappone). Per questo studio sono stati arruolati 60 pazienti (38 ± 12 anni, 64 % maschi) con una vasta gamma di volumi e frazioni di eiezione del VS. Lo strain longitudinale globale (3DLε), radiale (3DRε), circonferenziale (3DCε) e l'area strain (3DAε) sono stati ottenuti con il rispettivo software proprietario. Nel complesso, la concordanza del 3DRε, 3DCε e 3DAε misurati con Artida e Vivid E9 era scadente. Tra le varie component, il 3DLε ha mostrato i valori più vicini tra le due piattaforme (bias = 1,5 %, limiti di concordanza da -2,9 a -5,9%, $p<0,05$). Artida ha fornito valori significativamente più elevati di 3DCε e 3DAε rispetto a VividE9 (bias = 6,6% per 3DCε, 6,0% per 3DAε e -24% per 3DRε, rispettivamente, $p <0,001$). Tutti i componenti di deformazione 3D hanno mostrato una buona riproducibilità (coefficiente di correlazione intraclasse: 0,82-0,98), fatta eccezione per 3DRε da Artida, che ha mostrato solo una moderata riproducibilità. Pertanto, i valori di riferimento devono essere identificati per ogni apparechiatura 3DSTE, e i dati basali e di follow-up in studi longitudinali devono essere ottenuti utilizzando la stessa attrezzatura.

L'obiettivo dello **Studio #2** è stato quello di valutare i valori di riferimento per lo strain longitudinale 3D (3DLε) del VS in 218 volontari sani (età 18-76 , il 57% donne), misuarti con un softwares 3DSTE (Vivid E9 , software 4D AutoLVQ) . Per confronto, Lε è stato misurato utilizzando anche il software specifico per il 2DSTE, e un software 3DSTE independente dall'ecocardiografo che acquisisce i data set 3D. La fattibilità dello strain 3D con 4D AutoLVQ era 89%, essendo inferiore a quella del 2DLε (95%) e simile a quella del 2DCε (92%). La fattibilità di analisi 3DSTE segmentale variava dal 46% al 100%. Valori di riferimento dei parametri di deformazione 3D sono stati identificati in base al sesso e gruppo di età. 3DLε diminuiva, mentre 3DCε aumentava con l'invecchiamento ($p<0.001$). Gli uomini mostravano 3DLε, 3DRε, 3DAε e 2DLε minori rispetto alle donne ($p<0,02$). All'analisi multivariata di regressione lineare, i fattori demografici (età e sesso), cardiaci (volumi e massa VS) e tecnici (qualità dell'immagine e la risoluzione temporale) hanno indipendentemente contribuito alla varianza dello strain 3D. Tenendo conto dalle notevoli differenze inter-software nei valori di strain VS identificati ($p<0,001$ per tutti), i limiti di normalità per lo strain VS identificati con un software 3DSTE specifico non dovrebbero essere usati in modo intercambiabile con quelli di 2DSTE o di un software 3DSTE independente dal fornitore.

L'obiettivo dello **Studio #3** era di valutare se la deformazione VS mediante 3DSTE nei pazienti dopo infarto miocardico con sopraslivellamento ST (STEMI) potrebbe fornire una valutazione accurata e obiettiva delle dimensioni dell'infarto e della transmuralità della necrosi, in confronto con la risonanza magnetica con gadolinio (LGE - CMR). Un totale di 77 pazienti con STEMI sono stati arruolati con l'eco 2D e 3D, e in 46 pazienti sono stati eseguiti studi LGE - CMR entro 24 ore dall'esame ecocardiografico. La quantità relativa di DE per segmento è stata usata per definire la necrosi transmurale (51-100% DE). La funzione VS è stata valutata nelle 3 sezioni 2D apicali del VS, misurando il 2DLε, e dal volume di dati 3D, valutando il punteggio della cinetica segmentaria (WMS) e la misurazione del 3DLε, 3DCε, 3DAε e 3DRε. I parametri di deformazione del VS erano correlati con gli indici convenzionali di funzione sistolica VS (FEVS) e di estensione dell'infarto (troponina I, WMSI, dimensioni dell'infarto alla LGE - CMR). Nonostante una buona

accuratezza dello 2DLε e dei parametri di deformazione 3D (AUC = 0,81-0,73), la valutazione visiva della cinetica regionale da parte di un osservatore esperto su immagini 3D di buona qualità (AUC = 0.87) è risultata essere sempre superiore rispetto al valore predittivo dello strain per identificare la necrosi transmurale alla LGE - CMR.

Gli obiettivi dello **Studio #4** erano di descrivere la funzione miocardica del VS nei pazienti con cardiomiopatia ipertrofica (HCM) mediante 2DSTE e 3DSTE, e di confrontarla con la deformazione VS normale di soggetti sani. In 32 pazienti con HCM e 32 controlli simili per età e per sesso, abbiamo analizzato il valore globale del 2DLε e del 3DLε, 3DCε, 3DRε, 3DAε. La frazione di eiezione (FEVS), la massa del VS e l'area del tratto di efflusso (LVOTA) sono stati misurati mediante eco 3D. Lo stato sintomatico è stato definito dalla classe NYHA (II - IV). Anche se LVEF era simile nei pazienti e nei controlli (64 ± 6 % vs 62 ± 4 %, p = 0,29), lo strain VS era significativamente ridotto nei pazienti (p < 0,0001), fatta eccezione per 3DCε, che era solo marginalmente più basso. Nei pazienti con HCM, tutti i parametri di deformazione erano correlati con il volume telesistolico del VS (r = 0,55-0,67), la FEVS (r = -0,82 a -0,88) e la massa VS (r = 0,33-0,56). I pazienti sintomatici avevano una riduzione maggiore del 3DAε , 3DRε e 3DCε, ma avevano anche più ostruzione dell'efflusso, un maggior rimodellamento concentrico ed un rapporto E/e ' più alto. All'analisi delle curve ROC, 3DAε, 3DRε e 3DCε hanno avuto una buona precisione per individuare i soggetti sintomatici (AUC 0,72-0,73). La massa 3D del VS mostrò una correlazione inversa con la deformazione longitudinale del VS: r = -0,74 per 2DLε e -0,70 per 3DLε (p < 0,001 per entrambi). In HCM con FEVS conservata, la deformazione longitudinale è risultata significativamente ridotta, tuttavia lo sviluppo dei sintomi è multifattoriale e relativo al deterioramento aggiuntivo della deformazione VS nella direzione circonferenziale – radiale.
Conclusioni. Questo progetto ha affrontato diversi temi di importanza fondamentale per la validazione clinica dello 3DSTE. Ha fornito un'analisi completa della variabilità di misura mediante 3DSTE (intra- ed interosservatore, al test-retest, inter-macchina e inter-software), ha valutato la fattibilità del 3DSTE in ambiente clinico e confrontato I valori ottenuti con lo strain VS

mediante 2DSTE. Inoltre, questo è il primo studio a definire i limiti di riferimento per lo strain 3D utilizzando sia software specifici che indipendenti dal fornitore. Infine, questo progetto presenta il valore aggiunto di 3DSTE rispetto ai precedenti metodi per la valutazione della funzione VS in 2 condizioni patologiche comuni (STEMI acuto, come prototipo di lesione transmurale regionale necrotica, e l'HCM, come prototipo di malattia miocardica con funzione sistolica longitudinale compromessa nonostante FEVS conservata). Questa serie di studi contribuisce con dei dati originali alle conoscenze attuali basate sull'evidenza scientifica sul 3DSTE, che è essenziale per lo sviluppo e l'uso appropriato di questa nuova tecnologia.

Chapter 1. Introduction

1.1. Importance of quantitative assessment of LV function

Assessment of left ventricular (LV) function is an important requisite of clinical cardiology. Indices reflecting LV performance are of paramount importance for the diagnosis of cardiovascular diseases, for risk stratification and prognosis, as well as for selecting and guiding therapy (1). Assessing the most common measure of LV systolic function - LV ejection fraction (LVEF) - has direct implications for patient management. Suitability for device implantation, indication to cardiac surgery or heart failure drugs, to discontinue chemotherapy in cancer pacients are just a few among the most critical decisions that rely on accurate LVEF assessment in daily practice (2).

Two-dimensional echocardiography (2DE) is the most commonly used imaging tecnique to analyze LV function in terms of EF. It is non-invasive, harmless and cheap, readily available and repeatable, and an impressive body of evidence over the past half century certifies its clinical value and validity. However, 2DE calculation of LVEF is limited by several factors, mainly *technical* (quality of acoustic window and image acquisition, experience of the interpreter), *methodological* (geometric assumptions applied to few tomographic slices of a three-dimensional structure such as the LV) and *conceptual* (confounded by variable loading conditions and heart rate, and therefore not actually reflecting true LV contractility).

As a consequence, newer echocardiographic methods have been proposed and developed with the aim to improve the current capabilities to analyze the LV in clinical practice. 3D echocardiography (3DE) has been introduced for improving the quantitative assessment of LVEF, and gradually developed into a clinically useful tool, now applicable in

realtime in every day practice (1). However, one of the most important advances in LV functional quantification has been the development of techniques aimed to quantify tissue motion and deformation from ultrasound images. Two such echocardiographic techniques have dominated the research arena: Doppler-based measurements of myocardial velocity, frequently referred to as tissue Doppler, and speckle tracking-based measurements of tissue displacement and deformation. Both types of measurements lend themselves to the derivation of multiple parameters of myocardial function (3). Deformation imaging by 2DSTE has emerged as a reliable quantitative tool for LV myocardial function analysis, holding important diagnostic, prognostic and management implications (4, 5). Three-dimensional speckle-tracking echocardiography (3DSTE) represents a further advance in myocardial deformation imaging, allowing a fast and comprehensive evaluation of all LV segments from a single 3D dataset. In principle, 3DSTE should be more adequate than 2DSTE to capture the complex LV myocardial mechanics, by overcoming the issues of 2DSTE related to the "out-of-plane" motion of speckles and partial information contained in few thin slices of the LV. Although these new techniques are very promising and attractive, they are prone to technical and reproducibility issues, therefore extensive clinical testing is needed before adopting them for patient healthcare.

1.2. Rationale and aims of thesis

At present, 3DSTE technology is a research tool in its infancy of development, with potential clinical value which still remains to be demonstrated. With respect to prior technologies aiming to analyze LV myocardial function, 3DSTE comes with several advantages, but also with new challenges. It is currently unknown if the theoretical benefits of an additional third dimension to study LV mechanics are not actually outweighted by the new technical challenges derived from using a volumetric acquisition of the LV (i.e. lower spatial and temporal resolution of speckles than with 2DSTE).

Furthermore, the validation process of 3D strain is difficult due to the lack of adequate three-dimensional gold standard that can be applied noninvasively in human subjects to validate regional ventricular function in 3D (3). Despite positive results have been obtained from phantom and sonomicrometry studies (6, 7), these cannot be automatically extrapolated in patients and neither across different manufacturers. Therefore, its rigorous testing in a variety of clinical scenarious involving both normal and abnormal LV function becomes mandatory. In particular, there is an impelling need for clinical research studies in healthy subjects (to establish the reference for 3D strain normalcy and the normal pattern of 3D strain parameters) and in patients undergoing concomitent evaluation of LV function using a gold standard technique (such as cardiac magnetic resonance, CMR) or by other methods with established clinical value (such as 2D strain and regional wall motion score analysis etc).

Accordingly, the overall aim of this thesis was to explore the clinical feasibility and reliability of 3DSTE for advanced quantitative analysis of LV myocardial function from 3D datasets. The research project was designed to address a number of issues regarding 3DSTE, which clarification is of pivotal importance for the current research: feasibility; reproducibility (including at test-retest, and between vendors and softwares); normal ranges of 3D strain parameters; comparison with 2D strain; added value in comparison with previous methods for assessing LV function in landmark pathologic conditions involving the LV myocardium (ST-elevation myocardial infarction, as the prototype of transmural injury; and hypertrophic cardiomyopathy, as the prototype of myocardial disease with preserved EF despite impaired longitudinal systolic mechanics)(Figure 1.1).

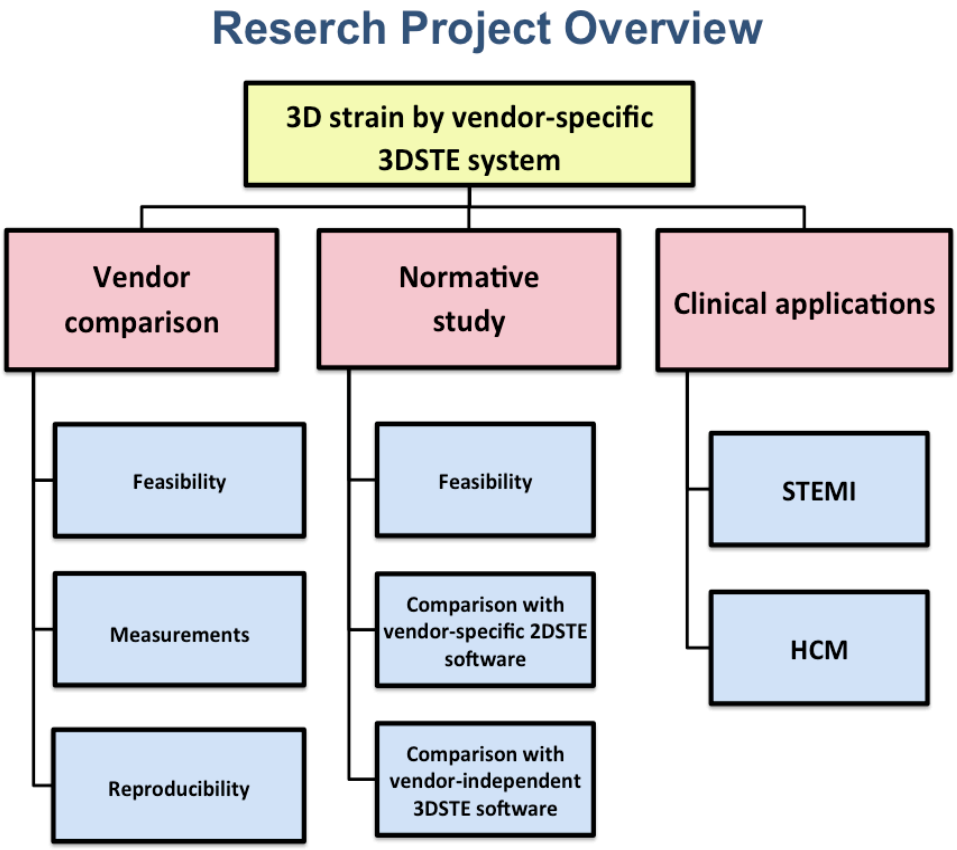

Figure 1.1. General plan of the research project presented in the thesis.

Using a series of clinical studies in healthy subjects and in patients, this work aims to contribute to the scientific evidence-based knowledge which is essential for the development and appropriate use of this novel technology.

The experimental part of the thesis (Chapters 5-9) is preceeded by a general first part aiming to provide a comprehensive review on LV myocardial mechanics (Chapter 2), on the strain concept and on previous echocardiographic techniques implemented in clinical and research practice to analyze LV myocardial deformation (Chapter 3), and finally an overview of the current 3DSTE technique, to which has been assigned a full separate chapter (Chapter 4).

Chapter 2. Myocardial Fiber Architecture and Function

2.1. Architecture of cardiac myofibers

The architectural arrangement of the myocardial fibers within the ventricular mass remains a highly controversial topic. Anatomic evidence supporting an overall helical nature for the ventricular myocardium exists for over 150 years. While the presence of helical patterns are throughout the LV walls is now universally accepted, surgeons have promoted the concept that myofibers are disposed in the form of a unique 'ventricular myocardial band' (8), while anatomists affirm that in no way they can constitute a unique myocardial band (9).

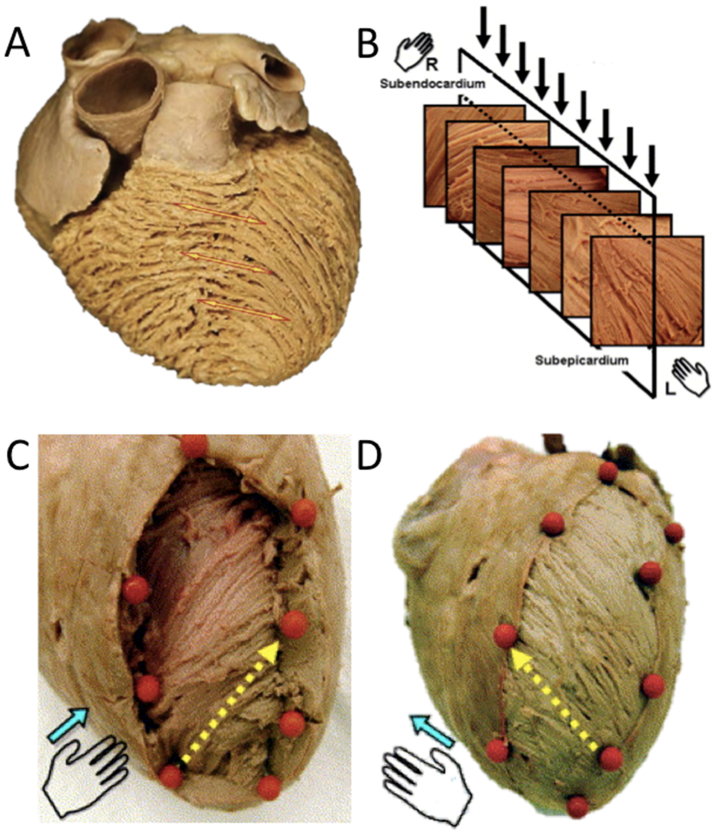

Figure 2.1. Myocardial fiber architecture (after Anderson (9) and Sengupta (15)), showing the multi-layered structure of LV myocardium, with a helical arrangement of subendocardial and subepicardial fibers in opposite directions.

Conventionally, LV myocardium is characterized by a multi-layered structure, with counter-directional layers meeting at the apex (Figure 2.1). According to this concept, LV myofibers are arranged in a counter-clockwise orientation (as viewed from the apex) in the subepicardial layer, circumferentially in the midwall layer and in a clockwise direction in the subendocardial layer (Figure 2.2)(8, 10-12).

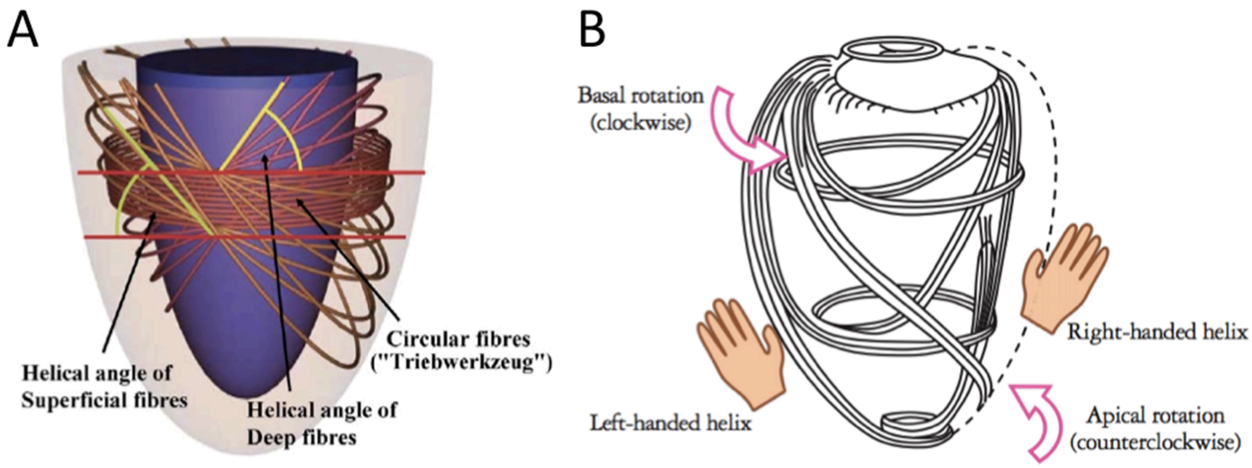

Figure 2.2. Myocardial fiber architecture (after Anderson (9) and Nakatani (12)). The scheme shows the shows the angles of myocardial fibers relative to the equator of the left ventricle, which vary at different depths within the ventricular wall. Note that the circular fibres of the middle layer are parallel to the ventricular equator.

Postmortem histologic studies showed that the geometry of myofibers within the LV wall changes gradually from endocardium to epicardium, and albeit that there are no fibrous partitions separating the ”layers”, the multi-layer concept is based on the rapidly changing angulation of myofibers from longitudinal to circular orientation (Figure 2.3)(13).

Therefore, the term “layers” is used in order to simplify anatomic description, indicating regions of LV wall where fiber orientation appears to change little with depth, in contrast to those where it changes rapidly (13).

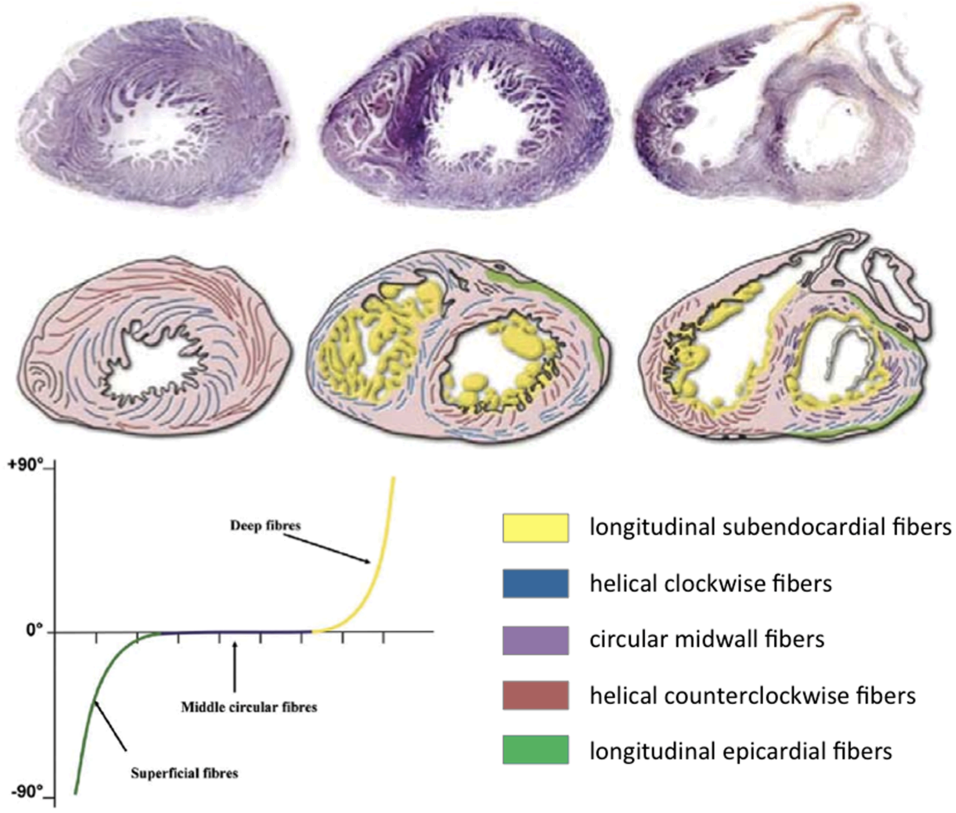

Figure 2.3. Myocardial fiber architecture (modified after Anderson (9)). The image conveys the findings of Greenbaum and colleagues (13), who obtained histological sections throughout the ventricular mass as shown in the upper panels, and then quantitated the angulation of the myofibres relative to the ventricular equator. The graph below shows the rapidly changing radial angulation of the fibres with increasing depth within the ventricular wall, underlining the concept of layers across the wall.

2.2. Myocardial mechanics and its link with cardiac myofiber arrangement

The complex orientation of the myocardial fibers results in intricate three-dimensional motion during contraction and relaxation. The potential functional significance of the fibre orientation of the LV mass has been described ever since the time of Vesalius and Harvey (1628)(14). They have recognised that the reduction in left ventricular cavity volume during systole involves longitudinal, as well as circumferential shortening, and that the latter plays the dominant role. Nowadays, it has been demonstrated that the helical fiber architecture of the LV helps maintain stability and minimizes energy expenditure (15). Mathematical models have shown that this counterdirectional helical arrangement of LV myofibers is energetically efficient and plays a crucial role for the equal redistribution of stresses and strain in the heart (16).

Myocardial contraction is normally initiated by the spontaneous depolarization of myocardial cells in the sinoatrial node and conducted through the atrio-ventricular node, depolarization rapidly spreading throughout the LV via the His bundle, the left and right bundle branches, and the Purkinje network. Electrical activation is nearly simultaneous within the entire LV, with the apex activated just a few milliseconds before the base and the endocardium activated just a few milliseconds before the epicardium. Repolarization occurs in the reverse fashion, with the base repolarizing first, followed rapidly by the apex (17, 18). Similar to electrical activation, longitudinal systolic shortening begins in the apex and rapidly progresses to the base (17). The rapid electrical transmission throughout the ventricle results in synchronous radial motion at any cross-sectional level of the LV (19).

Myocardial mechanics can be described as the summation of motion in three planes: 1) longitudinal shortening or lengthening in the long-axis plane extending from base to apex; 2) radial thickening or thinning in the short-axis plane; and 3) rotation about the long axis (as viewed from a short-axis plane) (Figure 2.4). Rotation of the LV base is opposite to that of the apex but is significantly lower in its magnitude. The difference in rotation at the base and apex creates a twisting motion of the LV, defined as torsion. Rotational motion is controlled not only by the helical fiber orientation, but also by the relative strength of the forces generated by the contracting epicardium and endocardium. During isovolumic contraction, there is a brief counterclockwise rotation due to the mechanical activity of the subendocardial fibers, which is followed by clockwise rotation (twist) during ejection when the subepicardal myofibers dominate the direction of LV rotation. As epicardial fibers relax, twisted fibers recoil rapidly with continued active contraction of the endocardial layers. This creates suction during the isovolumic relaxation period, and enhances early diastolic filling (20). Thus, rotational motion is an important link between systolic and diastolic function.

The three-dimensional motion created by the contraction of the helically structured myocardium generates efficient pumping action with minimal fiber shortening. Shortening in longitudinal and circumferential direction would result in radial thickening for conserving myocardial mass. However, LV wall thickening is not the resultant of simple shortening of individual myocytes, but also an effect of transmural shearing, i.e. sliding and rearrangement of myofiber sheets along cleavage planes during the cardiac cycle (Figure 5)(21).

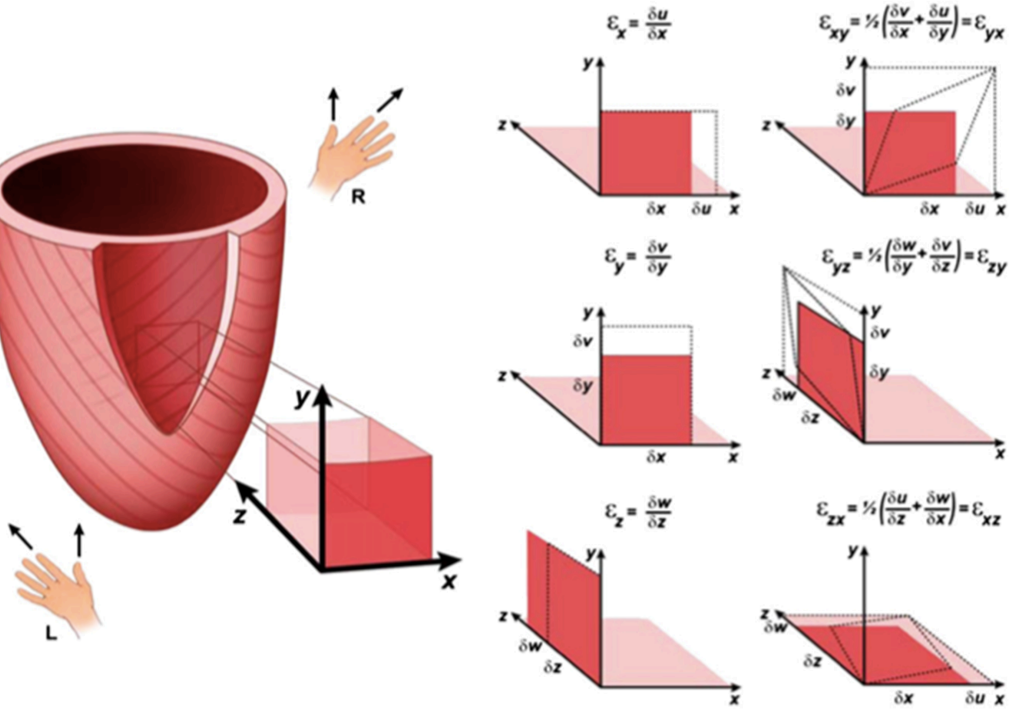

Figure 2.4. Myocardial mechanics and link to fiber arragement (after (4)). The *left panel* shows a schematic representation of the myocardial fiber orientation in the left ventricle that changes continuously from a right-handed helix (R) in the subendocardial region to a left-handed helix (L) in the subepicardial region. The *panels in the center and to the left* show the normal strain (ex, ey, and ez), and 3 components of shear strain (exy, exz, and eyz) in a block of myocardial tissue in which the *x-axis* is oriented at a tangent to the circumferential direction of the left ventricle, the *y-axis* is oriented longitudinally, and the *z-axis* corresponds to the radial direction, with *u, v,* and *w* representing displacements in the *x, y,* and *z* directions, respectively. The shear strain is the amount of deformation perpendicular to a given line rather than parallel to it. For example, the shear strain exy represents the average of the shear strain on the *x* face along the *y* direction and on the *y* face along the *x* direction.

It is estimated that, as a result of these complex mechanics, the LV can generate an

ejection fraction (EF) of 50% or more, with a fiber shortening of only 15% (8, 10). Maintaining this highly efficient mechanism of LV contraction is critical to ensure proper cardiac function.

2.3. LV myocardial function and contractility

Left ventricular myocardial function can be analyzed invasively and graphically displayed with a pressure–volume diagram, including both systolic and diastolic phases of a single cardiac cycle (Figure 2.5).

The width of the pressure–volume loop is the stroke volume (stroke volume = end-diastolic volume – end- systolic volume). The area inside the pressure–volume loop is an estimate of the myocardial energy (work = pressure × volume) utilized for each stroke volume. Pressure-volume assessment of LV myocardial function is influenced by multiple factors, such as preload, afterload, heart rate, and contractility.

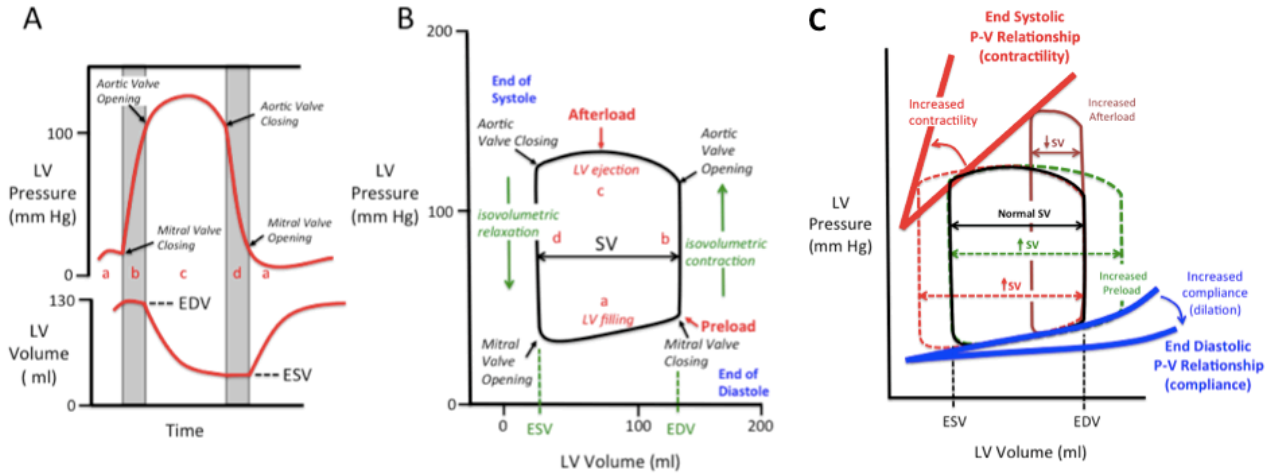

Figure 2.5. Ventricular pressure-volume loops. **A:** The left panel shows the time course of changes in left ventricular pressure and volume during a single cardiac cycle. As indicated in red, a: ventricular filling; b: isovolumetric contraction; c: ventricular ejection; d: isovolumetric relaxation. EDV: left ventricular end-diastolic volume, ESV: left ventricular end-systolic volume. **B:** The right panel shows corresponding changes in ventricular pressure vs ventricular volume (from the left panel) at different times during a single cardiac cycle. Stroke volume (SV) is equal to EDV-ESV. **C:** Effect of acute changes in hemodynamic parameters on SV.
Adapted after http://tmedweb.tulane.edu/tmedwiki/doku.php/the_cardiac_cycle

Contractility is the ability of the myocardium to pump blood without any changes in preload or afterload. Thus, a sudden increase in contractility will result in ejecting more volume out of the ventricle, i.e. increased stroke volume. Myocardial contractility is represented by the slope of the end-systolic pressure–volume relationship. Contractility is proportional to change in pressure over time (dP/dt). Myocardial contractility is influenced by the concentration of intracellular calcium, autonomic nervous system and/or pharmacological agents.

In research practice, LV myocardial function can be quantified in a number of ways. Invasive methods such as placing sonomicrometer crystals in the LV myocardium enable the accurate tracking of LV motion during the cardiac cycle. However, sonomicrometry is an invasive method reserved only for research purposes and limited by the fact that the actual procedure of implanting crystals may alter subsequent cardiac motion. Cardiac magnetic resonance imaging (CMR) and tagged CMR are common non-invasive alternatives to measure cardiac structure and myocardial function. CMR has excellent spatial resolution and allows tissue characterization, however its tomographic nature and the low temporal resolution limit its ability to study the LV three-dimensional mechanics in the beating heart. In addition, the relatively costly and time consuming nature of tagged CMR represent significant bareers for its clinical and research use. Finally, the electromagnetic field used with this imaging modality can interfere with the pacemakers or other metallic devices, generating heat and potentially damaging the myocardium or surrounding tissues.

Echocardiography is a relatively inexpensive and commonly used imaging technique that can be safely used in patients with cardiac devices. Strain measurements were reported to closely track classic physiological parameters of myocardial contractility in experimental and clinical settings under varying conditions (22-24). Therefore, deformation imaging

emerged as a promising and exciting echocardiographic method which finally enabled the clinicians to obtain insights on both regional and global LV contractility in a non-invasive and cost-effective manner.

The following paragraphs will focus on the assessment of LV myocardial function in terms of deformation (strain) and the currently available echocardiographic techniques used to measure strain.

Chapter 3. Echocardiographic Assessment of LV Myocardial Deformation

3.1. Importance and rationale

Echocardiographic imaging is ideally suited for the evaluation of cardiac mechanics because of its intrinsically dynamic nature and excellent temporal resolution (3).

Traditionally, cardiac motion and deformation analysis has been limited to a visual inspection of the ultrasound image sequence, in which each LV myocardial segment is assigned with a wall motion score. However, this methodology depends considerably on the expertise of the interpreter (25) and is limited by a relatively low interobserver agreement (26). In addition, the subjective interpretation of LV regional wall motion is predominately based on the assessment of radial thickening, while the longitudinal shortening is neglected by eye-balling, despite it was demonstrated to be one of the most sensitive and early signs of ischemia (27).

As discussed earlier, the evaluation of global LV systolic function is based mainly on LVEF calculation using Simpson's biplane method. Although LVEF still is the standard of current echocardiographic practice, many sources of error have been demonstrated as a consequence of poor endocardial definition, apical foreshortening, reliance on operator's experience and particularly due to unsatisfactory reproducibility among observers and at test-retest. The variability of LVEF by 2DE Simpson's biplane method has been found as high as 26% for inter-observer variability (28), and the minimum detectable true change in LVEF at sequential testing was reported as high as 11% (29). In clinical practice, cardiologists know they have to live with a measurement variability error in LVEF by 2DE of up to 10%, and so they consider cut-off values for absolute measurements or relative changes in LVEF by

2DE with a significant amount of tollerance (30). This is quite unsatisfactory for the current expectations from echo labs in terms of an early detection and follow up of the cardiac diseases course and treatment effects, not to mention for current research needs in cardiovascular imaging.

For these reasons, myocardial strain and strain rate imaging were introduced in cardiac ultrasound.

3.2. Definition of strain and strain-rate

Strain and strain rate are measures of changes in shape, i.e. deformations. The use of these measures to describe the myocardial mechanics has been introduced since 1973 by Mirsky and Parmley (31).

Strain *(ε)* is a mechanical characteristic that describes the deformation of an object normalized to its original shape and size (i.e. how much the object deforms). Strain Rate (*εR*) describes the rate of deformation (i.e. how fast the deformation occurs).

There are two common ways to measure one-dimensional deformations (shortening or lengthening) of an object: Lagrangian strain and natural strain.

For an object of initial length $\boldsymbol{L_0}$ that is being shortened or stretched to a new length $\boldsymbol{L}$, the Lagrangian (or conventional) strain is defined as: $\boldsymbol{\varepsilon = [L-L_0]/L_0}$. Strain is a dimensionless parameter reported as percent (%). For chardiac mechanics, the L_0 is the myocardial length measured at end-diastole and L at is the myocardial length measured at end-systole. The Lagrangian Strain Rate (*εR*) is the temporal derivative of Lagrangian Strain: $\boldsymbol{\varepsilon R(t) = dL(t)/dt}$. Conversely, natural strain employs a reference length L_0 that changes as the object deforms, describing the instantaneous length change of an object that is independent of a time reference.

These concepts apply to the evaluation of one-dimensional (i.e. longitudinal, circumferential and radial) strain by echocardiography (Figure 2.5). Negative strain indicates

fibre shortening or myocardial thinning, whereas a positive value describes lengthening or thickening (depending on the direction of strain measurement).

Natural strain calculation is the reasonable approach to use with Doppler Tissue Imaging (DTI), since the reference length L_0 must be defined at each frame of colour DTI, while speckle tracking methods will naturally lend themselves to the calculation of Lagrangian strain, since the baseline length L_0 is always known and can easily be used as reference. While the difference between Lagrangian and natural ε values is negligible when the extent of deformation is small (around 5-10%), however, for large extents of myocardial deformations during ventricular ejection and rapid filling, the difference between the two methods could become clinically significant.

If the deforming object is two-dimensional, then its deformation cannot be described anymore by shortening and lengthening only, since it may occur parallel, as well as perpendicular to a given border of the object (Figure 2.4). This type of deformation is called "shear strain". Consequently, the deformation of a two-dimensional object is defined by 2 linear strains (xx, yy) and 2 shear strains (xy, yx). Applying the concepts of linear and shear strain to a three-dimensional deforming object, nine different strain components can be distinguished, namely 3 linear strains (xx, yy, zz) and six shear strains (xy, xz, yx, yz, zx, and zy).

3.3. Quantitative parameters

In order to characterize the myocardial deformation in cardiovascular imaging, the following strain parameters are commonly measured: longitudinal, circumferential and radial linear strains, corresponding to the three coordinates x, y, and z (Figure 2.4). Imaging methods such as echocardiography also allow the assessment of longitudinal-circumferential

shear strain (i.e. torsion, the wringing LV motion), but this is beyond the scope of the present thesis.

Strain values are computed and displayed throughout the cardiac cycle, as strain versus time curves. Relevant strain values along strain-vs-time curves are:

- End-systolic strain: the strain value at aortic valve closure (preferred);
- Peak systolic strain: the peak strain value during systole;
- Positive peak systolic strain: a local myocardial stretching, sometimes occuring in a minor extent in early systole, or as a deformation abnormality in regional dysfunction;
- Peak strain: the peak strain value during the entire heart cycle: the peak strain may co-incide with the systolic or end-systolic peak; if it appears after aortic valve closure, it is defined as "post-systolic strain".

Both the segmental and the global values of strain and strain rate are of interest in cardiology. The *segmental* strain (or strain rate) is defined as the corresponding average value of strain in that particular segment. The *global* strain or strain rate is defined and calculated in different ways, depending on vendor. For instance, some speckle-tracking software packages compute global strain by using the entire myocardial line length while computing the deformation; other by averaging the values computed in a number of points within the myocardial line or by averaging the values computed at segmental level. If global parameters are calculated by segmental averaging, the badly tracked segments need to be identified and excluded by using a reproducible automatic way to differentiate good and bad tracking results (see Chapter 6).

Also the method for calculating the linear strain parameters may vary across various commercially available software packages. For instance, longitudinal strain can be calculated

as subendocardial strain, midwall strain or averaged over the entire cardiac wall, or provide multi-layer strain (subendocardial, midwall and subepicardial strain values displayed together). Since recent evidence showed that the various solutions provided by different vendors can induce themselves a significant variability of strain measurements, it is pivotal to know and understand the technical characteristics of each software package and the significance of the numerical results provided for each strain parameter. Next chapters will provide a detailed overview on the principles and the methodology used by the software algorithms employed in the present research.

3.4. Timing of mechanical events

Since cardiac function is a cyclic process, the selection of the beginning of the cardiac cycle is arbitrary. By convention, end-diastole is used as the point at which the reference length (L_0) can be measured in order to report deformation (strain). End-diastole is commonly defined by the timing of mitral valve closure. Other events which are time-related to mitral valve closure may be used as surrogate, such as the beginning of the QRS-complex in the ECG, ECG R-peak, the largest diameter or volume of the LV, the aortic valve opening click etc., however all surrogate time markers may be sub-optimal under certain circumstances. As a compromise between feasibility and accuracy, analysis software used in deformation imaging generally use the peak of the QRS complex to define end-diastole, but also offer the user the option to overrule this definition and set end-diastole manually if deemed inappropriate.

End-systole coincides with aortic valve closure which is typically visualized by two-dimensional echocardiography from the apical long-chamber view or by detecting the closure click on the pulsed wave Doppler tracing of aortic valve flow. Potential surrogate parameters are the nadir of the volume curve or the end of the T-wave. Again, generally the user is offered the option to overrule this definition and set end-systole manually if deemed inappropriate.

3.5. LV deformation analysis by echocardiography

One of the main clinical benefits of deformation imaging is the capability to provide an objective, more reproducible and less load-dependend measure of global LV systolic function in comparison with traditional LVEF, in terms of global LV longitudinal strain. Global LV longitudinal strain by 2DSTE has been shown to correlate better with LVEF by CMR than with LVEF by 2D Simpson's echocardiographic method (32), and has been demonstrated to provide incremental prognostic information over conventional echo parameters (33, 34).

Another clinical advantage is the capability to objectively assess and quantify LV regional dysfunction, while minimising the influence of tethering effects from normal neighbouring segment which may confound tissue velocity measurement.

Various parameters reflecting LV motion and deformation are calculated by echocardiographic methods: longitudinal strain (from apical views – also the most used parameter), radial strain (from short-axis and apical views, the latter called also transversal strain), and circumferential strain (from short-axis views). More complex deformations, such as rotation, twist, and torsion (longitudinal-circumferential shear) can be estimated as well by echocardiography. In Table 3.1, main terms and definitions used for describing various features related to strain imaging by echocardiography have been summarized.

To date, three different echocardiographic methods have been successively applied for estimating LV myocardial strain: Doppler tissue imaging (i.e. one-dimensional, DTI) and non-Doppler two-dimensional speckle-tracking (2DSTE) and three-dimensional speckle-tracking (3DSTE), which will be presented with their pros and cons in the following paragraphs.

3.5.1. One-dimensional strain by Doppler tissue imaging

Doppler tissue imaging (DTI) - also called tissue velocity imaging (TVI) or Doppler

myocardial imaging (DMI) - is a technique where the velocity of the myocardium toward or away from the transducer is measured and displayed. To distinguish between signals generated by moving tissue and blood flow, a "wall filter" is used, which can be a high-pass filter used to image blood velocities (high), or - in case of DTI - a low-pass filter used to display the myocardial velocities (low). Tissue velocities during the cardiac cycle can be displayed as a pulsed-wave (PW) Doppler spectrogram (showing the velocity corresponding to a single sample region of the myocardium) or as a color overlay on the gray-scale echocardiographic image (showing velocities corresponding to each pixel of the image).

Table 3.1. Terminology used in deformation imaging.

Term	Definition
Velocity	Vectorial quantitative parameter, characterized by a direction and an amplitude (speed or rate)
Displacement	Distance of motion (active or passive) and represents the time integral of velocity
Strain	Myocardial deformation (active shortening-lengthening)
Strain-rate	Myocardial deformation velocity
Longitudinal strain	Deformation from LV base to apex, in a direction parallel to the LV long-axis
Circumferential strain	Deformation along the LV perimeter observed in short-axis view, in a direction perpendicular to the LV long-axis
Radial strain	Deformation towards the center of LV cavity, in a direction perpendicular to the LV long-axis
Twist	Net difference between the opposite rotation angles of LV apex and LV base in the systolic phase
Torsion	Twist normalized to base-to-apex distance
Untwist	Net difference between the opposite rotation angles of LV apex and LV base in the diastolic phase
Bull's eye	Parametric color-coded display of segmental strain values for all 17 LV segments
ROI	Region of interest placed across myocardium for strain measurement (user-defined and editable)
Baseline drift	Measurement error due to inaccurate tracking or heart translation, resulting in strain curves not returning to zero at end-diastole

When the velocity of the tissue is known, several other parameters can be derived. The simplest is the *displacement,* which can be calculated as the integral of velocity over time. The *spatial velocity gradient* can be also derived from DTI recordings. Assuming that the spatial velocity distribution is linear, linear strain rate is equivalent to the spatial velocity gradient: $\varepsilon R = dv/dx$, where dv is the velocity gradient and dx is the instantaneous length of the object. When strain rate has been calculated for each time point during the deformation, strain can be computed as the temporal integral of the strain rate.

The DTI strain imaging has been validated in vivo versus sonomicrometry (35) and tagged CMR (36). However, DTI strain imaging is affected by artifacts related to random noise and reverberations, which may alter the quality of velocity measurements. As with any Doppler-based method, accuracy of strain measurements depends on a correct parallel alignment with tissue motion, therefore angle misalignment between the ultrasound beams and the examined structure may cause additional errors. This angle-dependency increases the variability of the measurement among observers and at serial examinations. Furthermore, DTI strain is one-dimensional, meaning that in a given echo view LV strain can be computed only in the direction parallel with the ultrasound beam (i.e. longitudinal in 4-chamber view) and in a limited number of LV segments where the optimal alignment is feasible. This technique requires high frame rates, which may be difficult to obtain in enlarged ventricles. Finally, extracting meaningful strain data requires manual adjustment of the region of interest, which is a tedious and time-consuming task, and requires a certain level of training and expertise.

3.5.2. Two-dimensional strain by speckle-tracking echocardiography

Non-Doppler-based, 2D strain estimation methods have been introduced to overcome the limitations of DTI strain. For 2D strain analysis using echocardiography, a “block-matching” technique is used on B-mode images, commonly called as “speckle-tracking” (37).

The fundamental principle of 2D speckle tracking (2DSTE) is based on the ultrasound image of myocardial tissue as a pattern of gray scale values, commonly referred to as a *speckle pattern.* The exact spatial distribution of the gray values within the echo image - the speckle pattern - can be attributed to constructive and destructive interference of reflections from the individual *scatterers* (reflections occuring at transitions between different types of tissue density) within the myocardium (38). This pattern is an acoustic characteristic of the underlying myocardial tissue and is assumed to be unique for each myocardial segment, therefore, serving as a "fingerprint" of that particular myocardial segment within the ultrasound image (39).

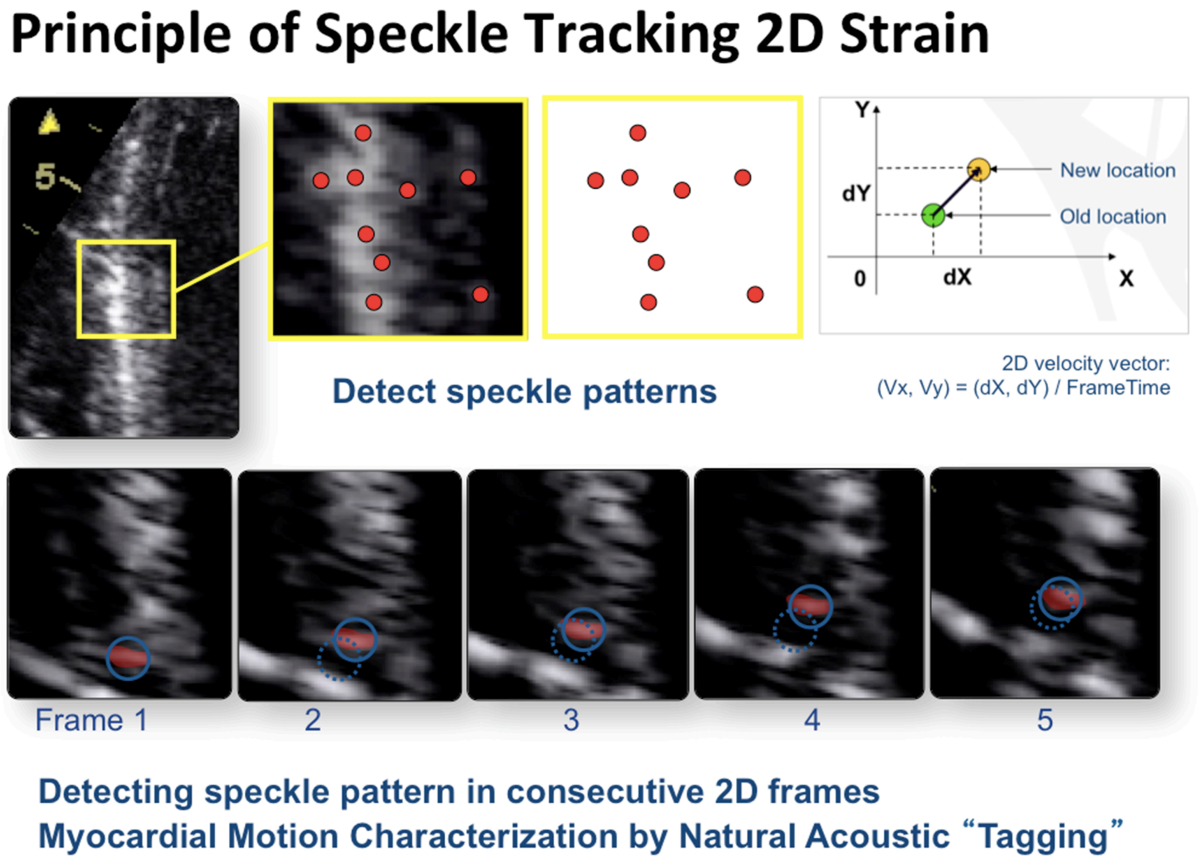

Figure 3.1. Principle of 2D speckle-tracking algorithm (courtesy of GE Healthcare).

The position of the acoustic fingerprint will change according to the position of the myocardial segment within the ultrasound image during the cardiac cycle. Tracking of the speckle pattern during the cardiac cycle ("block-matching") within the ultrasound image thus allows to follow the motion and the deformation of the myocardium (Figure 3.1). By applying several measures of similarity, the in-plane velocity vector is obtained, and repeating the procedure for all pixels in the image and between all image pairs within the image sequence, a dynamic velocity vector field is obtained. Since velocity vector estimates are generally noisy, they may require correction before further processing, a process called *regularization*.

The assumption that the speckle patterns are preserved between image frames is fundamental to this methodology. Myocardial rotation, deformation (i.e., strain), and out-of-plane motion will change the relative positions/ amplitudes of the scattering sites with respect to the transducer and will cause a change in speckle patterns between subsequent image frames. The only way to reduce speckle decorrelation between subsequent frames is by acquiring image frames quickly after one another (at high frame rates) to limit the amount of rotation, strain, and out-of-plane motion between subsequent frames. In addition, being an image-based analysis of strain, it seems logical that one should avoid as much as possible image artifacts and reverberations, in order to preserve the speckle patterns and ensure the quality of strain estimation.

2DSTE has been validated versus sonomicrometry (40, 41) and tagged CMR (40, 42). Speckle-derived strain is superior to DTI strain, particularly with regard to noise, angle dependency and reproducibiliy. These reasons, as well as its user-friendly and more automatic workflow, have promoted 2DSTE as the current standard method used for assessing LV deformation in clinical practice.

Clinical applcations of 2DSTE. A growing body of evidence suggests that assessment

of LV deformation by 2DSTE provides incremental information in clinical settings (4).

Myocardial deformation imaging by 2DSTE offers the possibility of quantifying regional cardiac deformation noninvasively. It is widely used for the detection of myocardial ischemia (43) and has been proposed as a clinically useful tool to detect heart disease at its preclinical stage, to differentiate among various hypertrophy etiologies, and to monitor therapy (5, 39). Application of 2DSTE has also been extended for studying regional and global function of other cardiac chambers including the right ventricle and the left atrium.

Most importantly, 2DSTE has provided new mechanistic insights into the diverse phenotypic expressions of heart failure, with a broad range of applications to detect the early stages of the progression of LV myocardial dysfunction (44). In general, longitudinal LV shortening, which is predominantly governed by the subendocardial fibers, is the most vulnerable component of LV mechanics and therefore most sensitive to the presence of myocardial disease. Conversely, the midmyocardial and epicardial function may remain relatively unaffected early in the disease course, and therefore circumferential strain and twist may initially remain normal or show exaggerated compensation for preserving LV systolic performance. However, concomitent increase in cardiac muscle stiffness (i.e. due to LV hypertrophy or fibrosis etc) may cause progressive delay in LV untwisting. Loss of early diastolic longitudinal relaxation and delayed untwisting attenuates LV diastolic performance, producing elevation in LV filling pressures and a phase of predominant diastolic dysfunction, when LVEF may remain in normal ranges. Conversely, an acute transmural injury or disease progression would result in concomitant midmyocardial and subepicardial dysfunction, leading to a reduction in all strain components (longitudinal, circumferential, twist mechanics), which consequently causes a reduction in LVEF.

According to the above principles, Sengupta PP and Narula J proposed a new algorithm for exploring the spectrum of altered cardiac muscle mechanics in patients with heart failure

based on the relative involvement of various strain parameters (Table 3.2)(44).

Table 3.2. Classification of left ventricular mechanics in heart failure (after Sengupta *et al.* (43)).

Predominant functional impairment	**Longitudinal mechanics**	**Circumferential mechanics**	**Torsional mechanics**	**Global EF**	**Diastolic filling pressures**	**Clinical syndrome**
Longitudinal	Impaired	Preserved	Preserved	Preserved	Elevated	Diastolic HF (HFNEF)
Subepicardial	Preserved	Impaired	Impaired	Preserved	Elevated	Diastolic HF (HFNEF)
Transmural	Impaired	Impaired	Impaired	Impaired	Elevated	Systolic HF

Abbreviations: HF, heart failure; HFNEF, heart failure with normal ejection fraction.

In other words, if the subendocardial region is unaffected, but subepicardial myocardial dysfunction predominates (e.g. pericardial diseases, myocarditis etc), there will be a predominant impairment in circumferential and twist mechanics. with relative sparing of subendocardial function in order to preserve EF. More commonly, if the subendocardial region is affected, the outcome predominantly affects the longitudinal shortening and suction performance, although EF is still maintained by compensation offered from the outer subepicardial region. Typical examples are the majority of progressive myocardial diseases and coronary ischemia. If compensation is not possible due to concomitant dysfunction of the subepicardial region in transmural disease, LVEF becomes reduced and the LV dilates (44). Common examples are progressive myocardial diseases in advanced stages with marked transmural involvement and acute transmural infarction, resulting in concomitant subendocardial and subepicardial dysfunction.

This novel approach of classifying LV mechanics would also explain why the simple calculation of LVEF is conceptually inappropriate to evaluate for non-transmural myocardial

diseases in early stages, as the reduction in one directional strain can be compensated by the strain in other direction(s) to maintain stroke volume and LVEF, advocating for more sensitive measures of LV function, such as strain.

This background knowledge has been used to provide a research framework for the novel 3DSTE technology to assess LV deformation, and the Chapters 6-9 will address key topics arised from the 2DSTE experience: sources of variability of 3D strain, normal pattern of 3D deformation, STEMI (prototype of transmural injury) and HCM (prototype of impaired longitudinal mechanics with preserved EF).

Limitations of 2DSTE. The accuracy of speckle tracking is dependent on 2D image quality and frame rates. Good image quality enhances the clarity of speckle patterns and improves the accuracy and robustness of their detection. Low frame rates result in unstable speckle patterns, whereas high frame rates reduce scanline density and affect speckle resolution.

The most critical limitation of speckle tracking techniques is the temporal stability of ultrasound speckle patterns. Their instability is not only due to through-plane motion, but also due to physiological changes of living tissue structures and changes of interrogation angles between moving tissue and ultrasonic beam. The accumulation of small random errors in the detection of speckled patterns during the tracking process may potentially lead to inaccurate strain results.

Other relevant limitations of 2DSTE originate from its two-dimensional nature. The speckles have a complex motion in the three-dimensional space and the speckle patterns in 2D echo images represent the in-plane projection of their actual 3D motion. This off-plane limitation issue is known to be more critical in short-axis than in apical views (i.e. affecting more radial and circumferential 2D stran than longitudinal 2D strain). In addition, 2DSTE analysis requires six image acquisitions obtained from different cardiac cycles and from

parasternal and apical LV views to compute all strain components in all LV segments. This can be an issue in specific experimental and clinical settings, particularly when the heart rate or LV loading conditions change rapidly (i.e. stress echo)(45). The ideal method would be to derive all strain measurements from a single 3D dataset, as explained in the following chapter.

Despite obvious clinical benefits of 2D strain imaging, one of the biggest challenges looming is the rapid pace of technological growth, which has resulted in a great variety of software and algorithms. As 2DSTE becomes commonplace, it seemed mandatory to ensure standardization of nomenclature, steps in data acquisition, as well as optimal training to reduce data variability. The European Association of Cardiovascular Imaging and the American Society of Echocardiography have undertaken such initiative in 2010 and have created a Task Force together with the industry representatives to standardize the 2D strain imaging across vendors and users (46). The Task force provides for the first time a neutral communication platform to discuss the problems inherent in current deformation imaging tools and to agree on definitions of the parameters to be measured. The first document including the recommendations from the Task force on 2DSTE will be published in 2014.

Chapter 4. Left Ventricular Myocardial Strain by Three-dimensional Speckle-tracking

Deformation imaging by 2DSTE has become an established clinically useful tool for LV myocardial function analysis, due to its diagnostic, prognostic and management implications. The recent developments of ultrasound transducer technology with capability of real-time full volume imaging of the LV, as well as of hardware and software computing, make it possible to perform speckle-tracking in three dimensions and thus track the complex deformation of the myocardium (47). Three-dimensional speckle-tracking echocardiography (3DSTE) represents the latest advance in myocardial deformation imaging, overcoming some of the limitations of 2DSTE and allowing the strain analysis of all LV segments from a single 3D dataset.

4.1. Principle.

3DSTE is an advanced post-processing tool that tracks inherent features ("speckles" or "acoustic markers") in a 3D volumetric image of the LV over time. 3DSTE uses a tracking algorithm based on frame-to-frame block matching in three-dimensions, which can be considered a direct development of 2DSTE to three dimensions (47). This involves successively searching for a match between 3D patterns found in one frame and in the following ones. Calculation is performed after defining a region of interest (ROI) that covers the entire LV myocardium.

The assumption of a stable local speckle pattern between subsequent volumes holds true also in the case of 3DSTE, as detailed above for 2DSTE in Section 3.5.2. The quality of each match is calculated, and any outliers are detected and removed before the weighted spatial averaging of the results is performed. The results are next mapped to an average myocardial mesh, so that the shape of the mesh model of the LV can be updated for all frames

(48). All quantitative results are derived from this mesh model (Figure 4.1).

It is worth emphasizing the fact that, the longer time there is between successive frames (i.e. with lower temporal resolution), the longer the tissue may have moved, and the larger the search areas for each block matching has to be.

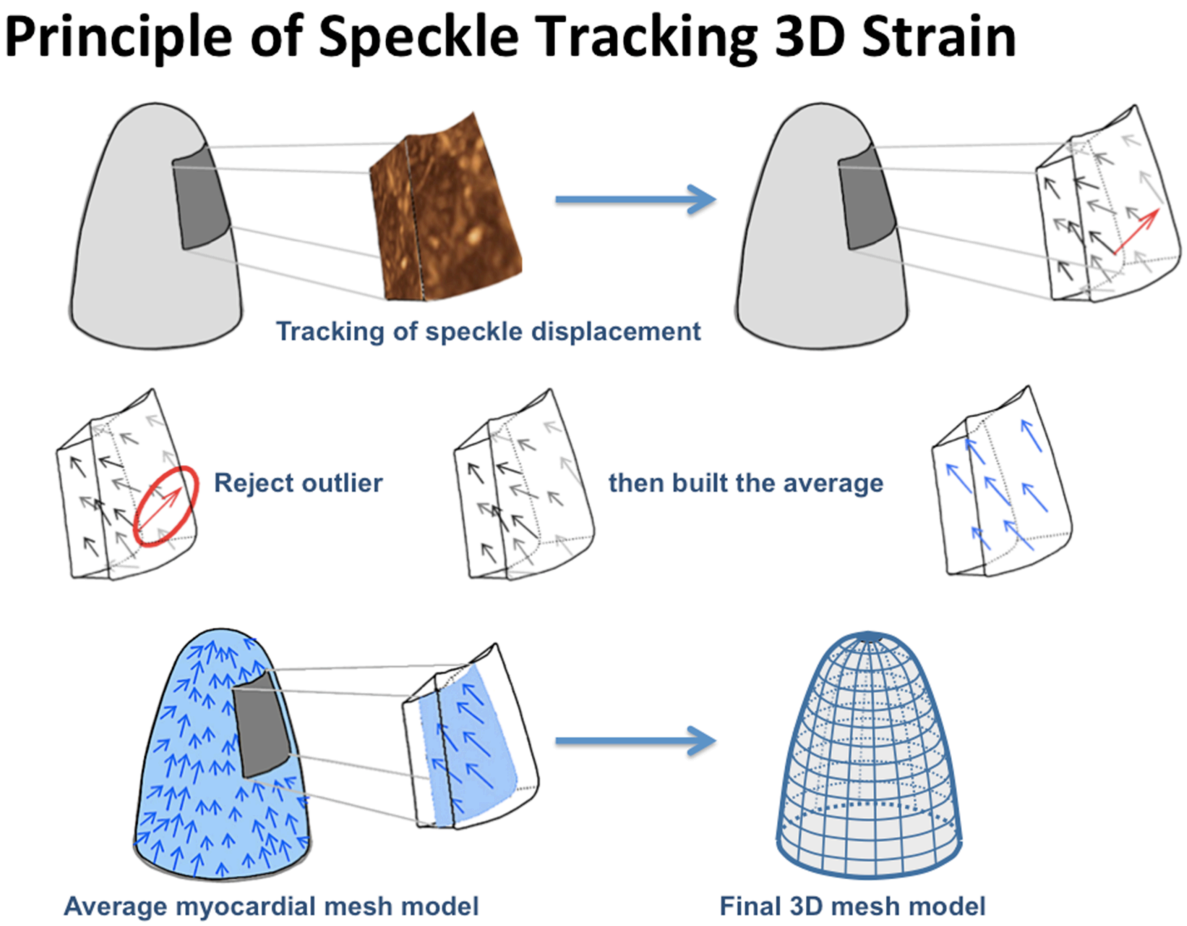

Figure 4.1. Principle of 3D speckle-tracking algorithm (courtesy of GE Healthcare).

Therefore, the necessary time of 3DSTE processing would shorten as the temporal resolution of the 3D data set increases. However, too much increase in temporal resolution will reduce the line density in the 3D image, and so the quality of speckles. The frame rate has to be above a minimum level for the natural acoustic markers to be recognizable in successive

frames. As a rule of thumb, the temporal resolution should be at least 40% of the heart rate, (24 volumes/s at 60 bpm, 40 volumes/s at 100 bpm etc) (48). Multi-beat ECG-gated 3D acquisition is the preferred way to achieve these levels of temporal resolution and still obtain large 3D datasets able to encompass the entire LV.

4.2. Advantages and limitations of 3D versus 2D speckle-tracking

The heart has a complex, three-dimensional deformation pattern, and speckles move in the three spatial directions. 3DSTE offers a new way to analyze the LV function by echocardiography, but most importantly a new concept for assessing myocardial function from volumetric acquisitions.

Advantages of 3DSTE. The fundamental difference between 2DSTE and 3DSTE is that the first tracks the projection of 3D movement of speckles confined into a fixed 2D plane, whereas the latter assesses real movement in 3D, not just a projection. With 3DSTE, performing tracking over time in three dimensions means there is no more out-of-plane motion issue of the speckles.

Time-saving is one of the main advantages of 3DSTE because all strain components (longitudinal, circumferential, radial) in all LV segments are calculated in one analysis step from a single dataset. Within a few minutes, the 3DSTE software provides a large variety of parameters to quantify LV size, geometry and function (volumes, stroke volume, ejection fraction, mass, sphericity), including strain parameters. Importantly, all these strain measures are derived from the same cardiac cycle length, avoiding the problems of 2DSTE related to the need of matching cardiac cycle length in separate LV image acquisitions in order to compute global strain.

3DSTE allows to compute a new strain parameter, i.e. area strain as a measure of relative area change that combines the effect of longitudinal and circumferential strain (Figure 4.2). The rationale behind computing area strain is that this parameter is potentially

more accurate than single strain parameters, and indeed MRI tagging showed that are strain could discriminate normal and ischemic zones better than most other strain indexes (48).

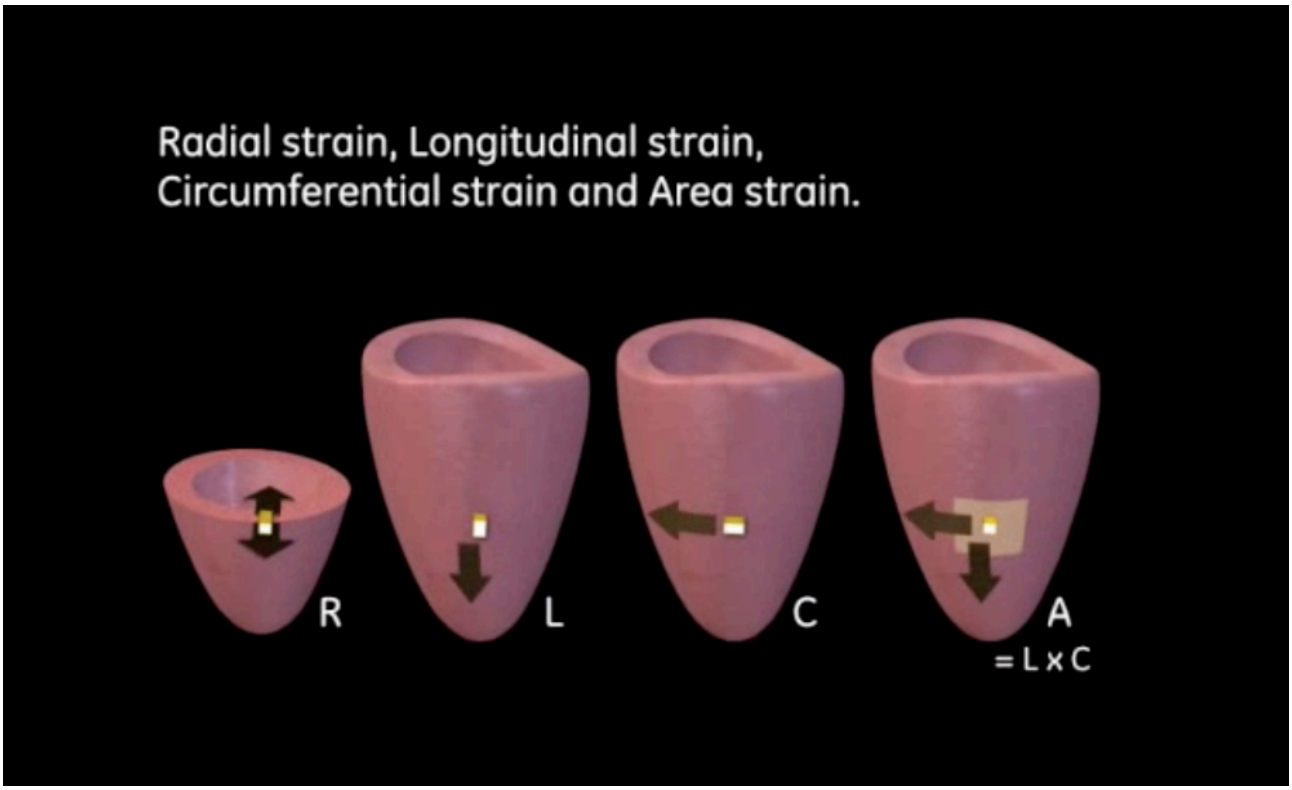

Figure 4.2. Left ventricular myocardial strain parameters measured by 3D speckle-tracking echocardiography using 4D AutoLVQ software. *Courtesy of GE Vingmed*

Limitations of 3DSTE. With the introduction of a new dimension with 3DSTE, new challenges arise. A 3D full volume is constructed from "stitching" four to six subvolumes. This could lead to problems in tracking the speckles across "stitches", as they belong to different heart cycles. However, since most of the deformation occurs in small segments, this may not be of major importance. Traditionally, frame rate (20–25 vps) and lateral resolution (number of lines in each direction) have been considered to be too low for effective tracking. However, the high end technology used in this research project allows to reach a superior temporal resolution (average 32-40 vps), close to the range used for 2DSTE.

4.3. Methodology.

3DSTE technique follows the subsequent steps to estimate 3D strain:

I. Key cardiac events - end-systole and end-diastole - are indicated either automatically (e.g., on the basis of the electrocardiogram) or manually (e.g., by visually inspecting the cardiac cycle and indicating the frames with the smallest and largest volumes, respectively);

II. The region of interest (ROI) for 3D strain estimation is defined: the endocardial border, sometimes in combination with the epicardial border, is delineated manually, semiautomatically, or automatically at end-diastole and/or end-systole (depending on the software);

III. Segmentation: LV is subdivided into segments for segmental strain analysis, usually ranging from 16 to 18 segments depending on the segmentation model used by the various software packages.

IV. Finally, the 3D LV region of interest is tracked throughout the cardiac cycle, and the deformation curves versus time are estimated and displayed in each segment, as well as averaged for the entire LV. The calculated parameters can be presented in various ways, and usually the output includes a color coded bull's eye plot.

In Table 4.1. the main features of 3DSTE software packages used in this research (i.e. 4D AutoLVQ) and the differences between 2D strain algorithms have been summarized.

With 4D AutoLVQ, the ventricle is divided into 17 segments, and the instantaneous strain throughout the cardiac cycle is displayed numerically and using color coding in the bull's eye plot (red=negative; blue=positive). As shown in Table 5.1, care should be taken when comparing numerical results from 2D strain and 3D strain bull's eye plot. The strain values displayed by 2DSTE are the peak systolic values in various segments irrespective of their timing in systole, including positive peaks (if any), while the strain values diasplayed by

3DSTE are simultaneus and from one current frame (may be end systolic frame or the frame of peak systolic strain or any other).

Table 4.1. Comparison between 2D strain and 3D strain by vendor-specific equipment (Q-Analysis and 4D AutoLVQ, respectively, GE Vingmed, Horten, Norway).

	2D strain	**3D strain**
Acquisition	3 parasternal and 3 apical 2D views	one apical 3D full volume
Temporal resolution[1]	40-80 fps	36.6 vps (*in vitro* validation study (12))
Heart rate	regular (consecutive 2D LV planes)	regular (ECG-gated multi-beat LV full-volume)
Parameters	all strains (longitudinal, radial, circumferential)	all strains (longitudinal, radial, circumferential)
Two-directional strain[2]	no	yes
Bull's eye map[3]	static	dynamic
Calculation of global strain	non-simultaneous segmental peaks[4]	simultaneous segmental values[4]
Positive peak rule[5]	yes	no
Drift compensation[6]	yes	no
Definition of end-systole	time of aortic valve closure	time of LV minimal volume

[1]higher range is advisable in tachycardia to avoid undersampling

[2] reflects a combination between longitudinal and circumferential strain.

[3] bull's eye maps of 2D longitudinal strain display one snapshot with peak values of segmental strain; bull's eye maps of 3D strain parameters display simultaneous segmental strain values continuously throughout the cardiac cycle.

[4]with 2D longitudinal strain bull's eye, peak segmental values are displayed irrespective of their reciprocal timing during systole; with 3D strain bull's eye, simultaneous segmental strain values are displayed in each frame.

[5] in the bull's eye display, a positive strain is displayed during systole for a certain segment, only if the positive peak strain exceeds 75% of the peak negative strain value in the same segment.

[6] all segmental strain curves are "forced" by the software to return to baseline at end-diastole.

Abbreviations: 2D, two-dimensional; 3D, three-dimensional; fps, frames per second; LV, left ventricular; vps, volumes per second.

For 3D speckle-tracking algorithms, the accurate estimation of radial strain is more problematic than for longitudinal or circumferential strain. This suboptimal performance could be related to the fact that radial strain must be calculated over a relatively smaller region (because of the limited wall thickness), in combination with relatively limited spatial resolution of speckles in apical LV 3D acquisitions.

Differences exist in the way radial strain is defined and obtained by different 3DSTE vendors. The 4D AutoLVQ software used in this research project estimates radial strain from the area strain assuming that the segment has a constant volume V. Radial strain is found as $3DR\varepsilon = 100*(R-R_0)/ R_0$, where R = V/A is the radial length of the segment, and A is the segmental area. R_0 is the initial length at end diastole (QRS). By substitution, the radial strain formula can also be written $3DR\varepsilon = -100*3DA\varepsilon /(3DA\varepsilon +100)$, where $3DA\varepsilon$ is the area strain (48).

4.4. Validation.

3DSTE algorithm has been validated with phantoms and sonomicrometry in several experimental studies (6, 7, 49, 50). Overall, these studies reported moderate to very good correlations (r = 0.49–0.91) between regional strain values obtained by 3D STE methods and sonomicrometry. The radial strain component showed the worst correlation and agreement with sonomicrometry for all the tested approaches. As mentioned in the previous section, in order to overcome this shortcoming, a solution provided by some vendors was to compute radial strain from other strain components which are more reliably measured.

Although the images in simulated phantom models and animal experiements have realistic image quality, image artifacts often encountered in clinical images are usually not present. Given the high susceptibility of 3DSTE algorithm to image quality issues, clinical validation in real life patients appears as the reasonable next step.

On the other hand, validating 3DSTE in a clinical setting is challenging because no reference measures of LV myocardial deformation are available. The new 3DSTE technique can be compared against only one of the currently established methods to assess LV myocardial function (e.g., DTI, 2DSTE, CMR tagging). However, the results of such comparisons should be interpreted with caution, because none of the available noninvasive imaging techniques for assessing LV deformation is a true gold-standard method. Such comparison would show only the comparability of strain values among different techniques rather than indicating if one method is more accurate than the other (27).

4.5. Clinical value of 3D speckle-tracking to date

Recent studies have provided encouraging results, showing the potential of 3DSTE to replace 2DSTE and DTI in a clinical setting in which the value of deformation imaging is already proven (e.g., the detection of myocardial ischemia etc).

Specifically, several researchers reported that LV global strain quantitation by 3DSTE is a reliable technique for the evaluation of global LV function, in comparison with conventional parameters (ejection fraction by 3DE and CMR, cardiac output, wall motion score index) and global 2D longitudinal strain (51-55).

By far, the most attractive clinical application of 3DSTE is in the setting of ischemic heart disease, for which detecting areas of regional myocardial dysfunction is equally important than measuring global LV function. Even though it still remains unclear whether 3D STE regional strain values are as reliable as those obtained by DTI or 2DSTE, preliminary evidence showed that 3DSTE has a good agreement with delayed-enhancement CMR to detect myocardial scar in patients with healed myocardial infarction (52), as well as with conventional visual wall motion score (53).

4.6. Reproducibility

A clinically important aspect for the reliable applicability of 3DSTE is the reproducibility of the strain measurements. A highly precise or reliable study will give the same measurement on sequential examinations and is a vital characteristic of a good follow-up test. Indeed, if the study is highly precise (reproducible) - even if it is of limited accuracy - most clinicians would find such a study useful, providing that the bias from the actual measurements was reproducible (56).

Overall the reproducibility of current 3DSTE was reported as acceptable to excellent (57, 58), including at test-retest (51, 54). In general, radial strain values showed higher variability than values of longitudinal or circumferential strain, and segmental strain showed greater variability than global strain values. The reproducibility of 3DSTE was either comparable, or superior than of 2DSTE particularly for radial and circumferential strain (51).

As stated for 2DSTE, the biggest concern regarding the reproducibility of 3DSTE is related to its consistency among vendors. 3DSTE-derived strain parameters currently exhibit a wide variation in the reported values depending on the imaging system and software used (see Chapter 6)(59).

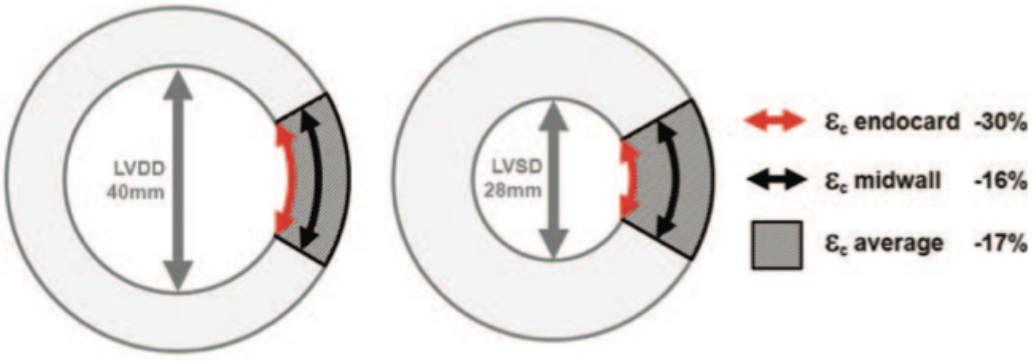

Figure 4.3. Assessment of circumferential strain. This simulation of a ventricle with a fractional shortening of 30% illustrates how the measurement of circumferential strain depends on the definition of the parameter. If circumferential strain is defined as shortening of the endocardium, the measurement result will be -30%. If defined as midwall shortening, only -16% will be measured. Averaging the entire wall will result in -17%. All these definitions are used in current systems (reproduced from Voigt J. (30)).

There are fundamentally three sources of variation: acquisition, postprocessing, and the hemodynamic status of the patient (afterload variations such as blood pressure etc).
A sufficiently high temporal resolution has traditionally been considered the most important aspect of acquisition in deformation ultrasound. For 3DSTE, the most important aspect is probably to achieve the optimal trade-off between temporal and spatial resolution, since higher frame rates may lead to some compromise in spatial resolution because of the sacrifice in line density. While the computational power is substantially similar, the various vendors may propose slightly different ways of managing the trade-off between temporal and spatial resolution (prioritizing more one at the expense of the other). The optimal temporal and spatial resolution for 3DSTE are yet unknown. Two preliminary studies have reported on optimal temporal temporal resolution: 3DSTE had the best agreement with 2DSTE for longitudinal strain estimation at a temporal resolution of 34-50 vps, and the highest correlations for longitudinal and circumferential strain estimation with sonomicrometry at 37 vps (6).

As discussed in previous sections, variations in 3DSTE post-processing may refer to various aspects, such as: global strain calculation, definition of linear strains, application of drift compensation and segment validation, including ways of controlling the outliers and the order of calculation etc. All these technical aspects can only be partially disclosed to the user, since this information is property of the vendors, making their software packages a sort of "black box" (30).

The study presented in Chapter 6 was among the first to provide clinical evidence on this issue. As a logical consequence of the intervendor variability, the reference values should be defined for each vendor and software (see Chapter 7).

4.7. Feasibility

The acquisition of volumetric LV datasets required for 3DSTE analysis is limited to patients with no heart rhythm irregularities and in a clinically good condition (able to cooperate for breathholding for up to 10 seconds). In addition, the accuracy of 2DSTE and, probably even more, of 3DSTE algorithm is critically dependent on the optimal image quality of the acoustic window, without reverberation or dropout artifacts. In addition, the acquisition of an adequate 3D dataset for LV strain analysis requires a sufficient amount of dedicated training and skill.

These basic technical requirements may dramatically limit the number of patients in whom 3DSTE is feasible in the world of clinical cardiology. To date, feasibility of 3DSTE in everyday practice is unknown, but is expected to be lower the feasibility of 2DSTE. After excluding patients with irregular rhythm and unable to breathhold, the reported feasibility of 3DSTE so far ranged between 63% and 83%, being lower than for 2DSTE (80-97%) (27).

All current 3DSTE approaches seem to have difficulties estimating deformation in the basal parts of the LV. The lowest correlation between the 3DSTE approach and 2DSTE or triplane imaging was seen in the basal LV segments (60). In addition, LV apical segments are often incompletely imaged in a pyramidal-shaped LV volumetric acquisition. Even though the volume of LV dataset can be increased to its maximum size, this would lead to an unacceptably low temporal resolution for 3D strain imaging and is not recommended. When more than 3 segments per ventricle cannot be analyzed, the global LV 3D strain parameters are no longer provided, as the strain average in that case would not be truly representative of global LV performance.

The research studies presented in the following chapters add relevant new data on the feasibility of 3DSTE and provide more detailed insights on the current technical limitations of

3DSTE.

Experimental Part

Chapter 5. Methodology

5.1. Selection of subjects

Several different patient populations were recruited for this series of studies included in the present thesis.

Chapter 6 presents the study exploring the clinical variability of 3D strain values at repeated measurements pertaining to different observers, software packages and vendors. The patient population was designed to reflect the current clinical practice and included consecutive, clinically stable patients with a full spectrum of cardiac conditions. A total of 71 patients referred for a clinically indicated routine echocardiography in the Echocardiography Laboratory of the Padua University Hospital (Italy) were screened for enrolment. The inclusion criteria were those imposed by the application of 3DE modality: presence of sinus rhythm, adequate apical acoustic window and ability to breathhold for 5-10 seconds during the 3D full volume acquisition of LV. Eleven patients (15%) were excluded due to poor 2D image quality (>2 LV segments not adequately visualized without contrast infusion) or persistent stitching artifacts despite re-attempted 3D dataset acquisition. Accordingly, the final population consisted of 60 patients. Studies were retrieved from the digital archive and analyzed offline on dedicated workstations.

Chapter 7 represents a prospective, normative study of LV 3D strain parameters. The population used for this study was enrolled as part of a larger research project aimed to establish the reference values for chamber and valve quantification by transthoracic 3DE. These subjects were healthy Caucasian volunteers prospectively recruited between 2011 and 2013 in the Echocardiography Laboratory and in the Research Echolab of the Padua University Hospital among hospital employees, fellows in training, their relatives and people who underwent medical visits for driving or working license. Study sample size was

determined according to Altman et al (61), who set 200 subjects as the minimum number to enrol in a study aimed to assess reference values for biological variables. Criteria for recruitment included: age > 17 years, no previous history of cardiovascular or lung disease, no symptoms, absence of cardiovascular risk factors (i.e. systemic hypertension, smoking, diabetes, dyslipidemia), no cardio-/vasoactive treatment, normal electrocardiogram and physical examination. Exclusion criteria included: trained athletes, pregnancy, body mass index > 30 kg/m^2, poor apical acoustic window (defined as more than two LV segments not adequately visualized without contrast infusion) and inadequate 3D datasets for global LV 3D strain analysis (either due to incomplete LV visualization or poor tracking in >3 segments). For the LV 3D strain normative study, from a total of 276 healthy volunteers screened, 218 met the entry criteria in the study. This healthy population was also used to analyze the variability of 3D strain normal values related to the software package used for measurements, sub-study presented in the Chapter 6 dedicated to 3D strain variability.

Chapter 8 is a prospective, observational study exploring the potential clinical impact of introducing LV myocardial functional analysis by 3DSTE in patients after a recent ST-elevation myocardial infarction. Patients were included if they had no history or documentation of previous old infarction, fulfilled the diagnostic criteria of acute STEMI and were successfully treated by primary PCI. Additional enrolment criteria was the performance of LV study by both echocardiography and LGE-CMR within 24 hours, fulfilled in 46 patients. The overall number of STEMI patients studied with echocardiography was 77, and included those patients in which LGE-CMR was either not performed or did not fulfill the entry criteria.

Chapter 9 is a prospective, observational study, aiming to explore the LV geometry and myocardial strain in 42 consecutive patients with hypetrophic cardiomyopathy by 3D echocardiography. Patients were identified in the specialized outpatient clinic dedicated to hypertrophic cardiomyopathy of the Padua University Hospital, either during their initial

evaluation or at routine yearly follow-up. A total of 42 patients who met the entry criteria (sinus rhythm, good apical acoustic window, LV EF > 50%) were studied in the Research Echo Lab at the Padua University Hospital. A group of 42 age-and gender-matched healthy subjects from the normative study were used as controls.

All the studies from this series were approved by the Ethics Committee of the University of Padua (protocols #2380 P, #2332 P, #2634). All patients included in this research have provided their written informed consent for enrolment in the respective study.

5.2. LV analysis by conventional 2D echocardiography and 2DSTE

Standard echocardiographic views were obtained using a commercially available Vivid E9 ultrasound system equipped with M5S and 4V probes. Grayscale images were acquired using second-harmonic imaging with frequency, depth, and sector width adjusted for frame-rate optimization (between 50-80 fps). Image settings and frame-rates were kept similar for LV short axes at basal, mid and apical level, as well as in four-chamber, two-chamber, and long-axis apical views, which were recorded immediately one after another. Peak early diastolic (e') mitral annular velocities were obtained by pulse-wave tissue Doppler imaging from the apical four-chamber view using both the septal and the lateral sites. The average e' was used to calculate the ratio of peak early-diastolic transmitral flow velocity E to e', to estimate LV filling pressures. Both two-dimensional and Doppler images were digitally stored as three consecutive cycles recorded during end-expiratory apnea.

Two-dimensional strain was evaluated from standard bidimensional acquisitions, using a dedicated software package (EchoPac PC BT 12, GE Vingmed, Norway) (37) by a single observer experienced in 2D strain quantitation by STE. By tracing the endocardial contour on an end-diastolic frame, the software automatically tracked the contour on subsequent frames. An automatically generated region of interest (ROI) divided into six segments was provided

for each view (i.e. 3 parasternal for radial and circumferential strain, 3 apical for longitudinal strain). Tracking quality was verified in real time and the region of interest was manually corrected by contour position refinements and width adjustments to fit the LV wall. The LV was divided into 17 segments and each segment individually analyzed. LV segments with inadequate tracking were rejected by the software/operator. If more than 2 segments had inadequate tracking, global strain values were not computed.

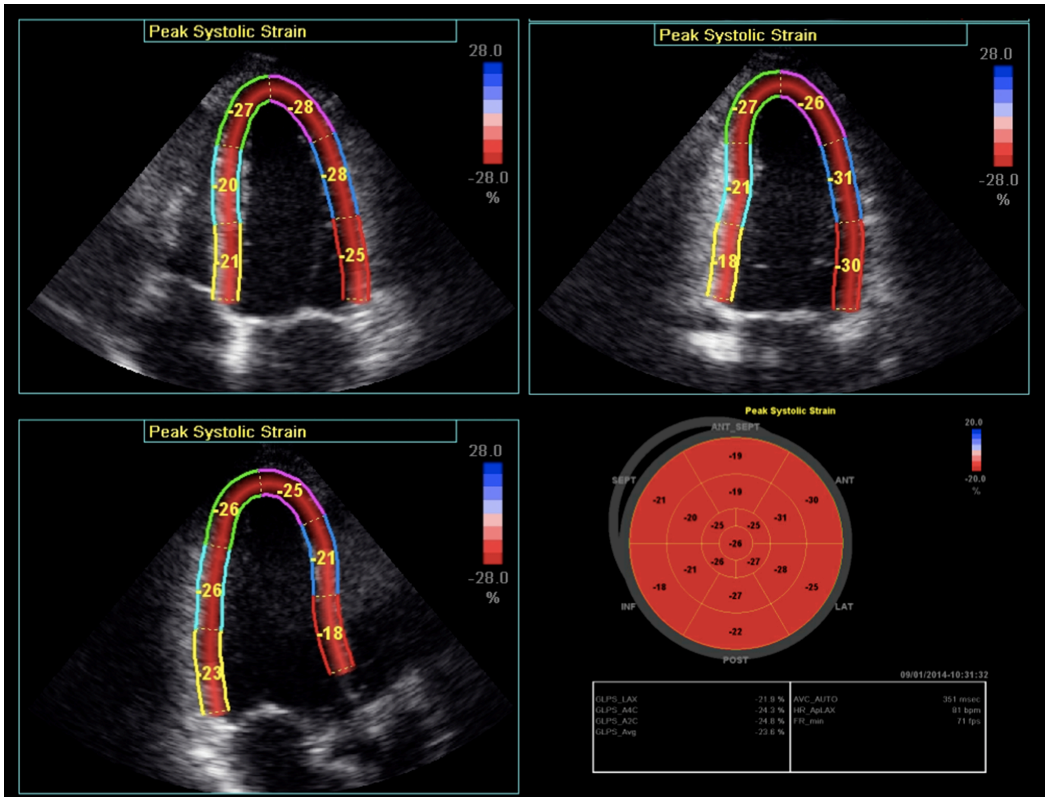

Figure 5.1. Example of LV longitudinal strain analysis by 2D speckle-tracking software (EchoPac BT 12, GE Vingmed, Horten, Norway)

5.3. LV analysis by conventional 3D echocardiography and 3DSTE

Consecutive 4 and 6-beat ECG-gated subvolumes were acquired from apical approach using second-harmonic imaging, during an end-expiratory apnea to generate the full-volume data set (62). Care was taken to encompass the entire LV cavity within the data set. The

quality of the acquisitions was then verified in each patient by selecting the multi-slice display mode available on the machines (Figure 5.2) to ensure optimal imaging of the entire LV wall at each short-axis level and, if unsatisfactory, the data set were re-acquired.

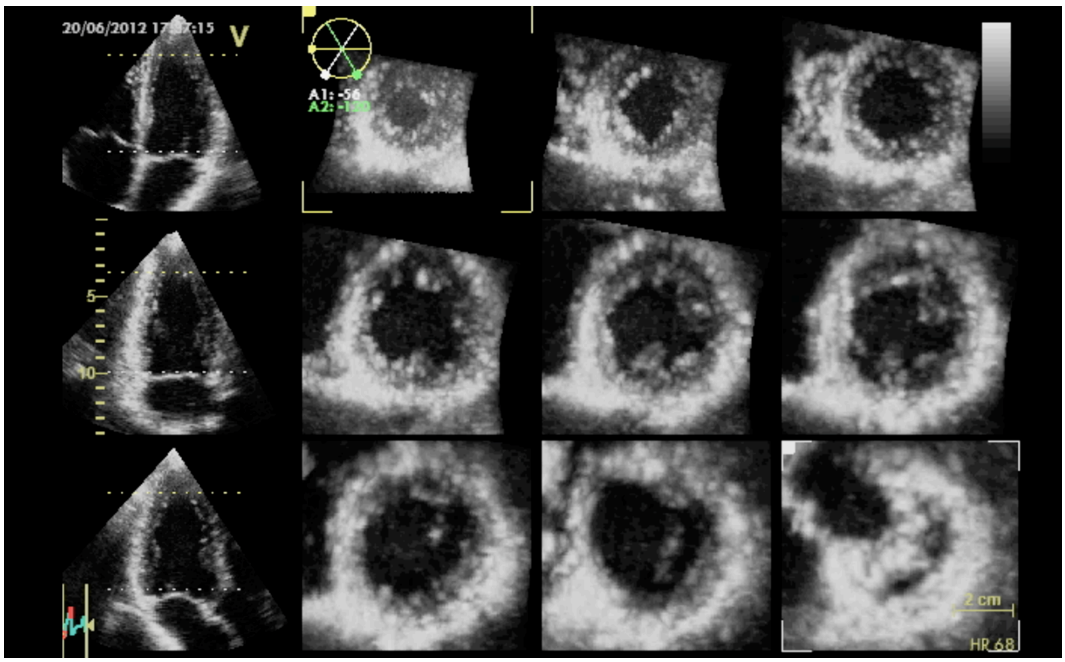

Figure 5.2. Multi-slice display of 3D LV dataset

Three-dimensional LV quantitative analysis was perfomed by a single experienced researcher using a commercially available software (4D AutoLVQ, EchoPac BT 12 and BT 13), dedicated for the analysis of proprietary 3D datasets acquired with the Vivid E9 scanner (GE Vingmed, Horten, Norway). The workflow for the quantitative analysis of LV 3D geometry and deformation consisted of several steps:

1. After an automated cropping of the 3D full volume in a quad screen display (i.e. apical four-chamber, two-chamber and long-axis views, as well as a short-axis view), manual adjustments to optimize each view were performed by pivoting and translating each plane so that the corresponding intersection line of the 3 LV planes was placed in the middle of the LV cavity, crossing the LV apex and the center of mitral valve in each view. Manual verification of the

timing of end-diastole and end-systole was performed, and adjustments were done when necessary;

2. Endocardial surface identification was manually initialized by placing 2 attractor points in each longitudinal view (at the apex and in the middle of mitral annulus), in end-diastole and then in end-systole;

3. If endocardial border detection was judged unsatisfactory by the examiner, LV endocardial borders could be manually adjusted in a multiplanar layout (3 apical and 3 transverse planes) by a point-click method, with secondary immediate automated refinement of boundary detection accordingly (63). Manual correction of endocardial surface was done to include trabeculae and papillary muscles in each view, as well as between the standard planes. The position of the contour was double-checked by observing motion images;

4. After the quantitative analysis derived from endocardial LV surface (3D volumes and EF), a similar contour on the LV epicardial surface was added in the next step, thus delimitating the region of interest from which LV 3D strain parameters were computed (Figure 5.3). Manual refinements of this second epicardial contour to precisely fit the LV wall in each segment were also performed;

5. Final analysis using 3DSTE algorithm yielded segmental and global values for each strain component (longitudinal, 3DLε; circumferential, 3DCε; radial, 3DRε; area strain, 3DAε) in each frame of the cardiac cycle, presented as color-coded polar maps and time-strain traces of a LV 17-segment model. 4D AutoLVQ package does not apply any drift compensation to strain curves, and LV segments showing a significant drift of Lε (more than 12 percentage points) of end-systolic strain curves from the baseline were rejected from the subsequent analysis. In addition to the automated validation of tracking quality performed by the software (rejecting segments with excessive drift at end-diastole), visual check was performed by the operator, who rejected additional segments (if their deformation was inadequately tracked in the

motion images or if they showed unsound curve patterns)(Figure 5.4). Global strain was automatically computed as a weighted average of the segmental strain values and displayed. Rejected segments were not included in the calculation of global strain. Global strain was not computed when more than three LV segments were rejected.

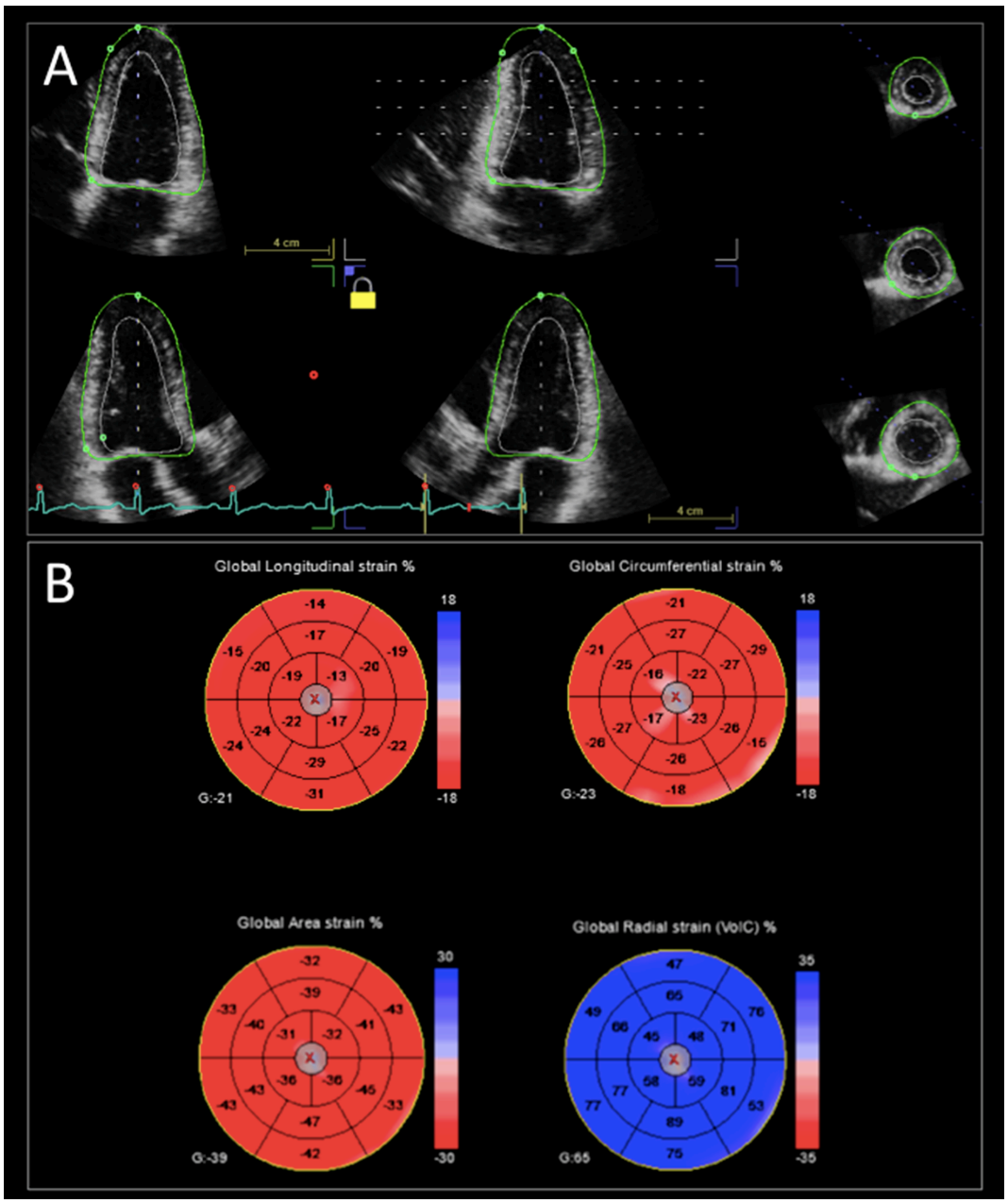

Figure 5.3. Example of LV strain analysis by 3DSTE using 4D AutoLVQ software. The ROI is edited manually by user in order to fit the LV wall thickness (excluding pericardium or atrial myocardium) on three apical views and three short-axes, but also in between them (as shown in the panel marked by a yellow locker)(B) Parametric color-coded (red-negative; blue-positive) display of 3D longitudinal, circumferential, area and radial strain at end-systole obtained from a single dataset. The 17th segment has been automatically rejected by sofware due to excessive drift at end-diastole.

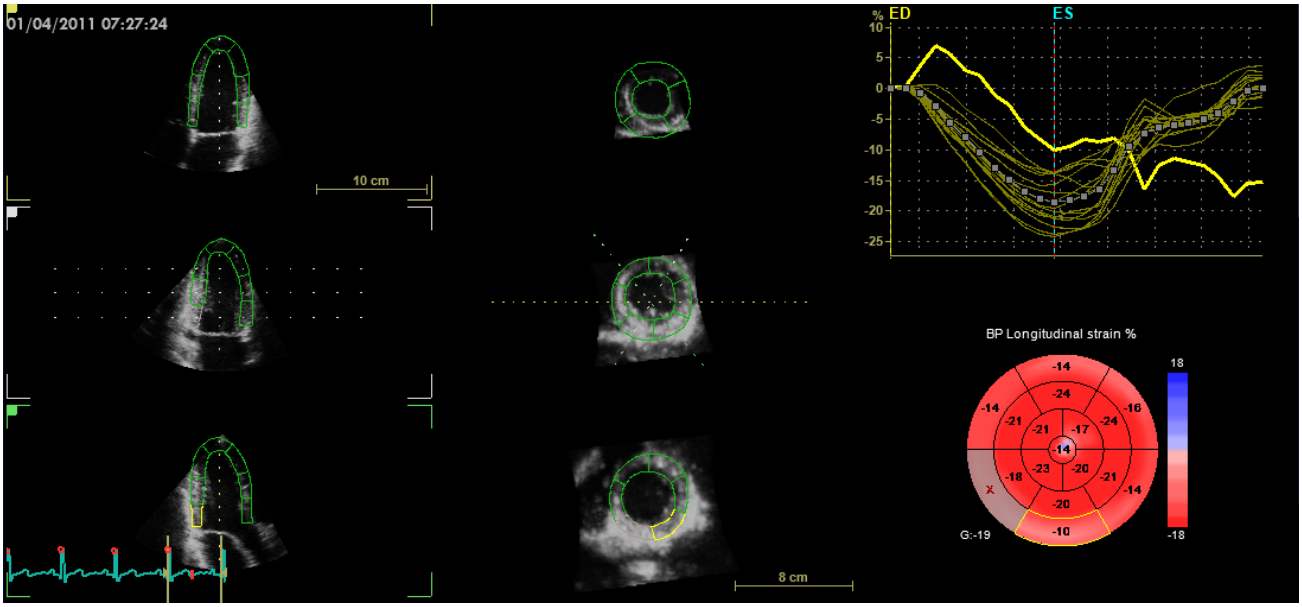

Figure 5.4. Example of poor 3DSTE tracking using 4D AutoLVQ software in the basal LV segments. The "X" mark at the inferior basal segment shows that it was rejected by software due to excessive drift. The strain curve of the posterior basal segment (also rejected) has been highlighted in yellow color to illustrate the aspect suggestive for poor tracking, with positive early systolic strain (stretching), double late peaks in diastole and large end-diastolic drift. Indeed, the peak end-sysolic strain in the posterior basal segment has an abnormally low value (-10%). These poorly tracked segments should be excluded from the computaton of global LV strain.

Chapter 6. Measurement Variability of 3D Strain

6.1. Introduction

The development of myocardial deformation analysis by echocardiography has allowed the quantitation of LV myocardial function at regional and global level, aiming to render its assessment more objective, accurate and reproducible (3). A significant concern raised for 2DSTE method was the inter-vendor inconsistency of LV strain measurements, namely when different 2DSTE platforms provided by various manufacturers have been applied to study the same subjects in the same setting, by the same examiner (64, 65). This discordance in the strain values output could reflect the technical differences of the acquired datasets (spatial and temporal resolution, overall image quality), as well as differences in post-processing (accuracy of myocardial tracking, definition and computation of strain parameters etc). Although research in this area is presently ongoing, this clear evidence has contributed to raise the awareness of inter-vendor differences of strain analysis and has led to joint strategic efforts aiming to achieve standardization of 2DSTE technology (46).

The newly developed 3DSTE based on 3D data sets has the potential to circumvent some of the limitations of 2DSTE in the assessment of LV myocardial deformation, mainly related to its tomographic nature and out-of-plane motion issue. Despite there is a growing interest for applying 3DSTE to measure LV myocardial deformation in various pathological conditions (66-68), data about its inter-vendor consistency in assessing routine patients in clinical setting is lacking. Since various 3DE platforms are now commercially available, this evidence is pivotal for the 3DSTE technique to be implemented in both clinical and research arenas and for an effective interpretation of study findings.

Accordingly, in the present study 2 commercially available 3DSTE platforms have been used to obtain LV 3D strain in the same patient population, in order to: 1. investigate and

compare their intrinsic variability in terms of their intra- and inter-observer reproducibility, as well as at test-retest; 2. assess the inter-vendor consistency of 3D strain measurements; 3. identify some of the sources of inter-vendor inconsistencies, if any. A sub-study of the normative study presented in Chapter 7, comparing the impact of 3DSTE software package applied on the same 3D datasets, has been reported herein to complement for Aim #3.

6.2. Methods

6.2.1. 3D Acquisition. All examinations were performed with commercially available echocardiographic systems (Vivid E9, GE Healthcare, Horten, Norway, and Artida, Toshiba Medical Systems Corporation, Tokyo, Japan) equipped with the 4V and the PST-25SX phased-array matrix transducers, respectively. Two 3D LV full volume datasets were acquired from apical approach by the same experienced examiner, at the beginning and at the end of the standard echocardiographic examination using both echo platforms in sequence and without changing patient position. The wide-angle default settings of each scanner recommended by the two manufacturers (48, 69) was used for all 3D acquisitions. Data sets were digitally stored in raw-data format and exported to separate workstations equipped with the two commercially available softwares (EchoPAC BT11, GE Healthcare, Horten, Norway, and 3D WMT, Toshiba Medical Systems Corporation, Tokyo, Japan) for offline analysis of LV myocardial deformation measurements by 3DSTE, together with LV volumes, mass and ejection fraction quantitation.

6.2.2. 3D Analysis. A single experienced investigator analyzed the data sets in random order, unaware of the identity of the patients. The mean time spent for the analysis with each software was recorded for subsequent comparison.

Data sets acquired with Artida were displayed in a 5-slice mode (Figure 6.1). The LV was automatically divided in 17 3D segments using standard segmentation (19). The

following parameters of global myocardial deformation (Lagrangian strain) were measured: longitudinal (Lε), circumferential (Cε), radial (Rε) and area (Aε) strain. Measurements were performed using a methodology extensively described by Seo et al (7), time-strain curves were displayed with drift compensation of any segmental trace and temporal strain-volume variations presented in a wide variety of color-coded displays. Global strain values for all 3D deformation parameters, as well as the other LV measurements were exported into an Excel spreadsheet for statistical analysis.

Datasets acquired with Vivid E9 were analyzed using the 4D AutoLVQ package (EchoPAC BT 11, GE Vingmed, Horten, Norway), as described in Chapter 5.3.

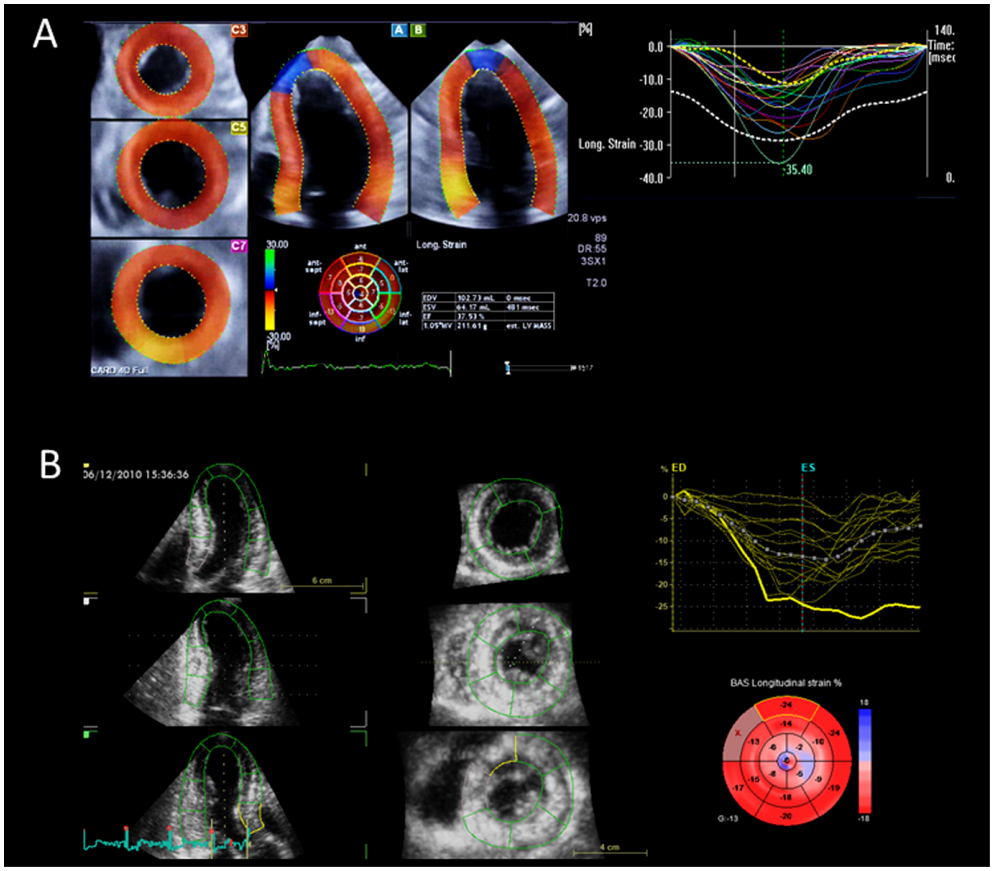

Figure 6.1. Left ventricular data set display with 3D speckle-tracking analysis of myocardial deformation using Artida (Panel A) and Vivid E9 (Panel B) platforms. On the right side of each panel, the derived time-strain curves are shown. Time-strain curves obtained with Artida show a drift compensation (i.e. all curves are forced to reach the zero baseline at end-diastole - upper right panel). This does not apply to the time-strain curves provided by Vivid E9 (lower right panel), a large drift (> 12%) leading to automated segment rejection by this software; a time-strain curve with a significant drift is highlighted in yellow.

6.2.3. Reproducibility assessment

(i) Intra-observer. To explore the impact of the intrinsic variability of each system at repeated measurements, 20 randomly selected LV datasets were analysed by a single observer on two different occasions separated by one week interval.

(ii) Inter-observer. A second observer, blinded to the results obtained by the first observer, independently analyzed the same 20 datasets.

(iii) Test-retest. Variability at sequential evaluations was assessed by comparing 3D strain measurements from two different LV datasets acquired in sequence, at the beginning and at the end of the echo study (around 40 minutes later), obtained in the same patient by the same observer using the same platform.

(iiii) Inter-vendor. The agreement between the 3D strain measurements provided by Artida and Vivid E9 was assessed by comparing the measurements of each strain component obtained with these two systems in the same patient, by the same observer.

6.2.4. Analysis of sources of inter-vendor inconsistency. In order to explore the reasons for the observed differences between the two vendors, various factors have been tested: (a) image quality of 3D datasets, (b) temporal resolution of 3D datasets and (c) the influence of the specific software used for post-processing 3D datasets.

(a) Image quality of 3D datasets was independently scored by two observers by looking at sliced images and was graded as poor (incomplete endocardial border visualization), fair (complete, but suboptimal visualization of endocardial border) and good (clear visualization of the whole endocardial border). In case of disagreement between the two observers, a consensus was reached by joint review. 3D strain measurements obtained from datasets scored as having good quality with both platforms were compared. In addition, the number of LV segments which did not enter within the image sector of the sliced datasets was collected.

(b) To test the influence of dataset temporal resolution on intervendor consistency of 3D strain measurement, in 15 patients an additional data set was acquired with Artida at 30 vps, immediately after the reference one, in order to achieve the same temporal resolution of datasets acquired with Vivid E9.

(c) In a first step, the influence of the software used to analyze the 3D datasets was assessed in 20 patients by comparing 3D strain results obtained by a single observer who analyzed all 3D datasets acquired with both platforms with a vendor-independent software (4D LV Analysis, TomTec Imaging Systems, Unterschleissheim, Germany). In a second step, 3D LV datasets obtained using Vivid E9 from 218 healthy volunteers were analysed with the vendor-specific software (4D AutoLVQ) and then with the vendor-independent TomTec software by the same observer, two months after the first analysis, and the resulting reference values of 3D strain were compared.

Statistical Analysis. Data are summarized as mean±SD, frequencies and ranges, as appropriate. Continuous data were compared with the two-tailed Student *t* test for paired and unpaired data, respectively. For each deformation parameter, the consistency between each pair of measurements obtained with the two platforms was assessed using Bland-Altman statistics, to calculate the systematic bias and limits of agreement, and with Pearson's correlation coefficients. Intra- and inter-observer, as well as test-retest variability were assessed using Bland-Altman statistics (coefficient of repeatability, CR) and intraclass correlation (intraclass correlation coefficient, ICC). Comparison of Pearson's correlation coefficients was performed using the Z score statistic. A probability value <0.05 was considered statistically significant. Data analysis was performed using SPSS version 15.0 (SPSS Inc., Chicago, IL, USA) and MedCalc for Windows, 11.4.3.0 release (Mariakerke, Belgium) statistical software.

6.3. Results

6.3.1. Feasibility

Feasibility of 3D LV data set acquisition was 85% (60 out of 71 attempted) and the final study group comprised 60 pts with a wide range of age and body surface areas (Table 6.1), LV volumes and ejection fractions (Table 6.2).

Table 6.1. Demographic and clinical characteristics of the study patients.

Variables	**N = 60 pts**
Males (%)	41 (68%)
Age (yrs)	58±15 (range 30-87)
Body surface area (m^2)	1.85±0.18
Heart rate (bpm)	64±12
Systolic blood pressure (mmHg)	120±18
Diastolic blood pressure (mmHg)	74±11
Clinical indications for echo study	
Ischemic heart disease	32 (53%)
Valvular heart disease	9 (15%)
Normal	5 (8%)
Cardiomyopathies	4 (7%)
Arterial hypertension	2 (3%)
Congenital heart disease	2 (3%)
Other	6 (10%)

Average heart rate was similar between datasets acquired with Artida and Vivid E9 (Table 6.2). Conversely, dataset volume size was significantly lower and temporal resolution was significantly higher for those acquired with Vivid E9. Quality of sliced images obtained from the 3D datasets was significantly better with Vivid E9 (Table 6.2).

Table 6.2. Echocardiographic characteristics of study patients.

Echocardiographic Variables	**Artida**	**Vivid E9**	**p value**
Data set size (degrees)	90° x 90° (default)	60° x 60° (large)	
Data set volume rate (vps)	21 ± 1	30 ± 3	< 0.001
Heart rate (bpm)	65 ± 14	65 ± 13	NS
Image Quality			0.01
Good, n (%)	30 (50)	38 (64)	
Fair, n (%)	17 (29)	20 (33)	
Poor, n (%)	13(21)	6 (3)	
Rejected segments (%)	0 (0)	64 (6.3)	< 0.0001
End-Diastolic Volume (ml)	121 ± 31 (range 52-197)	127 ± 35 (range 74-205)	NS
End-systolic Volume (ml)	63 ± 30 (range 22-161)	63 ± 32 (range 22-165)	NS
Ejection Fraction (%)	50 ± 13 (range 17-65)	53 ± 13 (range 19-70)	NS

However, the larger volume size obtained by Artida allowed to achieve a more complete visualization of LV segments using multi-slice display: incomplete visualization (i.e. 1 to 3 missing apical segments) was 28% with Vivid E9 and 2% with Artida ($p<0.0001$).

All segments from all available datasets (100%) were analysed with the 3D WMT software. Conversely, two patients with more than three LV segments rejected by automatic tracking using 4DAutoLVQ software by EchoPac were excluded because inadequate for global strain determination. Sixty-four LV segments (6.3%) from the remaining 58 patients were rejected because of significant drift of the strain traces. Inadequately tracked segments were more likely located at the basal level of the LV with a gradient towards mid-ventricle and apical regions (Figure 6.2).

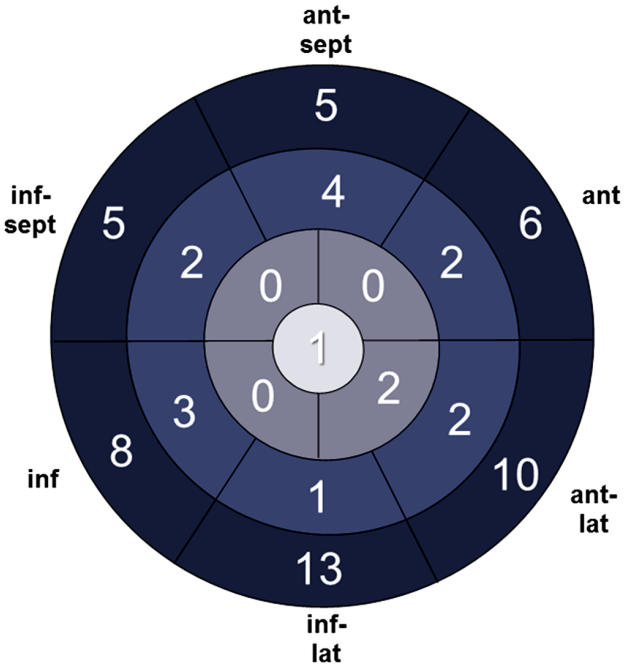

Figure 6.2. Bull's eye display showing the location of the left ventricular rejected segments by the EchoPAC software. A significantly larger number of patients had inadequately tracked segments at the basal LV region, with a basal-apical gradient (numbers represent patients).

The entire time required to analyse the 3D datasets and obtain the final results was not statistically different between the two platforms (3 min 58 sec ± 36 sec and 3 min 44 sec ±29 sec for Artida and Vivid E9, respectively; p= NS).

6.3.2. Observer and test-retest variability

Reproducibility of the strain measurements obtained with the two ultrasound systems are summarized in Table 6.3. Lε and Cε were found to be comparably and highly reproducible with both vendors (Table 6.3).

Table 6.3. Reproducibillity of 3D strain measurements obtained with Artida and Vivid E9.

(n=20 pts)	**Artida**		**Vivid E9**	
Intraobserver Variability	Bias±CR	ICC	Bias±CR	ICC
Peak Lε (%)	0.2 ± 3.4	0.95	0.5 ± 3.5	0.94
Peak Cε (%)	0.5 ± 4.2#	0.97	0.5 ± 2.2	0.98
Peak Rε (%)	0.5 ± 15.6#	0.56*	1.4 ± 7.5	0.97
Peak Aε (%)	0.6 ± 3.8	0.99	0.6 ± 3.4	0.98
Interobserver Variability				
Peak Lε (%)	0.4 ± 3.0	0.91	1.0 ± 3.8	0.89
Peak Cε (%)	0.4 ± 10.4#	0.84	1.1 ± 3.9	0.91
Peak Rε (%)	4.8 ± 22.2#	0.44*	3.6 ± 8.0	0.90
Peak Aε (%)	0.3 ± 10.8#	0.92	1.7 ± 4.1	0.96
Test-retest Variability				
Peak Lε (%)	0.6 ± 5.4	0.84	0.5 ± 3.7	0.94
Peak Cε (%)	0.2 ± 9.6#	0.82^	0.0 ± 3.7	0.95
Peak Rε (%)	1.5 ± 14.8#	0.66*	0.9 ± 7.7	0.96
Peak Aε (%)	0.3 ± 8.8#	0.91	0.5 ± 4.1	0.98

*p<0.0001; #p<0.001; ^p<0.05 for comparisons of coefficients of repeatability and of intraclass correlations
Abbreviations: Aε, area strain; Cε, circumferential strain; ICC, intra-class correlation; Lε, longitudinal strain; Rε, radial strain.
Bias represents absolute (i.e. strain-percent) values.

Among all strain components, Rε was the least reproducible parameter with both systems. Overall, reproducibility of the different strain components was significantly better with Vivid E9 than with Artida (Table 6.3).

6.3.3. Inter-vendor variability

For each vendor, there was no significant difference between global peak strain values and global strain measured at end-systole (Table 6.4).

Table 6.4. Results of global 3D strain measurements and comparison between Artida and Vivid E9 platforms.

Global ε (%)(n = 58)	**Artida**	**Vivid E9**	**Bias**	**LOA**	**ICC**
Longitudinal					
End-systolic	-13.5 ± 4.5	-14.6 ± 4.7#	1.1	6.4 to -4.2	0.830
Peak	-14.1 ± 4.2	-15.2 ± 4.8#	1.1	6.4 to -4.2	0.820
Circumferential					
End-systolic	-22.7 ± 8.3	-14.9 ± 4.6*	-7.8	2.7 to -18.3	0.683
Peak	-22.8 ± 8.3	-15.8 ± 4.9*	-7.0	2.5 to -16.4	0.750
Radial					
End-systolic	16.4 ± 9.1	40.5 ± 14.4*	-24.1	0.2 to 48.4	0.522
Peak	17.9 ± 8.4	42.1 ± 15.1*	-24.2	1.5 to 49.9	0.504
Area strain					
End-systolic	-33.7 ± 10.4	-26.4 ± 7.6*	-7.3	3.1 to -17.8	0.830
Peak	-33.8 ± 10.4	-27.2 ± 7.9*	-6.6	3.4 to -16.6	0.848

*p<0.001 and #p<0.01
Abbreviations: ε, strain; ICC, intra-class correlation; LOA, limits of agreement. Bias and LOA represent absolute (i.e. strain-percent) values.

Artida platform produced significantly higher absolute values of both Cε and Aε than Vivid E9 (Table 6.4). Lε and Rε obtained with Artida were significantly lower than those measured using Vivid E9 platform (Table 6.4, Figure 6.3). Among the various strain measurements, Lε showed the smallest bias and the narrowest limits of agreement between the two platforms. Conversely, Rε showed the largest bias and the widest limits of limits of agreement between vendors, as well as the poorest correlation among all strain components (Table 6.4).

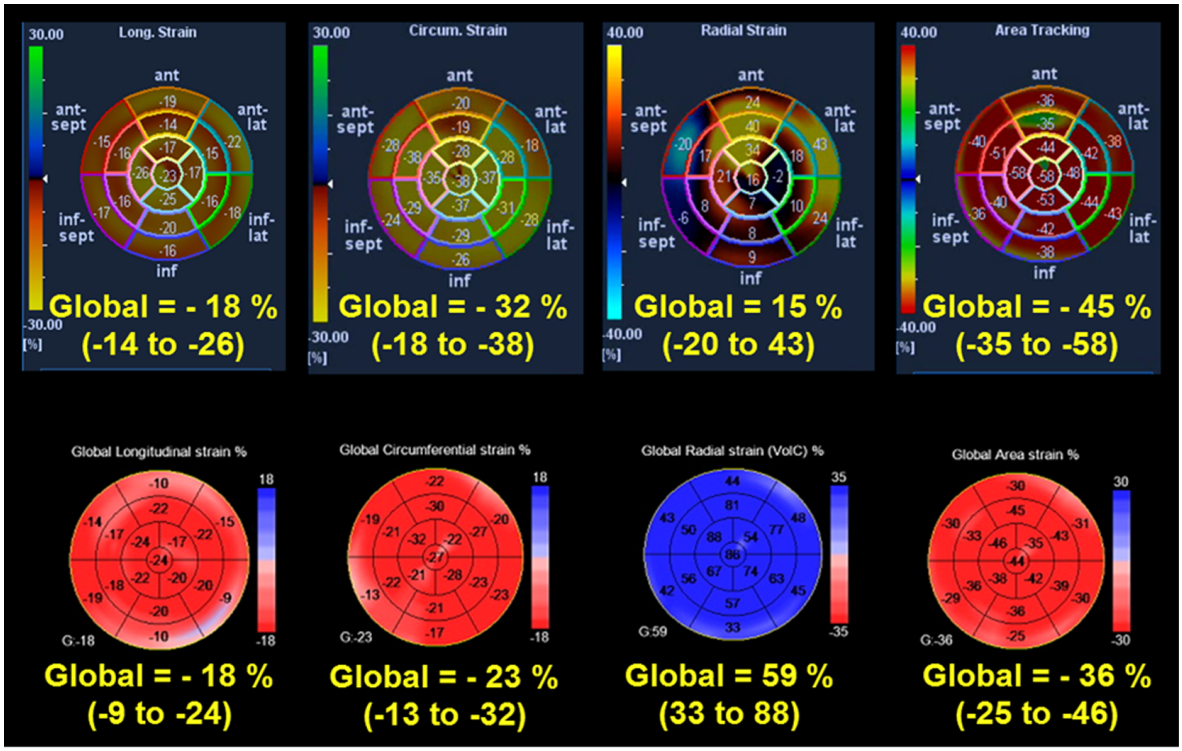

Figure 6.3. Comparison of longitudinal, circumferential, radial and area strain obtained from the same patient using Artida (upper panels) and Vivid E9 (lower panels). Only the global longitudinal component of the strain was comparable between the two platforms. However, looking at segmental values, also the longitudinal component of the strain showed significant differences between the two platforms. Notice that the bull's eyes in the lower panels are rotated clockwise by 60° and the segments at 12 o'clock represent the anterior septum.

6.3.4. Sources of inter-vendor inconsistency

Data sets obtained from 22 patients were graded as "good quality" with both software packages and underwent a subset analysis to assess inter-vendor consistency of 3D strain

measurements (Table 6.5). Selecting only the data sets with good image quality for analysis showed a trend towards an improved inter-vendor correlation of strain measurements, but it did not change the main results of the analysis performed on the whole study population. Apart Lε, all strain components differed significantly between the two ultrasound systems and the extent of biases and limits of agreement were comparable between the subset of patients with good image quality and the whole study population.

Table 6.5. Results of global 3D strain measurements and comparison between Artida and Vivid E9 platforms in a subset of 22 patients with good quality 3D data sets.

Global ε (%) (N = 22)	**Artida**	**Vivid E9**	**Bias**	**LOA**	**R**
Longitudinal					
End-systolic	-13.8 ± 4.6	-14.9 ± 4.7#	1.0	-3.1 to 5.2	0.888*
Peak	-14.1 ± 4.5	-15.6 ± 4.9#	1.5	-2.9to 5.9	0.886*
Circumferential					
End-systolic	-22.8 ± 8.7	-15.4 ± 5.5*	-7.4	-15.9 to 1.1	0.905*
Peak	-22.9 ± 8.7	-16.3 ± 5.7*	-6.6	-14.1 to 0.9	0.938*
Radial					
End-systolic	16.1 ± 9.4	42.2 ± 15.8*	-26.0	1.1 to 53,2	0.486#
Peak	17.1 ± 8.8	44.3 ± 16.6*	-27.2	0.6 to 54.9	0.518#
Area					
End-systolic	-34.1 ± 10.9	-27.1 ± 8.2#	-7.0	2.5 to -16.6	0.905*
Peak	-34.2 ± 10.9	-28.2 ± 8.6#	-6.0	2.5 to -14.5	0.928*

**p<0.001,#p<0.05.*

Abbreviations: ε, strain; LOA, limits of agreement.

Bias and LOA represents absolute (i.e. strain-percent) values.

To assess the impact of temporal resolution on 3DSTE deformation measurements, we compared 3D strain measurements obtained from Artida data sets acquired at 20 vps (default settings) and at 30 vps (a volume rate similar to the one reached with Vivid E9). All 4 strain components showed no significant difference in their values between data sets acquired at 20 vps and those acquired at 30 vps (Table 6.6).

Table 6.6. Comparison of global 3D strain measurements (peak systolic) from datasets acquired at different temporal resolution with Artida.

3D strain parameter (N=14)	**30 vps**	**20 vps**	**Bias ± SD**	**ICC**	**t-test**
Peak Lε (%)	-14.3 ± 3.9	-12.9 ± 3.4	1.4 ± 2.0	0.852	0.52
Peak Cε (%)	-22.5 ± 5.5	-22.4 ± 4.4	0.1 ± 2.7	0.847	0.796
Peak Rε (%)	24.4 ± 8.0	21.2 ± 4.4	-3.2 ± 7.8	0.246	0.264
Peak Aε (%)	-33.8 ± 7.2	-33.1 ± 6.3	0.7 ± 3.1	0.892	0.423

Abbreviations as in Table 6.3. Bias represents absolute (i.e. strain-percent) values.

When a vendor-independent software was used to assess Lε in order to eliminate the potential variability due to vendor-specific analysis softwares, we found a significant difference between Lε values obtained examining the data set acquired using Artida and Vivid E9 (-14.3±5.3% and -12.9±4.3%, respectively, p= 0.0001, bias=-1.4, LOA=4.9±0.1%).

When the same vendor-independent TomTec software was used to analyze 3D LV datasets from healthy subjects, LV strain parameters were significantly different then those when obtained by vendor-specific (4D AutoLVQ) softwares (Table 6.7). The vendor-specific software measured systematically lower values of strain than the vendor-independent software, with 3DLε showing the smallest inter-vendor variability among all strain parameters. The measurements provided by the two software packages for 3DRε were not on

the same scale (i.e. median 53% by 4D AutoLVQ versus 98% by 4D LV function), and therefore have not been compared.

Table 6.7. Reference values for left ventricular strain parameters by three-dimensional speckle-tracking: comparison between vendor-specific and vendor-independent softwares.

	All (n=218)		**Women (n=125)**		**Men (n=93)**	
	4D AutoLVQ	**4D LV**	**4D AutoLVQ**	**4D LV function**	**4D AutoLVQ**	**4D LV Function**
3DLε (%)						
Reference range	**-19** (-21, -17)	**-22** (-20, -23)	**-20** (-21, -18)	**-22** (-21, -24)	**-18** (-20, -17)	**-21** (-19, -23)
Normal limit	**-15**	**-18**	**-16**	**-18**	**-15**	**-17**
3DCε (%)						
Reference range	**-19** (-21, -17)	**-34** (-32,-37)	**-19** (-21, -17)	**-35** (-32, -37)	**-19** (-21, -17)	**-34** (-32, -36)
Normal limit	**-15**	**-29**	**-15**	**-30**	**-15**	**-28**
3DAε or 3D						
Reference range	**-33** (-36, -31)	**-37** (-39, -35)	**-35** (-36, -32)	**-38** (-39, -35)	**-33** (-36, -31)	**-37** (-39, -34)
Normal limit	**-28**	**-32**	**-28**	**-33**	**-25**	**-32**

Data are expressed as median (1st, 3rd quartiles). Normal limit is expressed as 95th percentile.

Abbreviations: 3D strain (4D LV function); 3DAε, 3D area strain (4D AutoLVQ); 3DCε, circumferential strain; 3DLε, longitudinal strain.

All comparisons between 4D AutoLVQ and 4D LV function are significant at $p<0.001$.

6.4. Discussion

The main results of our study can be summarized as follows: (i) the inter-vendor agreement of Rε, Cε and Aε measured with Artida and Vivid E9 was poor; (ii) only Lε was comparable between the two vendors and also with values obtained with TomTec® software; (iii) the intrinsic variability of the different strain components obtained with the two systems tested was relatively low (except for Rε), but varied significantly among strain parameters and between the two vendors; (iv) increasing data set temporal resolution from 20 vps to 30 vps and image quality do not seem to impact significantly on inter-vendor agreement of strain

measurements; and (v) the use of a vendor-independent analysis software did not solve the inconsistency of 3D strain measurements in both normal and abnormal LVs.

The development of the 3DSTE technique allows to detect in a fast and comprehensive manner all the components (vectorial and rotational) of the myocardial deformation, without the intrinsic limitations of previous technologies based on tissue velocity imaging or two-dimensional ST (57, 70). However, since an accurate and reproducible assessment of LV myocardial function is pivotal for both clinical and research purposes, 3D used for quantitation of myocardial deformation should be evaluated as rigorously as any therapeutic intervention before starting its systematic application in everyday clinical practice (2). For these reasons, along with the accuracy that should be determined by comparing measurements with those performed with a reference technique, reproducibility (represented by the reciprocal of the variability of measurements made by a single observer in different occasions - intra-observer variability - or by different observers - inter-observer variability) and repeatability (the reciprocal of variability of measurements made on the same patients, in the same conditions in two different occasions – test-retest variability, or made using different systems and analysis softwares - inter-vendor variability) are crucial factors in determining the clinical relevance and reliability of any diagnostic technique.

To our knowledge, this is the first study comparing intervendor consistency and intrinsic variability of 3D strain measurements obtained with two commercially available echocardiographic platforms in patients with a wide range of LV size and function. Gayat et al. (71) compared strain values measured on data sets acquired from 30 subjects with normal LV function using Artida and iE33 (Philips Healthcare, Andover, Massachusetts, USA) and analyzed them using 3DWMT and 4D LV function software packages. They found that inter-technique agreement was poor (it improved when data sets acquired with different platforms were analyzed using a vendor-independent software - i.e. 4D LV function), and that the

discordance level was beyond the intrinsic measurement variability of any of the tested combinations of software and hardware. However, they analyzed only subjects with normal LV function and measured only longitudinal and circumferential components of strain. Finally, they did not assess an important parameter to consider when a technique has to be used to follow patients, which is the test-retest variability of measurements.

In our study population, 3DSTE was reasonably feasible and measurements were reproducible (except for Rε, Table 6.3) with both echocardiographic platforms. However, our data show that, among the various strain components, only the Lε (despite being significantly different between the two systems) was at some extent comparable between Artida and Vivid E9. Cε and Aε showed mean differences between the two platforms around 30% and 23%, respectively. Rε values obtained with Artida and Vivid E9 were so different (absolute values of 17% vs. 44%, respectively), that it seems as if they were measured with different scales. However, Rε obtained with the two systems used in our study seems to measure different entities, since intraclass correlation between Rε measured with Artida and Vivid E9 was only moderate. This is mainly due to the different ways used by the two platforms to compute Rε. Rε by 3DWMT is estimated by both endocardial and epicardial speckle tracking, so that Rε measurements are highly dependent on image quality compared with those of the Lε and Cε components, which are estimated only by endocardial speckle data (50). This translates in a lower accuracy and reproducibility of Rε with this platform in comparison with Cε and Lε (7, 50), consistent with our data. Conversely, EchoPAC does not actually measure the Rε, but it estimates it from Aε, assuming that each LV segment maintains a constant volume throughout cardiac cycle. This explains the high reproducibility and repeatability of Rε calculations obtained with EchoPAC.

Noticeably, the inter-vendor biases for all strain measurements were significantly larger than the intrinsic technique variability of each ultrasound system, as detected by the reproducibility and repeatability analyses.

Trying to find out whether any technical reason could explain such different measurements, we found that neither temporal resolution (at least in the range of volume rates tested in our study, i.e. from 20 vps to 30 vps), nor image quality have a significant impact on the different measurements obtained from the two tested platforms. However, it should be acknowledged that data sets with poor image quality were excluded from our study and that, given the high intrinsic variability of 3D strain estimates, the impact of the remaining range of image quality could have been too small to be detected with the size of our study population. Moreover, Cε and Aε by Artida showed significantly higher amplitudes than those obtained by VividE9, while Rε by Artida was significantly lower than the one obtained by VividE9. Even if some differences can be explained by the fact that 3D WMT tracks mainly speckles located in the endocardial layer and global strains are calculated as mathematical averages of all segmental values, while EchoPAC tracks speckles across the whole wall thickness and global strains are calculated as weighted spatial averaging of segmental values, these seem to be only part of the problem.

On the other hand, this is confirmed by the fact that Lε measurements provided by the two vendors are quite close. However, we have found that two data sets acquired in the same patients during the same echocardiographic study by Artida and Vivid E9 and analyzed using a single vendor-independent software (i.e. 4D LV function) provide Lε measurements which are discordant beyond the intrinsic variability of the respective ultrasound systems. This is likely linked to the 3D dataset characteristics, which differ from vendor to vendor. The ability of a given software package to accurately track wall motion may be affected by these 3D dataset characteristics. Our study in healthy volunteers showed that specific reference ranges

should be used when interpreting 3D strain values obtained by various 3DSTE systems and software packages.

Our study confirms previous reports that the 3DSTE software used for myocardial deformation analysis may induce *per se* a major variability in the measurements (59, 71). We have provided the normality values and limits of normality of the various 3D strain components both for the vendor-specific, as well as for the vendor-independent 3DSTE softwares, the latter being useful in a multi-vendor setting to standardize the LV 3DSTE analysis on datasets acquired by different 3DE scanners.

Study limitations. First, our study population was relatively limited. However, we enrolled a two-fold higher number of patients than in similar papers addressing the issue of inter-vendor consistency of strain measurements (64, 71), and differently from the previous studies we included patients with impaired LV function. Second, dataset temporal resolution and volume size differed significantly between the tested ultrasound systems. However, we used standard machine settings on purpose in order to assess inter-vendor agreement of measurements performed with the systems settings used in the clinical routine. Moreover, we have also shown that strain measurements obtained with Artida at standard settings were similar to those obtained at higher volume rates which were similar to those obtained with Vivid E9. Third, image quality was judged visually and not assessed on an objective scale. Thus, the scoring of the datasets in term of image quality might have been inaccurate. However, we are not aware of any accepted objective grading system for quality of 3D images.

Conclusions. Since peak strain values obtained from different ultrasound systems are not comparable, clinicians willing to translate 3DSTE data from the literature into clinical decision making should take into account the specific system used in their echocardiographic laboratory and reference values of the strain components should be developed for each ultrasound system. Moreover, clinicians who want to use myocardial deformation parameters

in longitudinal studies should ensure that baseline and follow-up acquisitions are obtained using the same platform. Since these are major limitations to the implementation of myocardial deformation parameters in the clinical practice and to the spread of the technique across echocardiographic laboratories, manufacturers are urged to take initiatives in order to overcome those variations and provide a common standard of two-dimensional and 3D strain measurement across vendors.

Chapter 7. Normative Values of LV Myocardial Strain Measurements Using 3D Speckle-Tracking Echocardiography

7.1. Introduction.

Deformation imaging by 3D speckle-tracking (3DSTE) has emerged as a promising quantitative tool for left ventricular (LV) myocardial function analysis, allowing a fast and comprehensive evaluation of all LV segments from a single 3D dataset. Despite researchers are increasingly employing 3DSTE to study various pathologic conditions (27), the normal pattern of LV myocardial deformation in healthy adults, as characterized by 3DSTE, and possible influence of various factors (e.g. demographic, hemodynamic, cardiac or technical) on LV 3D strain values remain unknown.

As described in the previous chapter, a major issue of 3DSTE strain is the large inter-vendor variability of LV myocardial deformation parameters among the various commercially-available software packages (59, 71), which adversely affects their implementation in the clinical routine. Therefore, the definition of specific normative values for each of the available 3DSTE softwares becomes crucial for a reliable application and interpretation of 3D strain in research, as well as in the clinical arena. So far, no study was specifically aimed to establish the normative data of LV 3D strain parameters, nor to identify factors that contribute to their variation in healthy subjects.

Accordingly, this prospective study was designed to:

1) identify the normative values for LV myocardial 3D strain parameters using a commercially available 3DSTE platform;

2) analyze the relationship of LV 3D strain parameters with demographic, hemodynamic, cardiac and technical factors;

3) compare reference values of LV strain obtained by a vendor-specific 3DSTE software with those measured by both 2DSTE and a vendor-independent 3DSTE software in the same population.

7.2. Methods

Study population. The criteria of enrolment in the normative study cohort is summarized in Figure 7.1.

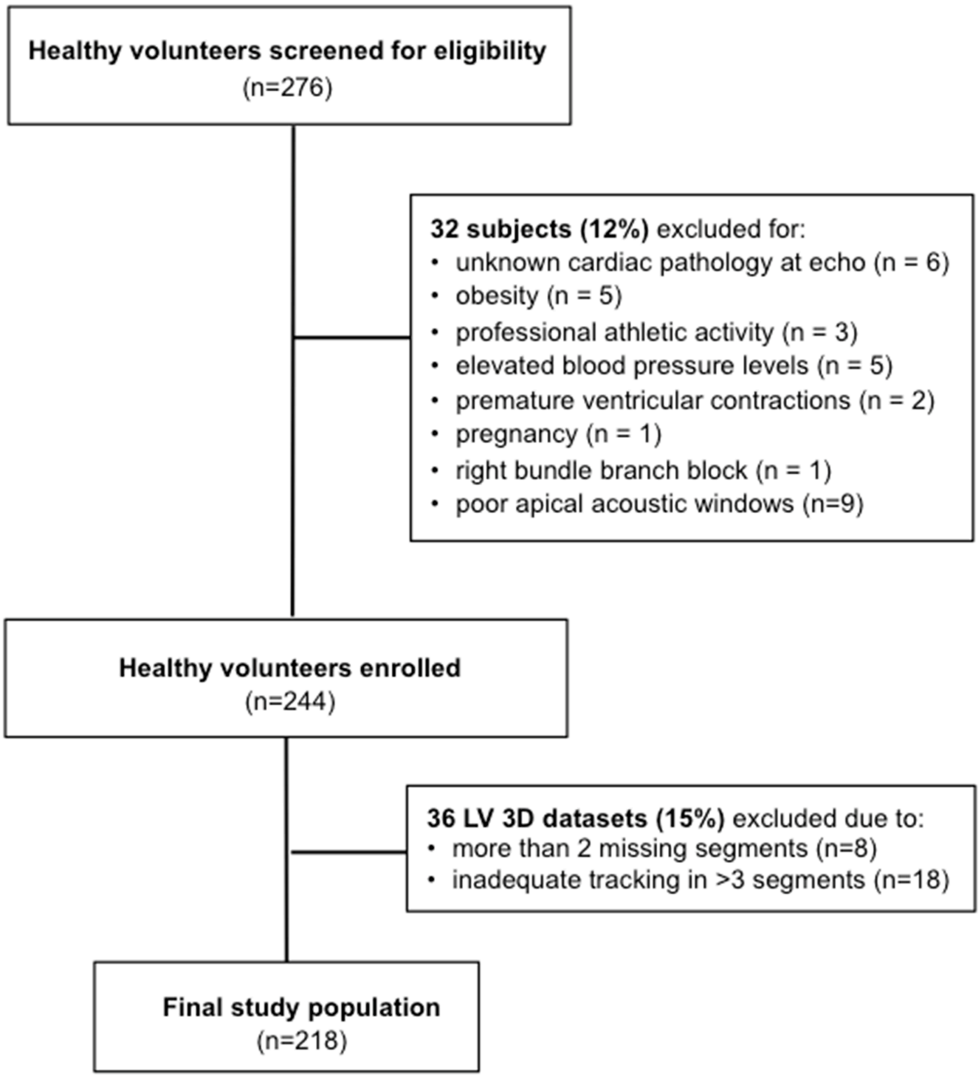

Figure 7.1. Flowchart showing the enrolment of healthy subjects in the present study.

Echocardiographic datasets were obtained using Vivid E9 (GE Vingmed Ultrasound, Norway) equipped with M5S and 4V probes for 2D and 3D acquisitions, respectively. Acquisition protocol included dedicated 2D datasets for measuring the LV myocardial strain parameters by 2DSTE (3) using Q-Analysis package (EchoPac BT12, GE Vingmed Ultrasound, Norway). Peak global 2D circumferential (2DCε) and radial (2DRε) strain were measured from the parasternal short-axis view at the midpapillary muscle level, while peak global 2D longitudinal (2DLε) strain was computed from the three apical LV views (72). When more than two LV segments were inadequately tracked in one view, global strain parameters by 2DSTE were not computed.

A detailed description of 3D datasets acquisition protocol and of 3DSTE analysis applied in this study has been presented in Chapter 5. 3D LV full volume datasets were acquired in all subjects, taking care to avoid any artifacts and to include all LV segments in the dataset. The image quality of 3D datasets was judged subjectively, considering the signal-to-noise ratio, the blood-tissue contrast and the completeness of LV wall visualization, and was cathegorized as either optimal or suboptimal. 3D datasets were analysed offline with 4D AutoLVQ (EchoPac BT12 and 13, GE Vingmed Ultrasound, Norway) by a single experienced researcher (63). 3D LV volumes, ejection fraction, sphericity and mass in this healthy cohort have been reported in a separate publication (73). For 3DSTE analysis, the region of interest (ROI) was set across the entire LV wall. The quality of segmental tracking was validated by the software, as well as by the operator (Figure 7.2). When more than three LV segments were inadequately tracked, the global strain values were not computed. The software provided four strain components: longitudinal (3DLε), circumferential (3DCε), radial (3DRε) and area strain (3DAε).

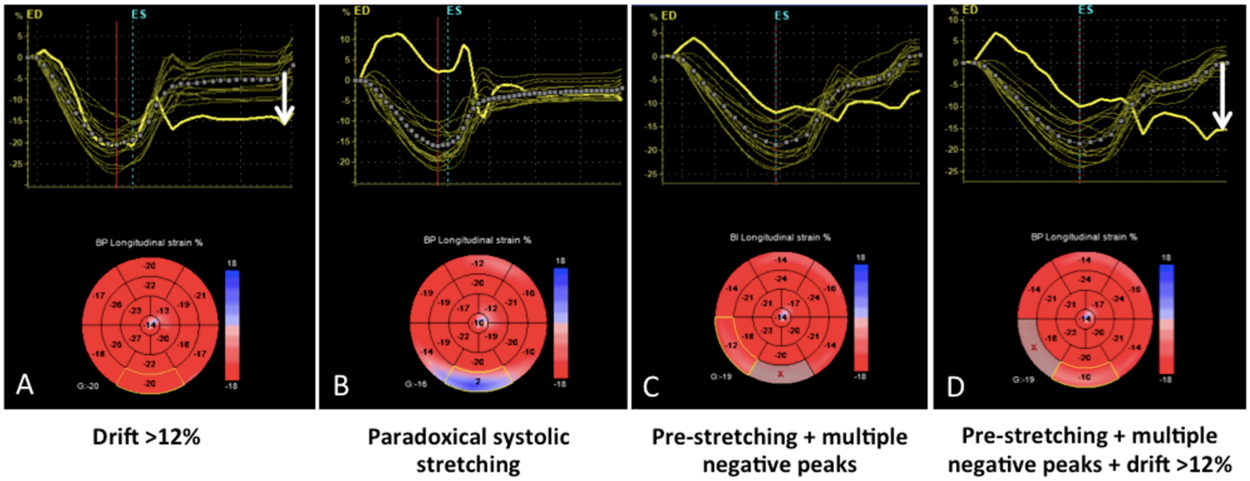

Figure 7.2. **Different examples of poor tracking in basal segments**. These examples illustrate the validation of 3D strain analysis based on several indicators of tracking quality. In A and D, the basal segments corresponding to the curves highlighted in yellow have been automatically excluded by the software due to excessive drift. Examples B and C show other cases in which the automated drift-based validation may fail to detect poor tracking, and where user's input is necessary to manually exclude the respective segments.

Statistical analysis. Normal distribution of variables and uniform distribution of subjects per age decade were assessed using the Kolmogorov – Smirnov test. Continuous variables were summarized as mean + SD or as median (first, third quartiles) when reporting reference ranges, while scalar variables were reported as percentages. The upper or lower limits of each strain parameter were defined as the 95th or, where appropriate, 5th percentile, respectively. Differences between values in men and women were assessed using the unpaired t-test for normally distributed variables, or the Mann–Whitney U-test otherwise. LV strain values obtained with the two softwares from the same subject were compared using the paired Student's t-test. Pearson's correlation was used to analyse the relationships between strain parameters and demographic, cardiac and technical variables. A stepwise multivariable linear regression analysis was used to assess the association of each 3D strain parameter with the following covariates: age, gender, weight, height, systolic blood pressure, temporal resolution and image quality (having $p<0.10$ in individual models). The association of echocardiographic LV parameters (LV 3D volumes and mass) with 3D strain indices was also tested in models

adjusting for age, gender, image quality and temporal resolution. All analyses were performed using SPSS 21.0 (SPSS Inc, Chicago, IL, USA). Differences among variables were considered significant at $p<0.05$.

7.3. Results.

The final study population comprised 218 subjects (Figure 7.1), whose characteristics are presented in Table 7.1.

Table 7.1. Clinical and demographic characteristics of the study population.

	All (n=218)	**Women** (n=125)	**Men** (n=93)	**p-value***
Age (years)	44±14	44±14	44±14	0.87
Height (cm)	170±9	165±7	177±7	<0.001
Weight (kg)	68±11	61±8	76±9	<0.001
Body mass index (kg/m^2)	23.3±3.0	22.5±2.9	24.2±2.9	<0.001
Body surface area (m^2)	1.78±0.18	1.66±0.12	1.93±0.13	<0.001
Systolic blood pressure (mmHg)	122±15	117±14	128±13	<0.001
Diastolic blood pressure (mmHg)	73±8	71±8	76±7	<0.001
Heart rate (bpm)	67±10	67±10	67±11	0.34
LV end-diastolic volume (ml/m^2)	59±10	56±8	63±11	<0.001
LV end-systolic volume (ml/m^2)	22±5	20±4	24±5	<0.001
LV stroke volume (ml/m^2)	37±6	36±6	39±7	0.001
LV ejection fraction (%)	63±4	65±4	62±4	<0.001
LV mass (g/m^2)	75±9	74±8	77±10	0.005

Data are expressed as mean ± standard deviation. *Women vs. Men comparison

Abbreviations: bpm, beats per minute; LV, left ventricular.

The age of subjects ranged between 18 and 76 years, and at least 37 subjects per age decade were included in the study (mean 47±9 subjects/age decade). Women were slightly prevalent (57%). Male gender was associated with higher blood pressure, larger body size, LV volumes and mass, and lower ejection fraction than women (Table 7.1).

Temporal resolution of 3D datasets was 35±7 (range 27-67) volumes/sec, while for 2D datasets, it was 73±5 (range 54-80) frames/sec. Image quality was scored as optimal in 74%, and suboptimal in 26% of subjects. There were 43% of 3D datasets having 1-2 LV segments incompletely visualized throughout the cardiac cycle, 90% of them being in the apical region. Overall feasibility of global 3DSTE analysis by 4D AutoLVQ was 89%. Feasibility of segmental 3DSTE analysis is presented in Figure 7.3. A large inter-segment variability in tracking quality can be observed, ranging from 100% at mid-ventricular level to 46% at basal infero-lateral level.

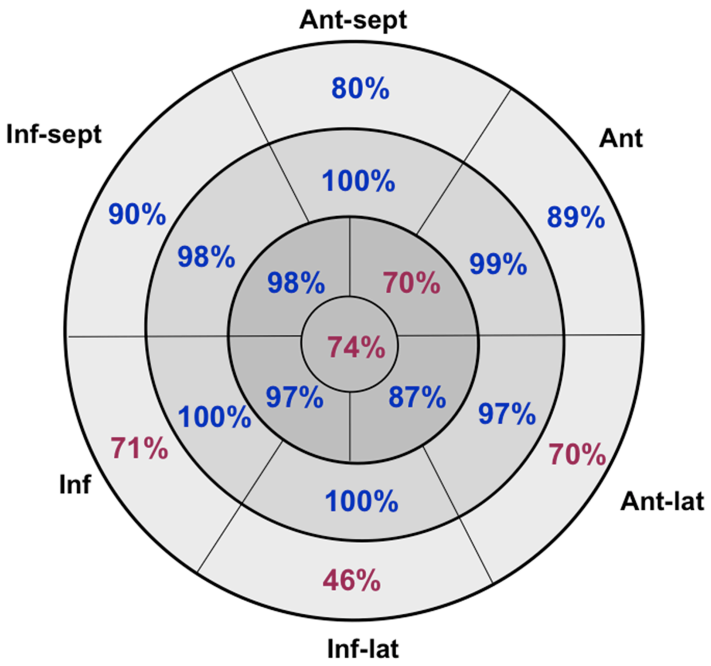

Figure 7.3. Feasibility of 3D speckle-tracking analysis in healthy subjects. Segmental feasibility is presented separately for each of the 17 segments and calculated as the percentage of segments included in the final analysis after rejecting those with inadequate tracking or incomplete visualisation. Segments excluded from global 3D strain computation in more than 25% of datasets are highlighted in red.

7.3.1. Reference values of LV 3D strain parameters. Reference values (limits of normality) for myocardial deformation by 3DSTE were: -19% (-15%) for 3DLε and 3DCε, -33% (-28%) for 3DAε and 53% (40%) for 3DRε (Table 7.2[1]).

Table 7.2. Reference ranges of left ventricular global strain parameters by age and gender obtained by three-dimensional speckle-tracking echocardiography (4D AutoLVQ software) in the study population.

		All		Women		Men		p-value[†]
		Normal Range	Limits of normality	Normal Range	Limits of normality	Normal Range	Limits of normality	
3DLε (%)	**All (n=218)**	**-19 (-21, -17)**	**-15**	**-20 (-21,-18)**	**-16**	**-18 (-20, -17)**	**-15**	**<0.001**
	18-29 y (n=38)	-20 (-21, -19)	-17	-20 (-21, -19)	-17	-20 (-21, -19)	-17	0.486
	30-39 y (n=46)	-19 (-21, -18)	-16	-20 (-21, -19)	-17	-18 (-20, -17)	-16	0.019
	40-49 y (n=57)	-19 (-22, -18)	-15	-21 (-22, -18)	-15	-18 (-20, -17)	-14	0.005
	50-59 y (n=34)	-18 (-21, -16)	-15	-20 (-20, -17)	-15	-18 (-19, -16)	-14	0.002
	≥60 y (n=43)	-18 (-20, -17)	-14	-19 (-20, -17)	-15	-17 (-19, -16)	-14	0.013
3DCε (%)	**All (n=218)**	**-19 (-21, -17)**	**-15**	**-19 (-21, -17)**	**-15**	**-19 (-21, -17)**	**-15**	**0.805**
	18-29 y (n=38)	-18 (-19, -16)	-15	-18 (-19, -16)	-14	-18 (-20, -16)	-14	0.179
	30-39 y (n=46)	-18 (-20, -17)	-14	-18 (-19, -16)	-14	-18 (-20, -17)	-15	0.047
	40-49 y (n=57)	-19 (-21, -17)	-15	-20 (-21, -18)	-15	-19 (-21, -16)	-15	0.329
	50-59 y (n=34)	-19 (-21, -16)	-15	-20 (-22, -16)	-15	-19 (-20, -16)	-15	0.409
	≥60 y (n=43)	-20 (-22, -19)	-16	-20 (-22, -19)	-16	-20 (-22, -19)	-16	0.661
3DRε (%)	**All (n=218)**	**53 (48-59)**	**40***	**54 (49, 60)**	**40***	**52 (48, 59)**	**39***	**0.015**
	18-29 y (n=38)	54 (49, 58)	41*	53 (48, 57)	40*	55 (50, 60)	42*	0.217
	30-39 y (n=46)	52 (48, 57)	40*	52 (49, 57)	39*	50 (47, 57)	40*	0.783
	40-49 y (n=57)	54 (48, 62)	41*	58 (50, 65)	45*	52 (46, 60)	39*	0.024
	50-59 y (n=34)	52 (47, 60)	40*	56 (48, 63)	40*	50 (46, 59)	38*	0.023
	≥60 y (n=43)	54 (49, 59)	40*	57 (49, 60)	44*	53 (49, 60)	38*	0.054
3DAε (%)	**All (n=218)**	**-33 (-36, -31)**	**-28**	**-34 (-32, -36)**	**-28**	**-33 (-35, -31)**	**-26**	**0.005**
	18-29 y (n=38)	-34 (-35, -32)	-28	-34 (-35, -31)	-28	-34 (-36, -32)	-28	0.270
	30-39 y (n=46)	-33 (-35, -31)	-28	-33 (-35, -31)	-28	-32 (-35, -31)	-28	0.925
	40-49 y (n=57)	-35 (-37, -31)	-28	-36 (-38, -32)	-30	-33 (-36, -31)	-25	0.007
	50-59 y (n=34)	-33 (-37, -29)	-26	-35 (-37, -31)	-27	-31 (-33, -28)	-25	0.006
	≥60 y (n=43)	-34 (-36, -32)	-28	-35 (-36, -32)	-28	-33 (-36, -31)	-25	0.155

Normal range is reported as median (1st-3rd quartiles), followed by the reference limit as 95th percentile (or 5th percentile where appropriate*). †comparison between Women and Men.

Abbreviations: 3DAε, area strain; 3DCε, circumferential strain; 3DLε, longitudinal strain; 3DRε, radial strain; seg, segments.

[1]*Reference ranges in Tables 7.2 and 7.3 present strain parameters as negative numbers, excepting 3DRε. Elsewhere, to avoid any confusion related to arithmetic versus physiologic lower values, all LV strain parameters were expressed and interpreted as absolute values (i.e. negative strain values were also judged as positive). In this paper, lower strain values stand for worse deformation, and higher strain values stand for better deformation.*

Overall, men had slightly lower 3DLε, 3DRε and 3DAε values than women, even if this effect was not evident in all age groups. Conversely, we found no effect of gender on 3DCε.

Significant regional and segmental differences were found for 3D strain values (Table 7.2, Figure 7.4). Basal segments displayed the lowest strain values, while midventricular segments had the largest strain values. Individual segment analysis showed high variability of 3D strain measurements in neighbouring segments (Table 7.3, Figure 7.4). The apical cap had the smallest deformation among all LV segments, and its inclusion significantly reduced apical regional strain.

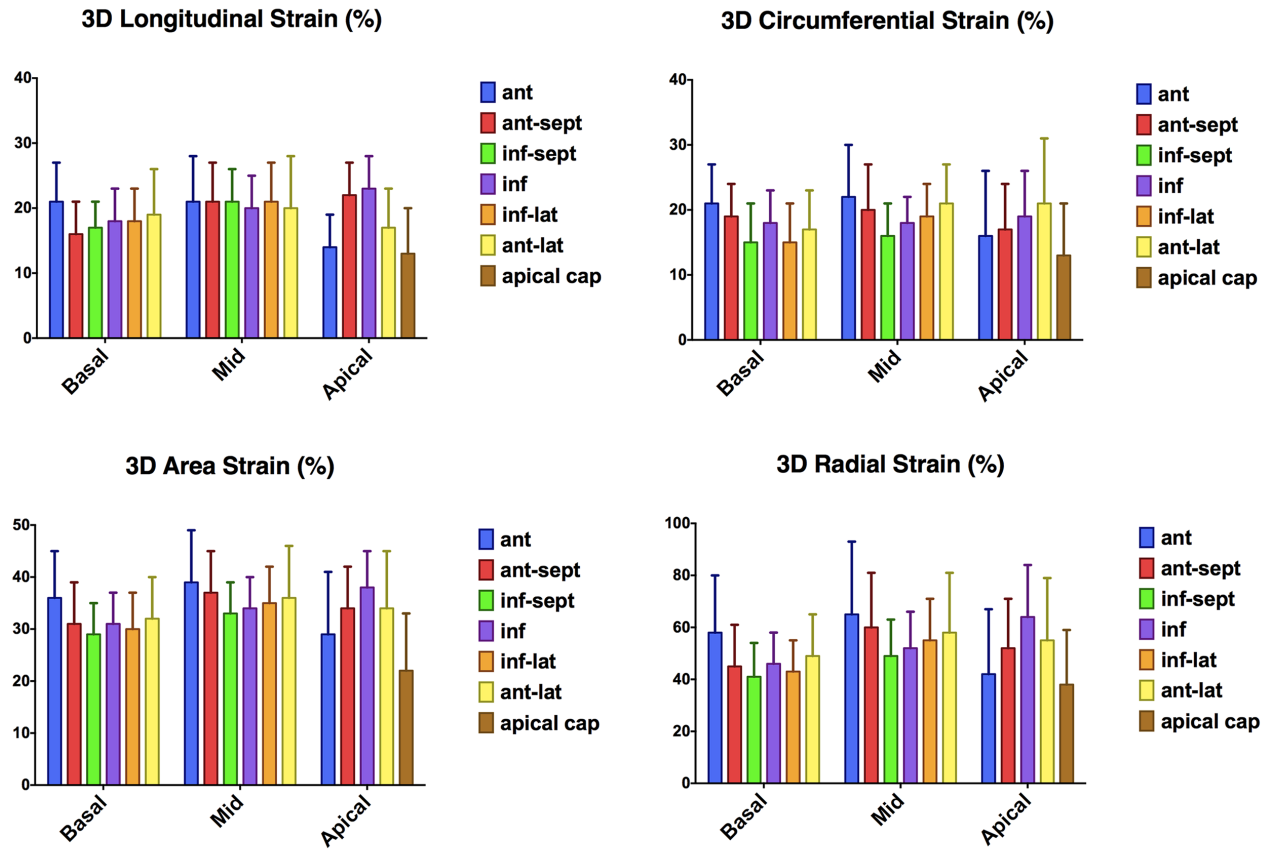

Figure 7.4. Bar plots showing segmental left ventricular strain values by 3D speckle-tracking. Among all strain parameters, 3D longitudinal strain had the lowest inter-segment variability (in basal and mid regions). However, there was a significant variability of average segmental strain, particularly for 3D circumferential and radial strain, as well as for all apical regions. Error lines show that 3D strain measurements per each segment have a quite large dispersion around the median.

Table 7.3. Regional differences of left ventricular strain parameters obtained by three-dimensional speckle-tracking (4D AutoLVQ software) in the study population.

	3DLε (%)		**3DCε (%)**		**3DRε (%)**		**3DAε (%)**	
	Median (1st, 3rd quartiles)	IQR	Median (1st, 3rd quartiles)	IQR	Median (1st, 3rd quartiles)	IQR	Median (1st, 3rd quartiles)	IQR
Global	**-19.0 (-21.0, -17.0)**	**4.0**	**-19.0 (-21.0, -17.0)**	**4.0**	**53.0 (48.0, 59.0)**	**11**	**-33.0 (-36.0, -31.0)**	**5**
Basal 6 seg	-17.5 (-20.0, -15.0)	5.0	-17.5 (-19.5, -15.6)	3.9	46.0 (40.5, 51.0)	10.5	-31.0 (-33.9, -28.5)	5.4
Mid 6 seg	-20.5 (-22.5, -18.0)*	4.5	-19.0 (-21.5, -17.0)*	4.5	55.5 (49.0, 63.5)*	14.5	-35.0 (-38.0, -32.5)*	5.5
Apical 4 seg	-20.0 (-21.5, -18)*†	3.5	-18.5 (-21.0, -15.5)*†	5.5	55.0 (46.0, 62.5)*‡	16.5	-34.5 (-37.0, -30.5)*†	6.5
Apical 5 seg	-18.5 (-21.0, -16.0)*†	5.0	-18.0 (-20.0, -14.0)*†	6.0	52.0 (42.0, 60.0)*†	18.0	-32.0 (-35.5, -28.0)*†	7.5

Apical 4 seg was obtained by averaging 4 apical segments (excluding apical cap or 17th segment), while Apical 5 seg includes the apical cap.
Abbreviations: IQR, interquartile range. Other abbreviations as in Table 7.2.
*p<0.01 for Mid 6 seg vs Basal 6 seg, Apical 4 seg vs Mid 6 seg, Apical 5 seg vs Apical 4 seg; †p<0.01 for Apical 4 seg vs Mid 6 seg and Apical 5 seg vs Mid 6 seg; ‡p=0.03 for Apical 4 seg vs Mid 6 seg.

7.3.2. Relationship with clinical, haemodynamic and technical factors. At bivariate analysis, age, gender and body size (r=0.3, p≤0.001 for all), but also systolic blood pressure (r=0.13, p=0.05), dataset image quality (r=0.19, p=0.005) and temporal resolution (r=0.20, p=0.003) showed significant correlations with 3DLε. The other 3D strain parameters had comparable relationship with the above factors. Conversely, heart rate did not correlate with 3D strain parameters (p>0.5 for all).

Figure 7.5 illustrates the opposite effects of ageing on the global 3DLε and 3DCε. Despite there was a large overlap of strain measurements among decades, the median of global 3DLε showed a significant decrease with aging, while global 3DCε progressively increased with age. The 3DLε/3DCε ratio was approximately 1 around middle age (40-60 years, Figure 7.5) and was inversely correlated with age (r=-0.5, p<0.0001), this relationship being closer than with either of 3DLε or 3DCε alone (r=-0.4 and r=0.3, respectively, p<0.001).

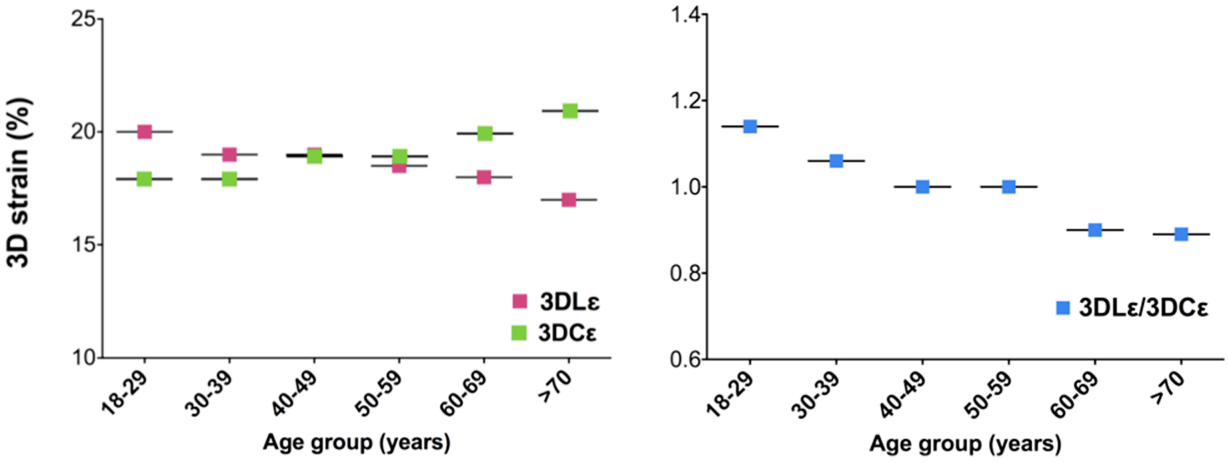

Figure 7.5. Graph illustrating the trends in 3D longitudinal strain and circumferential strain changes across age groups in healthy subjects. Left graph shows that global 3D longitudinal strain progressively decreased, while 3D circumferential strain increased with ageing (colored boxes represent the medians of global strain measurements by age decade). Right graph shows that the ratio between 3D longitudinal and circumferential strain typically was >1 in young, while elderly were likely to have a ratio <1.

In Table 7.4, the independent correlates of global 3D strain parameters are summarized. Several demographic, haemodynamic, cardiac and technical factors influenced 3D strain measurements, accounting for a modest percentage of the variability of strain measures: 22% for 3DLε, 14% for 3DCε, 9% for 3DRε and 13% for 3DAε (based on estimates of the adjusted R^2 calculated for each model). The inclusion of technical factors (dataset image quality and temporal resolution) improved the overall variance of 3DSTE analysis,

and the image quality of 3D datasets was the only covariate independently associated with all 3D strain measurements (Table 7.4). The 3DLε/3DCε index was no longer influenced by image quality when it was included as dependent variable in the linear regression model from Table 7.4.

Table 7.4. Independent correlates of 3D longitudinal strain (model-adjusted R^2=0.22), 3D circumferential strain (model-adjusted R^2=0.14), 3D radial strain (model-adjusted R^2=0.09) and 3D area strain (model-adjusted R^2=0.13).

	3DLε		**3DCε**		**3DRε**		**3DAε**	
	β	*p*	*β*	*p*	*β*	*p*	*β*	*p*
Age	-0.25	<0.001	0.29	<0.001	-0.01	0.85	-0.02	0.82
Gender	-0.31	<0.001	-0.25	0.80	0.08	0.34	-0.09	0.29
Height	-0.13	0.13	-0.05	0.47	-0.17	0.011	0.19	0.003
Weight	-0.07	0.42	0.02	0.74	-0.02	0.79	0.06	0.53
SBP	0.09	0.13	0.05	0.48	0.01	0.81	0.01	0.83
Temporal resolution	-0.18	0.003	-0.08	0.23	-0.13	0.04	-0.16	0.015
Image quality	0.18	0.004	0.24	<0.001	0.24	<0.001	0.30	<0.001

Abbreviations: SBP, systolic blood pressure. Other abbreviations as in Table 7.2.

7.3.3. Relationship with LV echocardiographic parameters. LV volumes were independently associated with 3DCε, 3DRε and 3DAε (accounting for 5-12% of their individual variance, p<0.04 for all). LV mass was inversely correlated with 3DLε, 3DRε and 3DAε (explaining 3% of their individual variance, p=0.01 for both), even after adjusting for the effect of age and systolic blood pressure.

7.3.4. Comparison with LV strain by 2DSTE. Feasibility of global 2DLε was higher than of global 3DLε (95% vs 89%, p=0.03), while the feasibilities of 2DSTE and 3DSTE for global 2DCε and 2DRε analysis were similar (92% vs 89%, p=0.34). Reference ranges of LV strain by 3DSTE [median % (1st-3rd quartiles)] were significantly different than those by 2DSTE for all strain parameters. Specifically, 3DLε was lower than 2DLε, and 3DCε was lower than 2DCε: 19% (18-21) vs 21% (20-23), and 19% (17-21) vs 22% (20-24), respectively (p<0.001 for both). Conversely, 3DRε was higher than 2DRε: 54% (48-60) vs 39% (31-46) (p<0.001). Age and gender had a significant effect on 2DLε, however this relationship was weaker than for 3DLε (model-adjusted R^2=0.13 for 2DLε versus model-adjusted R^2=0.16 for 3DLε). No independent relationships with age were identified for 2DCε and 2DRε.

7.4. Discussion.

This is the first prospective study specifically designed to establish normative values of global LV myocardial strain by 3DSTE. The main findings of this study can be summarized as follows: 1. Ageing had a significant effect on global 3DLε and 3DCε; 2. Women had higher values of 3D strain than men, except for 3DCε; 3. Accordingly, reference values and limits of normality for global 3DSTE strain parameters were reported by age and gender; 4. Image quality and temporal resolution had a significant influence on LV strain measurements by 3DSTE, independently of clinical and hemodynamic variables; 5. Limits of normality of LV strain obtained using vendor-specific 3DSTE should not be used interchangeably neither

with those obtained by 2DSTE from the same vendor, or by vendor-independent 3DSTE software packages.

Technical considerations. The advent of 3DSTE has enabled the quantitative assessment of LV myocardial mechanics from 3D datasets. However, the impact of image quality of 3D datasets and acoustic markers on the reliability of 3DSTE analysis remains to be established. In our study, image quality was the only variable that independently correlated with all 3DSTE strain parameters, emphasizing that 3DSTE is indeed affected by acoustic properties and speckle quality, even in healthy subjects selected for satisfactory 2D image quality. Kawamura and coworkers (74) showed that the image quality of the 3D datasets impacts also on the accuracy in LV volume measurement by 3DSTE in comparison with cardiac magnetic resonance. Interestingly, in our study none of 2DSTE-derived strains were independently related with image quality, suggesting that 2DSTE is relatively less influenced than 3DSTE by the image quality.

LV apical segments were the most frequent segments to be incompletely visualized. This is likely due to the pyramidal shape of 3D LV dataset and its relatively limited volume size, necessary to preserve the temporal resolution close to optimal values [37 volumes/s at 60 beats/min *in vitro* (6)]. In addition, we found that basal segments (inferior, infero-lateral and lateral) were the most likely to be poorly tracked by 3DSTE. This limitation has already been reported for 2DSTE as well (75). Because of their active excursion and their position in the far field, which adversely affects the spatial resolution of speckles in lateral (and azymuthal, for 3D volume acquisitions) directions in apical datasets, basal LV segments are the most challenging to track for speckle-tracking algorithms. Accordingly, segmental strain measurements showed a large dispersion of values, preventing the recommendation of 3DSTE reference values for individual segments. Among all segmental strain components, 3DRε had the largest inhomogeneity across segments (but also the largest absolute values).

This technical issues may limit the reliability of 3DSTE in assessing localized myocardial diseases and regional ischemia in right coronary/circumflex artery territory. Despite these technical limitations, we have recently documented that global strain parameters obtained by the vendor-specific 3DSTE used in this study have an overall good reproducibility at repeated measurements (including test-retest)(59).

Relationship with age. To our knowledge, there is a single study reporting on the relationship of 3D strain parameters with age in healthy adults (76). In previous 2DSTE studies, the influence of age on LV strain has been controversial (72, 77, 78). Our data show that 3DLε, 3DCε and 2DLε were independently associated with age. Moreover, 3DLε decreased, while 3DCε increased across age groups, the two parameters having similar values around middle-age. The 3DLε/3DCε ratio showed a closer correlation with age and could be a more robust parameter than 3DLε, and 3DCε taken separately, as the effect of image quality on individual strain values was cancelled.

Relationship with gender. Our study is the first to report significant gender differences in 3DSTE-derived strain, with higher 3DLε, 3DRε and 3DAε in women than in men. The explanation is yet unclear, but it is likely that increased myocardial deformation contributes to the higher LV ejection fractions seen in women than in men across age spectrum, particularly in the setting of smaller LV cavity sizes (79, 80). Indeed, we have previously reported in the same healthy cohort that women had higher LV ejection fractions and smaller cavities - even after adjusting for body size - than men (73). However, only 3DLε was independently correlated with gender, suggesting that apparent gender-related variations in radial and area strain are likely attributable to gender-related confounding factors (i.e. smaller body size and LV volumes, lower blood pressure etc). Gender effect on LV strain by 2DSTE was controversial (72, 81). Recently, a large study including 739 healthy subjects reported significant age- and gender-differences for all 2DSTE strain parameters (79).

Relationship with LV geometry. Smaller LV volumes were independently associated with larger myocardial deformation in circumferential and radial directions. This finding may be interpreted as a compensatory mechanism to maintain cardiac output. Larger LV mass was independently correlated with smaller 3DLε and 3DAε, even after controlling for age or blood pressure. This confirms the observations from hypertensive patients (82), that 3DLε and 3DAε can serve as highly sensitive markers to detect early changes in LV deformation associated with larger LV mass even in healthy subjects, possibly in relation with variations in afterload (i.e. aortic elastic properties and stiffness etc) and/or myocardial fibrosis.

Comparison with 2DSTE. This is the largest study to compare 2DSTE and 3DSTE measurements in the same population of healthy subjects. We found that limits of normality are lower for 3DLε and 3DCε, and higher for 3DRε than for 2DLε, 2DCε and 2DRε, repectively. Our normal values for 2DLε and 2DCε are very similar to those reported by Yingchoncharoen et al (78) in their meta-anaylsis including nearly 2600 healthy adults.

Previous studies comparing the 2DSTE vs 3DSTE measurements reported conflicting results (51, 57, 83-85). Due to major differences in study population (type and sample size) and methodology (software, definition of global 3DCε and 3DRε), these studies are difficult to interprete in relation with our results. The only consistent finding appears to be that significant differences in strain measurements are to be expected when using either 2DSTE or 3DSTE. Part of the differences betweeen 2DSTE and 3DSTE may be related to the myocardial deformation in 3D space, with through-plane and twisting motion, which may be too complex to be captured within fixed slices of myocardium analyzed by the tomographic 2DSTE approach, particularly in healthy subjects with active LV mechanics (85). Other may be related to the different features of the tested softwares for 2DSTE and 3DSTE, respectively.

Clinical perspective. 3D strain was found to be a sensitive marker of mechanical dyssynchrony (86), early ischemia (66) and subtle LV impairment (82, 87), and a predictor of cardiovascular events (88). Other studies reported the usefulness of 3DSTE assessment in patients with myocardial infarction (58), transcatheter aortic valve replacement (89) and hypertrophic cardiomyopathy (90). Physiologically sound measurements, good reproducibility and time efficiency make 3DSTE very attractive for researchers as well as for clinicians. Looking at most recent literature, it is clear that the popularity of 3DSTE is increasing, and that research studies exploring its clinical added value will surge. However, multiple factors can affect the performance and reliability of 3D strain measurements performed with the current 3DSTE technology. Therefore, the definition of normal ranges of 3D strain parameters for each vendor and understanding the factors that influence 3DSTE variability are mandatory, and our study will hopefully assist the 3DSTE testing in clinical environment. Despite relevant from research and pathophysiologic standpoints, the observed age and gender differences in 3D strain values documented in our study are relatively much smaller than their average measurement variability. Based on present findings, we believe that, in its current stage of development, 3DSTE does not require age and gender-specific reference values for its clinical application.

Study Limitations. This is a single-center, single-ethnic study. The samples of men and women were not equal, particularly in the middle age groups, raising the possibility that some gender differences may have been amplified or not adequately detected. In addition, the number of subjects older than 70 years of age was limited. However, the enrolment of truly healthy volunteers according to the strict criteria applied in this study is rather challenging, particularly in the elderly subgroup.

Multi-center and multi-ethnic 3DSTE studies including larger cohorts of healthy volunteers studied with different 3D platforms would be highly desirable. However, the

interinstutional variability is an additional challenge in the use of 3DSTE, requiring specific interventions to achieve uniform training and standardization of both 3D dataset acquisition and analysis (91).

Conclusions. This study reported the normal ranges and limits of normality of global LV strain by 3DSTE from a large cohort of healthy volunteers, using quartiles in order to limit the impact of outliers. The present normal values are pertinent only for the 3DSTE equipment used in this study, and they cannot be used interchangeably neither with 2DSTE, or other 3DSTE vendor-specific software. At the current stage of 3DSTE development, no strain reference values for individual segments can be recommended. In healthy individuals, global indices of LV myocardial deformation obtained by 3DSTE are significantly influenced by clinical, cardiac and technical factors.

Chapter 8. Value of LV Myocardial Strain by 3D Speckle-tracking to Estimate Infarct Size and Transmurality after ST-elevation Myocardial Infarction.

8.1. Introduction.

Myocardial infarction is a leading cause of death worldwide (92). Decades of advances in the management and therapies of patients presenting with ST-elevation myocardial infarction (STEMI) have increased their survival and treatment time horizon, but subsequently led to a growing prevalence of systolic heart failure (93). Notwithstanding a timely restoration of myocardial perfusion, an accurate identification of the extent of irreversible damage and regional myocardial dysfunction is critically important after STEMI and has important therapeutic and prognostic implications (94).

Cardiac magnetic resonance imaging with late-gadolinium enhancement (LGE-CMR) is now an established and widely used method for delineating irreversibly injured myocardium after STEMI, independently of wall motion, infarct age and reperfusion status (95, 96). However, in the acute phase of STEMI, resting echocardiogram is the mainstay of imaging evaluation, while LGE-CMR requiring patient transportation in dedicated laboratory, a long examination time with limited monitoring facillities, is recommended at pre-discharge or after discharge (94). In addition, its limited availability, contraindications and costs limit the routine use of LGE-CMR in many patients who might potentially derive benefit.

Greater advantages might arise when the risk prediction and the initiation of preventive therapies for heart failure are accomplished early after STEMI, especially if large amounts of myocardium are jeopardized. Traditional markers like LVEF, when measured

early after STEMI, are known to be imperfect predictors of late LV dysfunction. A combination of an objective assessment of regional myocardial function and infarcted mass, with the transmural extent of infarcted tissue would be desirable. Longitudinal strain has been reported to accurately predict the global burden of LGE-CMR and its transmural extent in STEMI patients, thus providing valuable insights on infarct size and myocardial viability using ultrasound deformation imaging (97, 98). The recent advancement of three-dimensional speckle-tracking (3DSTE) technology has the potential to overcome some of the limitations of one and two-dimensional methods to capture a such complex and three-dimensional phenomenon as LV myocardial deformation.

However, 3DSTE lacks proper clinical validation and no studies have explored so far the value of 3DSTE for assessing myocardial function early after STEMI. In our study, we hypothesized that 3D strain parameters could be more accurate and promising markers of LV regional and global myocardial damage than two-dimensional longitudinal strain (2DLε) and wall motion assessment in STEMI patients. Our aims were to evaluate if: (1) myocardial deformation parameters obtained using 3DSTE in patients early after a first STEMI could provide an accurate and objective assessment of infarct size and transmurality, in comparison with LGE-CMR; (2) assessing segmental LV strain by 2D/3DSTE can improve the prediction of transmural myocardial necrosis over visual wall motion by experienced reader.

8.2. Methods.

A total of 46 consecutive patients were prospectively included according to the following criteria: (I) admitted with acute STEMI, diagnosed according to current practice guidelines (94); (II) successfully treated by primary PCI (successful reperfusion being defined as TIMI 3 flow and <30% residual stenosis of the culprit lesion); (III) scheduled for echocardiography at predischarge and for a LGE-CMR study within 24 hours distance from the echocardiographic examination; (IV) having a good-quality apical acoustic window at 2D

echocardiography. Exclusion criteria were: previous healed myocardial infarction, previous fibrinolysis, unstable clinical condition, inability to cooperate for breathholding and significant arrhythmias. Further exclusion criteria for patients referred to CMR were contraindications such as implanted pacemakers, defibrillators, metallic intracranial implants, claustrophobia or severe renal dysfunction (eGFR<30 mL/m^2). Patients who did not undergo CMR due to contraindications or by physician's decision, or in which the limited time frame of 24 hours between echo and CMR could not be achieved, have been evaluated by 2DE and 3DE only. The total number of patients studied by echo (+/-CMR) was 77 (Figure 9.1).

Primary PCI was performed according to standard clinical practice and decision to use of bare-metal or drug-eluting stents was at the discretion of the interventional cardiologist. The use of antiplatelet therapy, angiotensin-converting enzyme inhibitors, beta-blockers and statins was recommended according to guidelines. Plasma samples for troponin I levels (TnI) were collected on admission and subsequently during the hospitalization every 6 h for 2 days.

8.2.1. Echocardiography.

Image Acquisition. All 77 patients with STEMI were examined at 8±3 days after the event using a commercially available ultrasound scanner (Vivid E9, GE Vingmed, Horten, Norway) equipped with phased-array 2D imaging transducer (M5S) and fully-sampled matrix-array 3D imaging transducer (4V). A comprehensive 2D and 3D echocardiographic examination was done by an experienced echocardiographer, including parasternal long-axis and short-axis views, and three standard apical views of the LV. For each view, three consecutive cardiac cycles were recorded during breathhold and attention was paid to avoid foreshortening in apical LV views. Grayscale recordings were optimized for 2DSTE at a mean frame rate of 50-80 frames/sec (3). As part of the same echocardiographic study, 3D LV full-volume acquisition were performed and triggered to the ECG R wave on 4 to 6 consecutive heartbeats, in order to achieve an optimal spatial resolution and temporal resolution (≥30 vps). Care was taken to

include the entire LV myocardial thickness within the pyramidal scan volume in all segments. The quality of each 3D full-volume acquisition was immediately verified in twelve-slice display mode to ensure that in all segments the entire LV wall thickness is included in the dataset and that no stitching artifacts were present.

All examinations were digitally stored in raw-data format and exported to a separate workstation equipped with commercially available software for LV 2D and 3DSTE analysis (EchoPAC BT12, GE Vingmed, Horten, Norway).

Analysis of Two-dimensional Data Sets.

Wall motion score on 2D data sets (2DWMS). Two experienced readers, blinded to the clinical and angiographic data, assessed wall motion from the 2-dimensional images. Wall motion scoring was performed using a 16-segment model. Wall motion abnormalities were considered in terms of vascular territories LV regional function was visually interpreted on the basis of wall motion and systolic thickening from at least 2 separate views. Segment scores from 1 to 5 (i.e. from normal to aneurysmal) were assigned and 2DWMSI was calculated (99). Disagreements between reviewers were settled by consensus.

2*D longitudinal strain (2DLE).* Analysis of 2DLE by 2DSTE was performed on the four-chamber, two-chamber, and long-axis apical LV views, as previously described in Chapter 6. Peak segmental and peak global 2DLE were collected for analysis.

Analysis of Three-dimensional Data Sets

Wall motion score on 3D data sets (3DWMS). 3D echocardiography enabled the postacquisition cropping of the LV full-volume into 12 slices (three longitudinal and nine transversal). Adjustment of the LV planes in three vectors facilitated geometric correction in each view and ensured that no plane is foreshortened or off-axis (1). Moreover, by rotating each longitudinal plane around the LV central axis a full scan of the entire surface of each segment was

performed, for a throrough assessment of myocardial wall motion in and between displayed views. A 3DWMSI was then calculated similarly with 2DWMSI.

3D strain parameters. As detailed in Chapter 6, LV myocardial strain analysis by 3D speckle-tracking enabled the computation of 3DLƐ, 3DCƐ, 3DAƐ and 3DRƐ from a single LV dataset. Peak global, as well as peak segmental strain values have been collected for statistical analysis.

8.2.2. Cardiac magnetic resonance. CMR image acquisition was performed using 1.5-T Avanto scanner (Siemens Medical Solutions, Erlangen, Germany) with a phased-array receiver coil. All images will be acquired during breath-hold at end-expiration (1 or 2 slices per breath-hold depending on the subject heart rate and tolerance to breathhold), following a previously described protocol (100). The extent of late gadolinium enhancement (LGE) was scored for each LV segment by an expert reader and expressed in percents of LV wall thickness (0-25%, 25-50%, 50-75% 75%-100%). Segmental analysis considered LGE to be "transmural" when LGE was at least 50% transmural in >50% of the segment's total extension. The infarct size index (ISI) was calculated as sum of LGE score (0-4) for every LV segment divided by 17 (100). The transmural extent of necrosis at CMR in infarcted segments was compared with corresponding segmental strain values, while the infarct size index at LGE-CMR for whole LV was compared against global 2D and 3D strain parameters.

Statistical analysis. Continuous variables were summarized as mean ± standard deviation or percentage, when appropriate. Myocardial segments were divided in groups based on the transmural extent of infarction, and peak strain values between groups were compared by using 1-way analysis of variance with Bonferroni adjustment. Receiver-operating characteristic (ROC) curves were used to evaluate the ability to distinguish transmural from nontransmural infarction and non-infarcted segments and to determine optimal cutoff values for sensitivity and specificity. To establish a cut-off for strain parameters to identify segments

transmural LGE at CMR, the patient group was splitted into a definition group and a validation group (Figure 8.1). The ability to distinguish transmural infarction from the other segments (having no infraction or subendocardial infarction) was evaluated by developing a ROC curve, for which a dichotomous (yes/no) separation of segments on the basis of the extent of LGE (>50% for transmural infarction) was used. Relationship between global strain parameters and infarct size indices were explored using the Pearson correlation. A p value of <0.05 was considered statistically significant.

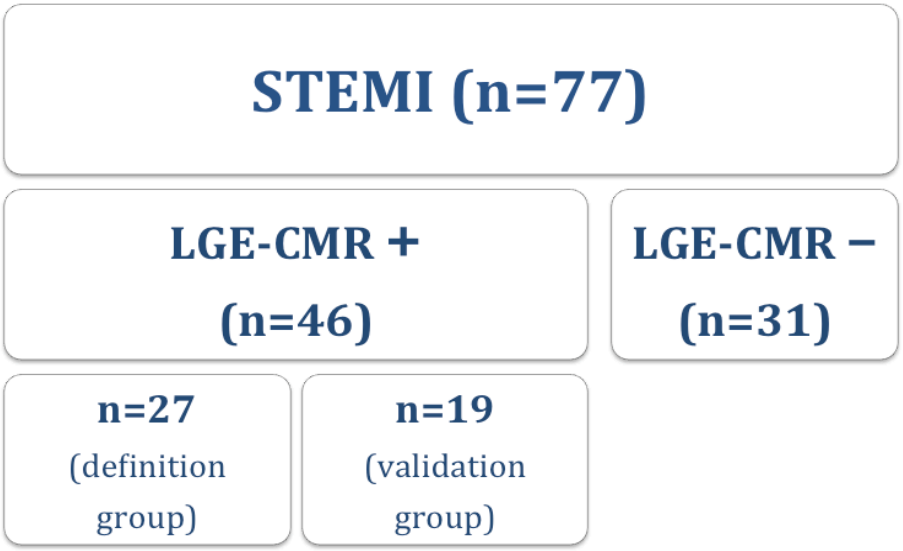

Figure 8.1. Patient flowchart.

8.3. Results.

8.3.1. Feasibility. To obtain LV 3D strain parameters required < 1 min/dataset for acquisition and <5 minutes/dataset for analysis. However, the acquisition of an optimal quality LV 3D full volume for 3D strain analysis commonly required several attempts, which needed an average total time of 3 minutes (range 30 seconds-12 minutes). At multi-slice display, image quality was judged optimal in 41% of datasets, good in 47% and fair to poor in

the remaining 12%. There were 0 to 2 segments incompletely visualized throughout the cardiac cycle, of which 85% were in the LV apical region.

Overall, segmental tracking by 3DSTE was feasible in 91% of LV segments. In 3 patients, more than 3 segments/LV were not interpretable by 3DSTE and the global strain values were not computed. The feasibility of segmental analysis by 3DSTE is reported in Figure 8.2.

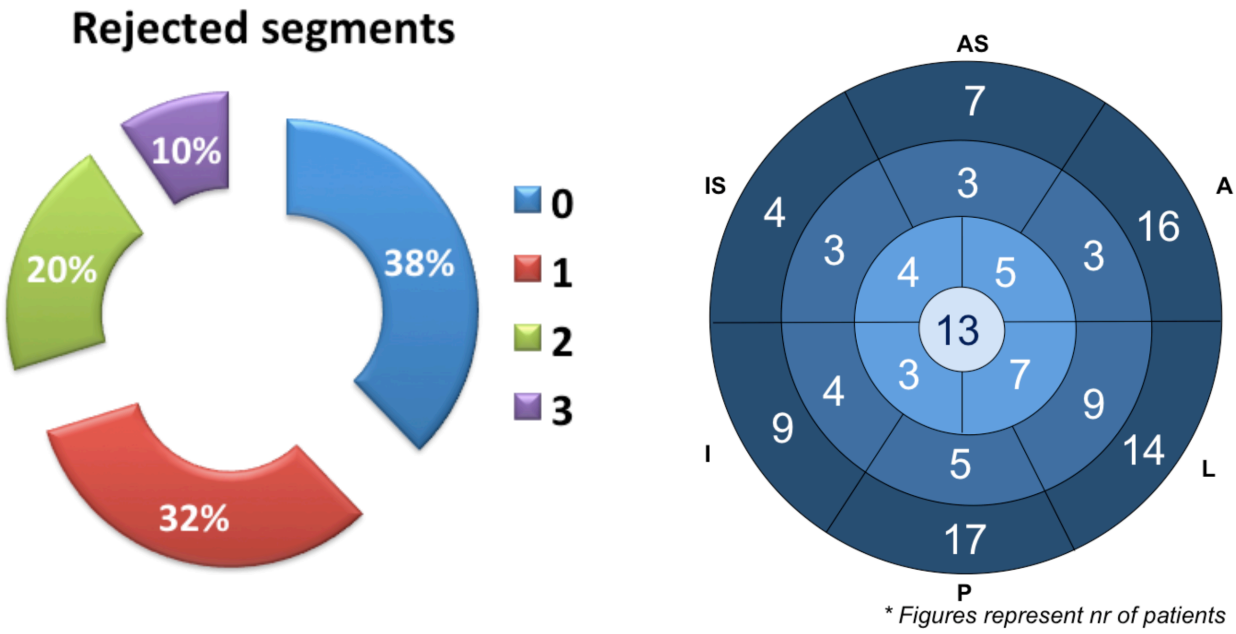

Figure 8.2. The proportion of patients having from 0 to 3 segments rejected by software due to poor tracking in the study population (*left*). Polar map showing the localization of rejected segments, i.e. poorly tracked segments rejected by software were more frequently localized in the basal segments and at the apical cap.

A total of 782 segments were analyzed by LGE-CMR. Among these, there were 274 segments (35%) showing transmural infarction.

Table 8.1. Characteristics of the study populations

	All patients (n=77)	**LGE-CMR patients (n=46)**
Age (years)	61±14	58±13
Gender (M, %)	84%	87%
Peak TnI (μg/L)	145±162	156±183
Culprit lesion (%)		
LAD	60%	56%
RCA	31%	36%
LCX	9%	9%
Multivessel disease (%)	57%	59%
3D LVEDV (mL/m^2)	72±14	73±14
3D LVESV (mL/m^2)	38±13	39±13
3D LVEF (mL)	49±9	48±9
2DWMSI	1.79±0.33	1.76±0.35
3DWMSI	1.89±0.33	1.85±0.39
ISI	n/a	1.40±0.73

Abbreviations: 2D, two-dimensional; 3D, three-dimensional; ISI, infarct size index at LGE-CMR; LAD, left anterior descendent coronary artery; LCX, left circumflex artery; LGE-CMR, cardiac magnetic resonance with late gadolinium enhancement; LVEDV, left ventricular end-diastolic volume; LVEF, left ventricular ejection fraction; LVESV, left ventricular end-systolic volume; RCA, right coronary artery; TnI, troponin I; WMSI, wall motion score index.

Characteristics of the study populations are presented in Table 8.1. There were no significant differences in terms of demographic, clinical and echocardiographic characteristics of the two groups. 3DWMSI was higher than 2DWMSI in both study groups ($p<0.0001$ for both).

8.3.2. Relationship of global LV strain parameters with infarct size indices

Parameters of global LV myocardial function measured by 2DSTE and 3DSTE (i.e. peak global strain values) were correlated with conventional indices known to reflect infarct size and LV functional impairment after STEMI (Table 8.2).

Table 8.2. Relationship between LV strain parameters and conventional indices of infarct size and LV systolic dysfunction.

	Blood	2D Echo	3D Echo	3D Echo	LGE-CMR
	Peak TnI	**WMSI**	**WMSI**	**LVEF**	**ISI**
	(N=70)	**(N=77)**	**(N=77)**	**(N=77)**	**(N=46)**
2DLε	0.50	0.74	0.78	-0.70	0.65
3DLε	0.31*	0.59	0.58	-0.60	0.36*
3DCε	0.48	0.75	0.76	-0.84	0.61
3DAε	0.43	0.75	0.73	-0.79	0.53
3DRε	-0.40	-0.68	-0.68	0.76	-0.53

Abbreviations as in Table 8.1. $p < 0.001$ for all, except *$p \leq 0.01$.

Among all tested strain parameters, peak global 2DLε and 3DCε exhibited the closest correlation with ISI at LGE-CMR (Figure 8.3).

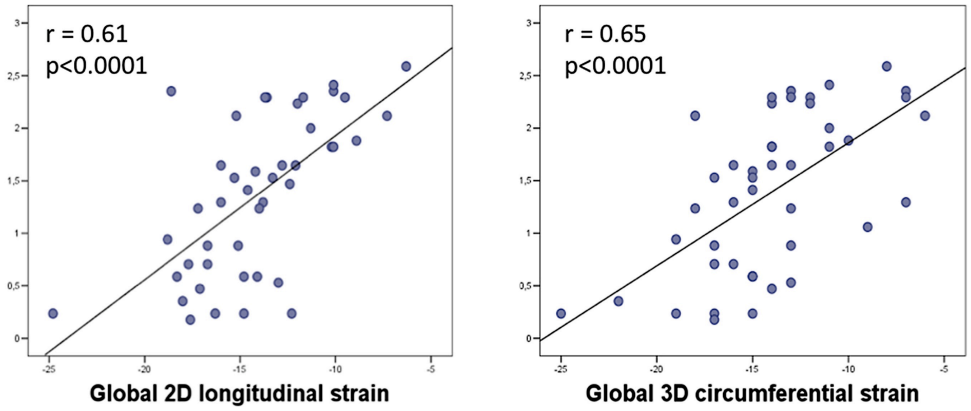

Figure 8.3. Correlations between LV strain parameters and infarct size index (ISI) at LGE-CMR.

8.3.3. Relationship of LV segmental strain with infarct transmurality.

LV segmental strain was significantly impaired in segments with transmural infarction, in comparison with the strain measurements of segments with no infarction or subendocardial infarction (Table). The best separation of segments according to the extent of LGE was provided by 2DLE (F ANOVA=144), 3DCE (F ANOVA=114) and 3DAE (F ANOVA=117)($p<0.0001$ for all). Interestingly, 3DLE had the lowest ability to reliably discriminate between the various extents of infarction transmurality (F ANOVA=50).

A first ROC curve analysis was performed in the definition group (101), which revealed that 2DLE and 3DCE have comparably good accuracy to discriminate segments with transmural infarction from other LV segments (area under curve, AUC=0.81 and 0.82, $p<0.001$). The optimal cut-offs identified in the definition group (i.e. 3DCE > -10.5% and 2DLE > -11.5%) were prospectively tested in the validation group, in order to assess their accuracy, sensitivity and specificity. ROC curve analysis in the validation group confirmed that, based on the selected cut-offs, 3DCE and 2DLE have similar accuracy (75%) for discriminating segments with >50% LGE at CMR, with 2DLE (69% sensitivity, 80% specificity) being relatively more sensitive and 3DCE being more specific (60% sensitivity, 84% specificity).

Figure 8.4 shows the ROC curve analysis in the validation group, after including also 2D and 3DWMS, in order to verify the relative accuracy of strain parameters (as objective measures) versus conventional regional wall motion assessment (as subjective visual assessment) by expert echo readers. Among all indices, 3DWMSI had the best ability to identify correctly the segments with >50% LGE than those with 0-50% LGE. 2DLE was more accurate than any 3D strain indices, and better than 2DWMSI. Among all 3D strain parameters, 3DAE, 3DCE and 3DRE had comparable capability to predict transmural infarction, performing significantly better than 3DLE (102, 103).

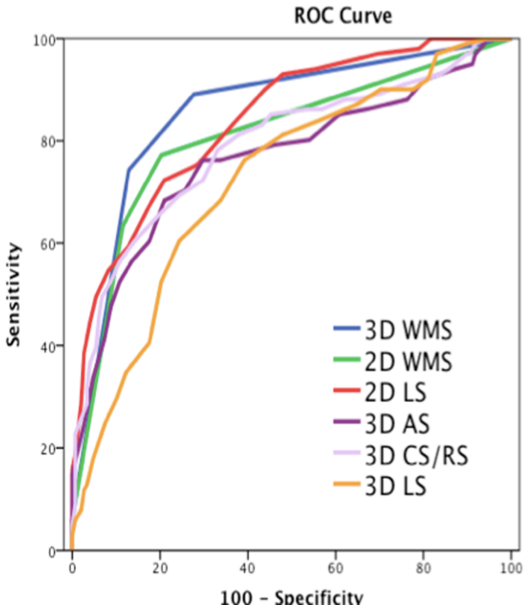

	AUC	95% CI
3D WMS	0.86	0.81–0.91
2D LS	0.84	0.79–0.89
2D WMS	0.81	0.75–0.87
3D AS	0.79	0.73–0.85
3D CS	0.77	0.71–0.83
3D RS	0.77	0.70–0.83
3D LS	0.72	0.66–0.79

Figure 8.4. ROC curve analysis for assessing the relative predictive power of various regional indices to accurately identify the segments with transmural infarction at LGE-CMR.

The incremental predictive value of 2D and 3D strain parameters over 3D WMSI was significant, but small (Figure 8.5).

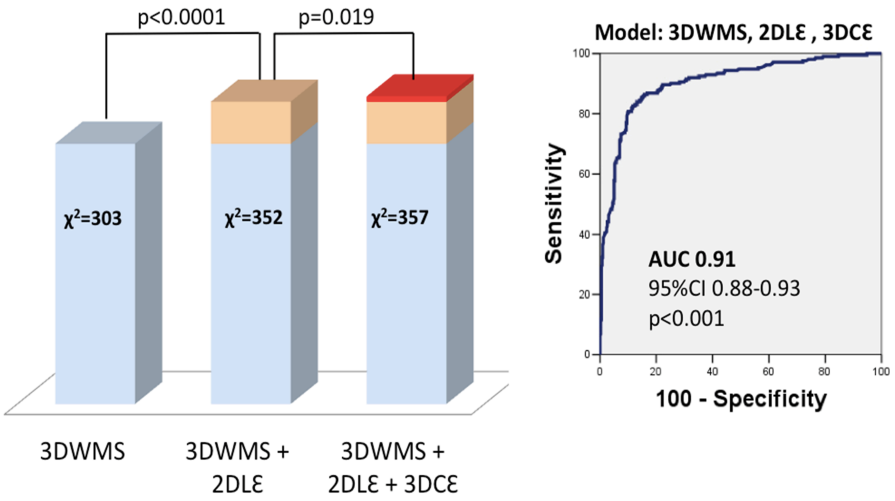

Figure 8.5. Incremental value of LV myocardial strain parameters (2D longitudinal strain and 3D circumferential strain) over visual wall motion assessment on 3D datasets (3DWMS) to accurately differentiate the segments with transmural infarction from those with no infarction and with non-transmural infarction at LGE-CMR.

8.4. Discussion

In STEMI, the effects of reperfusion are quite variable and depend on the duration and severity of preceding ischemia. The amount of salvaged myocardium is related to the duration of total coronary artery occlusion, the level of myocardial oxygen consumption, and the collateral blood flow (104). Transmural infarction may develop when recanalization occurs late (>6 h) or is not effective (persistent coronary occlusion or no reflow), otherwise is frequently limited to the subendocardium. The discrimination between transmural and non-transmural infarction after a STEMI holds important clinical and prognostic significance, since the latter is characterized by a lower incidence of expansive remodeling and related complications (e.g. cardiogenic shock, myocardial rupture, aneurysm and pseudo-aneurysm formation, thrombolism, pericardial involvement etc) (105, 106).

LGE measurements during the acute phase of infarction provide additive value to predict late LV systolic dysfunction than established predictors of adverse outcome, such as LV ejection fraction (LVEF) (107, 108).

3DSTE could be safely applied at bedside, also during the acute phase of STEMI and subsequently to monitor changes, and may rapidly provide objective informations on global and regional myocardial function, especially when CMR is not available, too risky or contraindicated. 3D circumferential strain had a better accuracy than 3D longitudinal strain to identify transmural infarction, presumably because circumferential function arises from the midwall fibers and was shown to be relatively preserved in subendocardial infarction, which mainly affects longitudinal shortening (98). Interestingly, 2D longitudinal strain had a comparable accuracy with 3D circumferential strain, and superior than 3D longitudinal strain (Figure 8.6). This finding suggests that, with the current state of ultrasound technology, the superior temporal and spatial resolution in 2D vs 3D datasets may lead to a still more accurate and robust analysis at segmental level by 2DSTE than by 3DSTE. In this regard, we have shown in Chapter 7 that the robustness of 3DSTE at segmental level is not optimal and that the observed inter-segment variability of 3D strain is likely reflecting the great dependence on image quality and some tracking issues even in healthy hearts. This evidence is relevant for the ongoing development and improvement of 3DSTE technology.

On the other hand, several factors are likely to have contributed to the good predictive value of qualitative wall motion analysis (3DWMS) versus quantitative strain measurements, when both were compared with DE-CMR: overall good image quality of LV data sets; obtaining a reliable wall motion interpretation of each LV segment from two orthogonal perspectives by slicing a single apical 3D data set, even in patients with difficult parasternal window; the possibility to adjust LV slices offline to ensure a full scan of each segment, thus avoiding erroneous interpretation due to off-axis plane position; the large predominance of segments with transmural necrosis among all infarcted segments which made easier the identification of abnormal regional thickening (109); and integrating abnormal wall

thickening with increased tissue echogenicity in the qualitative interpretation of regional abnormality.

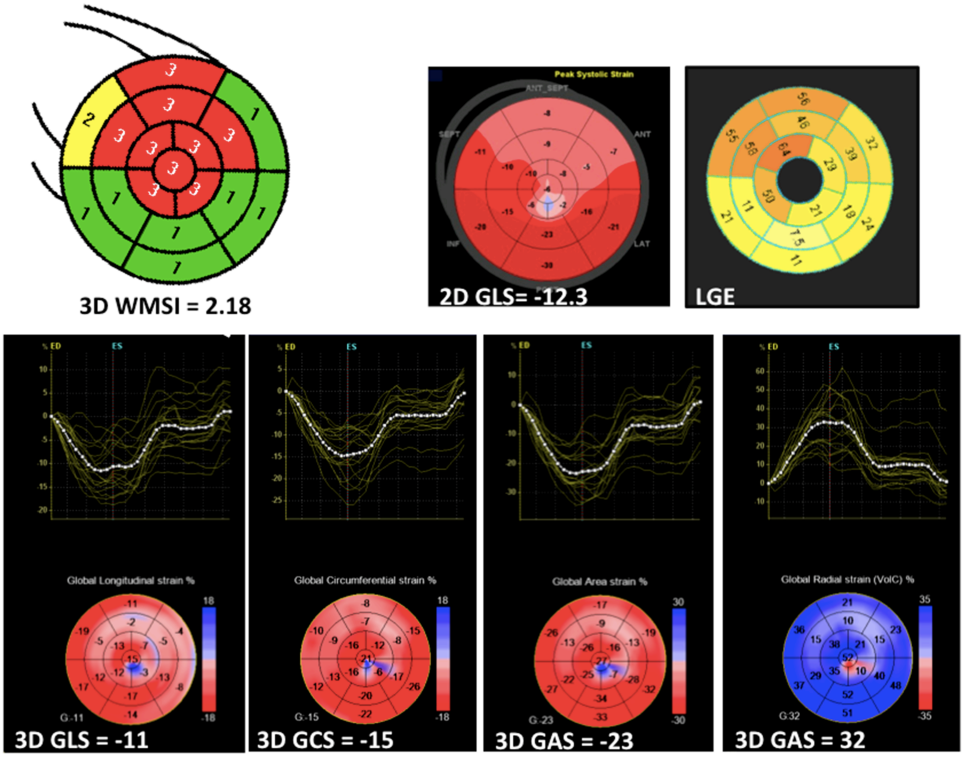

Figure 8.6. Multi-modality LV imaging in a patient with acute anterior myocardial infarction secondary to LAD occlusion. Note the correspondence of regional abnormalities localized at anterior, antero-septal and apical regions across various techniques and methods.

The healing phase of STEMI after successful reperfusion is a dynamic process. The time chosen for imaging during the healing process of myocardial infarction may influence the regional function assessment (as stunned myocardium is progressively recovering its function), as well as the LGE burden (as the myocardial edema resorbs and scar area shrinks during several month period (108). In all our patients, LGE-CMR and echo studies were performed within 24 hours, and the relative magnitude of any changes is likely insufficient to negate the value of measurements during this time frame. On the other hand, early prediction

of outcomes after STEMI is highly desirable, because it would allow a tailored therapy in a timely fashion, when the benefits might be greatest. We have chosen the pre-discharge time for imaging STEMI patients (7-10 days after the index event), since this is a moment of utmost clinical importance for planning future strategy and reasonably distant from the hyperacute phase. Both experimental (110) and clinical CMR studies (108) have shown that LGE during the acute phase of STEMI holds a strong independent association with late heart failure and adverse events, being clinically significant and not just a simple overestimation of myocardial damage.

Study limitations. Our study population is a selected one, due to: (I) technical constrains related to 3D speckle-tracking feasibility; (II) study design. Good image quality is a prerequisite for all ultrasound methods and particularly for those based on speckle-tracking algorithms. Moreover, only patients with first recent STEMI were enrolled by study design, therefore only a small proportion of the myocardial segments had LGE limited at subendocardial layer. Yet, our study focus was the identification of segments showing transmural necrosis, since infarct transmurality is one of the strongest prognostic markers after STEMI.

Conclusions. This study demonstrated that, early after a succefully reperfused STEMI, 3D strain (i.e. circumferential and area strain) can be used to assess infarct size and necrosis transmurality with good accuracy in comparison with DE-CMR, being comparable to the accuracy of 2D longitudinal strain. Deformation imaging may provide important informations in STEMI patients at bedside, when DE-CMR is unavailable, unfeasible or contraindicated. In our study, wall motion scoring on 3D data sets by experienced reader remained superior than quantitative deformation analysis for identifying segments with transmural necrosis early after STEMI. Follow-up studies to clarify the relative importance of the „new" versus „old" imaging parameters to stratify the individual risk and to best predict prognosis after STEMI

deserve high priority. Despite showing promising preliminary results, further improvements of 2D/3D speckle-tracking technology will bring benefit in future research studies.

Chapter 9. Left Ventricular Geometry and Myocardial Function Analysis by 3D echocardiography in Hypertrophic Cardiomyopathy

8.1. Introduction.

Hypertrophic cardiomyopathy (HCM) is the most common genetic cardiac disease, with a prevalence of 1:500 in the general population (111). HCM is associated with a variety of disease courses, age of onset, symptom severity, left ventricular outflow (LVOT) obstruction and risk for sudden cardiac death. The clinical diagnosis of HCM is usually established with echocardiography, which traditionally demonstrates nondilated, excessively hypertrophied LV in the absence of hemodynamic stresses (arterial hypertension or aortic stenosis) or systemic disease (for example, amyloidosis or storage diseases), and regardless of the presence of LVOT obstruction. According to conventional echocardiographic indices, the systolic LV properties were thought to remain intact, at least in the initial disease period when only the diastolic function is typically found impaired. Actually, in patients with HCM, the LV systolic function has been traditionally described as hyperdynamic due to the frequent observation of normal or supranormal LV ejection fractions measured by conventional echocardiography such as M-mode echocardiography and biplane Simpson area measurements. However, significant myocardial systolic dysfunction has been identified by DTI and 2DSTE deformation imaging, typically affecting the longitudinal shortening of the LV, despite a normal/supranormal LV ejection fraction (112).

Despite the substantial information available regarding the pathophysiology and natural history, the mechanisms of progressive heart failure and functional disability in HCM

are complex and remain incompletely understood, particularly in the absence of overt LV systolic dysfunction or LVOT obstruction. The phenotype of non-obstructive HCM with preserved EF is responsible for the largest proportion (nearly 50%) of HCM patients, and was reported to have a particularly malignant prognosis, patients becoming symptomatic and experiencing advanced heart failure and adverse outcome even earlier than those with obstructive forms or end-stage (113). The pathophysiological variables incriminated in the heart failure mechanism were atrial fibrillation and diastolic dysfunction. No study has explored so far if there is any relationship between LV systolic deformation using 3DSTE and heart failure symptoms.

Another important issue of HCM is that the clinical diagnosis is not always straightforward in patients presenting with LV hypertrophy, especially if an underlying cause (athletic training or arterial hypertension) is present. A substantial overlap is present between conventional echocardiographic findings in patients with HCM and those with other causes of LV hypertrophy, which represents a serious and not so infrequent problem given the dramatically different prognosis and implications of such diagnosis (i.e. risk of sudden death in athletes (114)). A thorough understanding of the myocardial mechanics pattern in the LV hypertrophy due to HCM, beyond the simple measure of LV ejection fraction, would have important diagnostic and managment implications.

Accordingly, the aim of this study was to describe the LV myocardial mechanics in HCM patients using 2DSTE and 3DSTE, and to compare it with the normal deformation pattern in healthy subjects.

9.2. Methods.

Thirty-six HCM pts and 32 healthy controls were enrolled. HCM was diagnosed by a hypertrophied non-dilated LV, with maximal wall thickness ≥15 mm (or borderline LV

hypertrophy 13-14 mm in the presence of positive family history and/or genetic testing), in the absence of an underlying cardiac or systemic etiology that might explain the LV hypertrophy (115). Patients with abnormal regional or global systolic function (LVEF < 50%) were excluded.

Echocardiographic examinations were performed in all subjects using a Vivid E9 ultrasound system (GE Vingmed, Horten, Norway). Three cardiac cycles were stored in cineloop format for offline analysis. Quantitative analysis of LV geometry, mass and function was performed by 3D echo. Peak global 2DLε and 3D strain (longitudinal, 3DLε; circumferential, 3DCε; radial, 3DRε; area, 3DAε) were analyzed according to the methodology described in Chapter 6. LV outflow tract area (LVOTA) has been planimetered on 3D rendered images of LVOT en face. Diastolic function was evaluated by analysis of mitral Doppler inflow and tissue Doppler imaging (DTI), and LV filling pressures were estimated by E/e'. Maximal LVOT gradient at rest and with Valsalva maneuver were systematically recorded from the apical 5-chamber view by continuous-wave Doppler. LV outflow tract obstruction was defined as a peak gradient > 30 mm Hg at rest or during Valsalva maneuver.

Heart failure symptomatic status was defined by NYHA class (II-IV). Statistical analysis was performed as described in Chapter 8.

9.3. Results.

Two HCM patients were excluded due to LVEF<50% and 4 due to poor quality of 3D datasets. Overall feasibility of 3D acquisition in patients with good apical acoustic window in 2D was 91%. Table 9.1 summarizes the clinical and echocardiographic characteristics of the HCM patients and control group.

Table 9.1 Characteristics of the study populations.

	HCM patients (n=42)	Healthy controls (n=42)
Age (years)	51±13	50±11
Male gender (n)	20	20
BSA (m^2)	1.85±0.22	1.84±0.18
3D LV end-diastolic volume	53±10	58±10*
3D LV end-systolic volume	19±6	22±5*
3D LV ejection fraction (%)	64±6	62±4
3D LV stroke volume (ml/m^2)	34±6	35±9
3D LV mass (g/m^2)	109±24	75±9**
3D LV mass/EDV (g/ml)	2.11±0.43	1.30±0.16**
3DLε (%)	-14.6±3.7	-19.5±2.3**
3DCε (%)	-18.3±3.5	-19.9±1.9*
3DRε (%)	46.6±11.6	57.1±6.9**
3DAε (%)	29.6±5.7	35.0±2.7**

*p<0.05, **p<0.001

Although LVEF was similar in pts and controls, LV systolic 3D deformation was significantly impaired in pts (p<0.0001) for all strain components, except for 3DCε which was only marginally lower (p=0.04). 2DLε was also significantly impaired in patients with respect to controls (-16.7±3.4 vs -21.2±1.3%, p<0.0001).

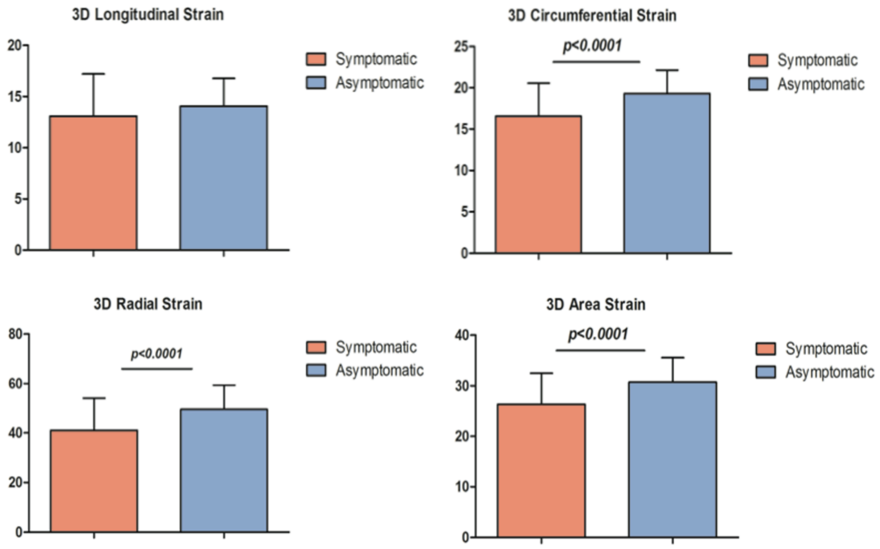

Figure 9.1. Left ventricular 3D strain parameters displayed according to the symptomatic status.

In HCM pts, all strain parameters were more closely correlated with LV end-systolic volume (r=0.55 to 0.67), LVEF (r=-0.82 to -0.88) and mass (r=0.33 to 0.56) than in controls ($p<0.0001$ for all).

Symptomatic pts (n=11) had more impaired 3DAε, 3DRε and 3DCε, while 3DLε was similar in comparison with asymptomatic patients. In addition, symptomatic HCM patients but also had more LVOT obstruction and concentric remodelling, and higher E/e' than those asymptomatic (Table 9.2, Figure 9.1). Interestingly, despite being significantly impaired with respect to controls, neither 2DLε or 3DLε were significantly related to symptomatic status in HCM patients. At ROC curve analysis, 3DAε, 3DRε and 3DCε had a similar accuracy to identify symptomatic pts (AUCs 0.72-0.73) (Figure 9.2).

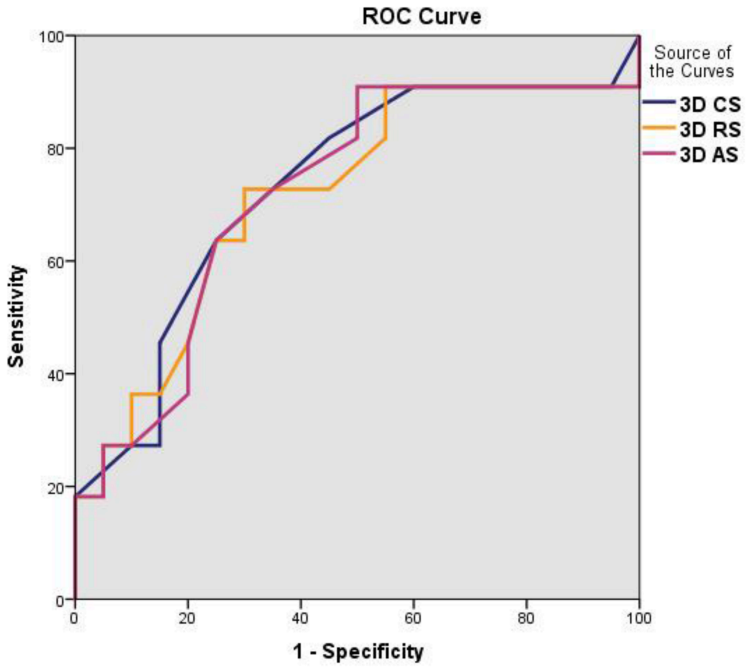

Figure 9.2. ROC curve analysis to determine the relative accuracy of 3D strain parameters to reliably predict heart failure symptoms in HCM patients.

Table 9.2. Comparison of symptomatic vs asymptomatic HCM patients.

	HCM patients Symptomatic	**HCM patients Asymptomatic**
	n=12	**n=20**
3D LV ejection fraction (%)	64±6	62±3
3D LV mass (g/m²)	119±29	104±19
3D LV mass/end-diastolic	2.4±0.5	1.9±0.5*
3DLε (%)	-13.1±4.1	-15.4±3.2
3DCε (%)	-16.6±4.0	-19.3±2.8*
3DRε (%)	41.0±13.1	49.6±9.7*
3DAε (%)	-26.4±6.1	-30.7±4.9*
2DLε (%)	-15.2±3.7	-17.4±3.1
E/e' average	20.7±9.4	9.4±2.7*
LVOT area (cm²)	2.3±0.9	3.4±0.7*
Max gradient >30 mmHg (%)	73	10*

*p<0.01

9.4. Discussion.

Strain imaging by DTI and 2D strain for the noninvasive evaluation of LV regional function in HCM has been proposed as a sensitive tool to detect early systolic function abnormalities in patients with HCM (116). However, clinical application of deformation imaging has been rather limited by complexity of data postprocessing and limited

reproducibility, as well as by the lack of site-specific normative values.

This study assessed the role of 3D strain, a new method to measure LV systolic strain from 3DE acquisitions, in evaluating global and regional function in HCM. Our results show that the 3D strain analysis is feasible in HCM and that different components of global LV strain (longitudinal, radial and area strain) are significantly reduced in HCM patients versus healthy subjects. LV 3D strain parameters were found to be significantly reduced despite normal LV function as assessed by standard criteria, suggesting the presence of a global subclinical LV systolic dysfunction. Interestingly, circumferential strain was relatively more preserved than the other strain components, presumably as a compensatory mechanism in order to maintain stroke-volume and ejection fraction within normal range. Therefore, global 3D strain analysis by 3DSTE appears to be a more sensitive index of global LV myocardial function than standard LVEF assessment. Potential applications include differentiation of HCM from hypertensive cardiomyopathy or from athlete's heart, treatment monitoring, and eventually identification of preclinical disease in carriers of HCM mutations (117).

In our study, alteration in global radial and circumferential strain, and not in longitudinal strain was related to heart failure symptoms. Previous studies based on 2DSTE reported only on the significance of 2D longitudinal strain in HCM to predict fibrosis, arrythmias and major adverse cardiac events (118, 119), and only one other recent study with 3DSTE reported that circumferential myocardial shortening seems to be directly involved in preservation of LV systolic performance in HCM, however it did not explore the relationship between circumferential strain and heart failure symptom development (120).

Conclusions. In HCM with normal LVEF, a significant LV systolic longitudinal dysfunction exists, irrespective of the presence of heart failure symptoms. Although in HCM symptom development is multifactorial, in the present study it was also related to further impairment in LV myocardial function in circumferential-radial direction.

References

1. Lang RM, Badano LP, Tsang W, Adams DH, Agricola E, Buck T, et al. EAE/ASE recommendations for image acquisition and display using three-dimensional echocardiography. Eur Heart J Cardiovasc Imaging 2012;13:1-46.

2. Muraru D, Badano LP, Ermacora D, Piccoli G, Iliceto S. Sources of variation and bias in assessing left ventricular volumes and dyssynchrony using three-dimensional echocardiography. Int J Cardiovasc Imaging 2012;28:1357-68.

3. Mor-Avi V, Lang RM, Badano LP, Belohlavek M, Cardim NM, Derumeaux G, et al. Current and evolving echocardiographic techniques for the quantitative evaluation of cardiac mechanics: ASE/EAE consensus statement on methodology and indications endorsed by the Japanese Society of Echocardiography. Eur J Echocardiogr 2011;12:167-205.

4. Geyer H, Caracciolo G, Abe H, Wilansky S, Carerj S, Gentile F, et al. Assessment of myocardial mechanics using speckle tracking echocardiography: fundamentals and clinical applications. J Am Soc Echocardiogr 2010;23:351-69.

5. Blessberger H, Binder T. Two dimensional speckle tracking echocardiography: clinical applications. Heart 2010;96:2032-40.

6. Hjertaas JJ, Fossa H, Dybdahl GL, Gruner R, Lunde P, Matre K. Accuracy of real-time single- and multi-beat 3-d speckle tracking echocardiography in vitro. Ultrasound Med Biol 2013;39:1006-14.

7. Seo Y, Ishizu T, Enomoto Y, Sugimori H, Yamamoto M, Machino T, et al. Validation of 3-dimensional speckle tracking imaging to quantify regional myocardial deformation. Circ Cardiovasc Imaging 2009;2:451-9.

8. Torrent-Guasp F, Kocica MJ, Corno A, Komeda M, Cox J, Flotats A, et al. Systolic ventricular filling. Eur J Cardiothorac Surg 2004;25:376-86.

9. Anderson RH, Ho SY, Redmann K, Sanchez-Quintana D, Lunkenheimer PP. The anatomical arrangement of the myocardial cells making up the ventricular mass. Eur J Cardiothorac Surg 2005;28:517-25.

10. Buckberg GD. Basic science review: the helix and the heart. J Thorac Cardiovasc Surg 2002;124:863-83.

11. Ashikaga H, Criscione JC, Omens JH, Covell JW, Ingels NB, Jr. Transmural left ventricular mechanics underlying torsional recoil during relaxation. Am J Physiol Heart Circ Physiol 2004;286:H640-7.

12. Nakatani S. Left ventricular rotation and twist: why should we learn? J Cardiovasc Ultrasound 2011;19:1-6.

13. Greenbaum RA, Ho SY, Gibson DG, Becker AE, Anderson RH. Left ventricular fibre architecture in man. Br Heart J 1981;45:248-63.

14. Harvey W. An anatomical disquisition on the motion of the heart and blood in animals (1628). In: Willis FA, Keys TE, editors. Cardiac classics. London: Henry Kimpton; 1941. p. 17-9.

15. Sengupta PP, Krishnamoorthy VK, Korinek J, Narula J, Vannan MA, Lester SJ, et al. Left ventricular form and function revisited: applied translational science to cardiovascular ultrasound imaging. J Am Soc Echocardiogr 2007;20:539-51.

16. Vendelin M, Bovendeerd PH, Engelbrecht J, Arts T. Optimizing ventricular fibers: uniform strain or stress, but not ATP consumption, leads to high efficiency. Am J Physiol Heart Circ Physiol 2002;283:H1072-81.

17. Sengupta PP, Khandheria BK, Korinek J, Wang J, Jahangir A, Seward JB, et al. Apex-to-base dispersion in regional timing of left ventricular shortening and lengthening. J Am Coll Cardiol 2006;47:163-72.

18. Ashikaga H, Coppola BA, Hopenfeld B, Leifer ES, McVeigh ER, Omens JH. Transmural dispersion of myofiber mechanics: implications for electrical heterogeneity in vivo. J Am Coll Cardiol 2007;49:909-16.
19. Tops LF, Suffoletto MS, Bleeker GB, Boersma E, van der Wall EE, Gorcsan J, 3rd, et al. Speckle-tracking radial strain reveals left ventricular dyssynchrony in patients with permanent right ventricular pacing. J Am Coll Cardiol 2007;50:1180-8.
20. Buckberg GD, Castella M, Gharib M, Saleh S. Active myocyte shortening during the 'isovolumetric relaxation' phase of diastole is responsible for ventricular suction; 'systolic ventricular filling'. Eur J Cardiothorac Surg 2006;29 Suppl 1:S98-106.
21. LeGrice IJ, Takayama Y, Covell JW. Transverse shear along myocardial cleavage planes provides a mechanism for normal systolic wall thickening. Circ Res 1995;77:182-93.
22. Abraham TP, Laskowski C, Zhan WZ, Belohlavek M, Martin EA, Greenleaf JF, et al. Myocardial contractility by strain echocardiography: comparison with physiological measurements in an in vitro model. Am J Physiol Heart Circ Physiol 2003;285:H2599-604.
23. Edvardsen T, Skulstad H, Aakhus S, Urheim S, Ihlen H. Regional myocardial systolic function during acute myocardial ischemia assessed by strain Doppler echocardiography. J Am Coll Cardiol 2001;37:726-30.
24. Abraham TP, Nishimura RA. Myocardial strain: can we finally measure contractility? J Am Coll Cardiol 2001;37:731-4.
25. Picano E, Lattanzi F, Orlandini A, Marini C, L'Abbate A. Stress echocardiography and the human factor: the importance of being expert. J Am Coll Cardiol 1991;17:666-9.
26. Hoffmann R, Lethen H, Marwick T, Arnese M, Fioretti P, Pingitore A, et al. Analysis of interinstitutional observer agreement in interpretation of dobutamine stress echocardiograms. J Am Coll Cardiol 1996;27:330-6.

27. Jasaityte R, Heyde B, D'Hooge J. Current state of three-dimensional myocardial strain estimation using echocardiography. J Am Soc Echocardiogr 2013;26:15-28.
28. Gopal AS, Shen Z, Sapin PM, Keller AM, Schnellbaecher MJ, Leibowitz DW, et al. Assessment of cardiac function by three-dimensional echocardiography compared with conventional noninvasive methods. Circulation 1995;92:842-53.
29. Otterstad JE, Froeland G, St John Sutton M, Holme I. Accuracy and reproducibility of biplane two-dimensional echocardiographic measurements of left ventricular dimensions and function. Eur Heart J 1997;18:507-13.
30. Voigt JU. Making a black box transparent. Eur Heart J Cardiovasc Imaging 2013;14:201-2.
31. Mirsky I, Parmley WW. Assessment of passive elastic stiffness for isolated heart muscle and the intact heart. Circ Res 1973;33:233-43.
32. Brown J, Jenkins C, Marwick TH. Use of myocardial strain to assess global left ventricular function: a comparison with cardiac magnetic resonance and 3-dimensional echocardiography. Am Heart J 2009;157:102 e1-5.
33. Cho GY, Marwick TH, Kim HS, Kim MK, Hong KS, Oh DJ. Global 2-dimensional strain as a new prognosticator in patients with heart failure. J Am Coll Cardiol 2009;54:618-24.
34. Stanton T, Leano R, Marwick TH. Prediction of all-cause mortality from global longitudinal speckle strain: comparison with ejection fraction and wall motion scoring. Circ Cardiovasc Imaging 2009;2:356-64.
35. Urheim S, Edvardsen T, Torp H, Angelsen B, Smiseth OA. Myocardial strain by Doppler echocardiography. Validation of a new method to quantify regional myocardial function. Circulation 2000;102:1158-64.
36. Edvardsen T, Urheim S, Skulstad H, Steine K, Ihlen H, Smiseth OA. Quantification of left ventricular systolic function by tissue Doppler echocardiography: added value of measuring pre- and postejection velocities in ischemic myocardium. Circulation 2002;105:2071-7.

37. Leitman M, Lysyansky P, Sidenko S, Shir V, Peleg E, Binenbaum M, et al. Two-dimensional strain-a novel software for real-time quantitative echocardiographic assessment of myocardial function. J Am Soc Echocardiogr 2004;17:1021-9.
38. Blessberger H, Binder T. NON-invasive imaging: Two dimensional speckle tracking echocardiography: basic principles. Heart 2010;96:716-22.
39. Mondillo S, Galderisi M, Mele D, Cameli M, Lomoriello VS, Zaca V, et al. Speckle-tracking echocardiography: a new technique for assessing myocardial function. J Ultrasound Med 2011;30:71-83.
40. Amundsen BH, Helle-Valle T, Edvardsen T, Torp H, Crosby J, Lyseggen E, et al. Noninvasive myocardial strain measurement by speckle tracking echocardiography: validation against sonomicrometry and tagged magnetic resonance imaging. J Am Coll Cardiol 2006;47:789-93.
41. Korinek J, Wang J, Sengupta PP, Miyazaki C, Kjaergaard J, McMahon E, et al. Two-dimensional strain--a Doppler-independent ultrasound method for quantitation of regional deformation: validation in vitro and in vivo. J Am Soc Echocardiogr 2005;18:1247-53.
42. Notomi Y, Lysyansky P, Setser RM, Shiota T, Popovic ZB, Martin-Miklovic MG, et al. Measurement of ventricular torsion by two-dimensional ultrasound speckle tracking imaging. J Am Coll Cardiol 2005;45:2034-41.
43. Hoit BD. Strain and strain rate echocardiography and coronary artery disease. Circ Cardiovasc Imaging 2011;4:179-90.
44. Sengupta PP, Narula J. Reclassifying heart failure: predominantly subendocardial, subepicardial, and transmural. Heart Fail Clin 2008;4:379-82.
45. Badano LP, Muraru D, Rigo F, Del Mestre L, Ermacora D, Gianfagna P, et al. High volume-rate three-dimensional stress echocardiography to assess inducible myocardial ischemia: a feasibility study. J Am Soc Echocardiogr 2010;23:628-35.

46. Thomas JD, Badano LP. EACVI-ASE-industry initiative to standardize deformation imaging: a brief update from the co-chairs. Eur Heart J Cardiovasc Imaging 2013;14:1039-40.

47. Crosby J, Amundsen BH, Hergum T, Remme EW, Langeland S, Torp H. 3-D speckle tracking for assessment of regional left ventricular function. Ultrasound Med Biol 2009;35:458-71.

48. Heimdal A. 4D Strain: Advanced research application for quantitative echocardiography. GE Healthcare White Papers [cited; Available from: http://www.vividechoclub.net/emea/whitepapers

49. Heyde B, Cygan S, Choi HF, Lesniak-Plewinska B, Barbosa D, Elen A, et al. Regional cardiac motion and strain estimation in three-dimensional echocardiography: a validation study in thick-walled univentricular phantoms. IEEE Trans Ultrason Ferroelectr Freq Control 2012;59:668-82.

50. Seo Y, Ishizu T, Enomoto Y, Sugimori H, Aonuma K. Endocardial surface area tracking for assessment of regional LV wall deformation with 3D speckle tracking imaging. JACC Cardiovasc Imaging 2011;4:358-65.

51. Reant P, Barbot L, Touche C, Dijos M, Arsac F, Pillois X, et al. Evaluation of global left ventricular systolic function using three-dimensional echocardiography speckle-tracking strain parameters. J Am Soc Echocardiogr 2012;25:68-79.

52. Hayat D, Kloeckner M, Nahum J, Ecochard-Dugelay E, Dubois-Rande JL, Jean-Francois D, et al. Comparison of real-time three-dimensional speckle tracking to magnetic resonance imaging in patients with coronary heart disease. Am J Cardiol 2012;109:180-6.

53. Kleijn SA, Aly MF, Terwee CB, van Rossum AC, Kamp O. Three-dimensional speckle tracking echocardiography for automatic assessment of global and regional left ventricular function based on area strain. J Am Soc Echocardiogr 2011;24:314-21.

54. Kleijn SA, Aly MF, Terwee CB, van Rossum AC, Kamp O. Reliability of left ventricular volumes and function measurements using three-dimensional speckle tracking echocardiography. Eur Heart J Cardiovasc Imaging 2012;13:159-68.
55. Kleijn SA, Brouwer WP, Aly MF, Russel IK, de Roest GJ, Beek AM, et al. Comparison between three-dimensional speckle-tracking echocardiography and cardiac magnetic resonance imaging for quantification of left ventricular volumes and function. Eur Heart J Cardiovasc Imaging 2012;13:834-9.
56. Marwick TH. Consistency of myocardial deformation imaging between vendors. Eur J Echocardiogr 2010;11:414-6.
57. Saito K, Okura H, Watanabe N, Hayashida A, Obase K, Imai K, et al. Comprehensive evaluation of left ventricular strain using speckle tracking echocardiography in normal adults: comparison of three-dimensional and two-dimensional approaches. J Am Soc Echocardiogr 2009;22:1025-30.
58. Abate E, Hoogslag GE, Antoni ML, Nucifora G, Delgado V, Holman ER, et al. Value of three-dimensional speckle-tracking longitudinal strain for predicting improvement of left ventricular function after acute myocardial infarction. Am J Cardiol 2012;110:961-7.
59. Badano LP, Cucchini U, Muraru D, Al Nono O, Sarais C, Iliceto S. Use of three-dimensional speckle tracking to assess left ventricular myocardial mechanics: inter-vendor consistency and reproducibility of strain measurements. Eur Heart J Cardiovasc Imaging 2013;14:285-93.
60. Negishi K, Negishi T, Agler DA, Plana JC, Marwick TH. Role of temporal resolution in selection of the appropriate strain technique for evaluation of subclinical myocardial dysfunction. Echocardiography 2012;29:334-9.
61. Altman D. Practical statistics for medical research. London: Chapman & Hall; 1991.

62. Badano LP, Boccalini F, Muraru D, Bianco LD, Peluso D, Bellu R, et al. Current clinical applications of transthoracic three-dimensional echocardiography. J Cardiovasc Ultrasound 2012;20:1-22.

63. Muraru D, Badano LP, Piccoli G, Gianfagna P, Del Mestre L, Ermacora D, et al. Validation of a novel automated border-detection algorithm for rapid and accurate quantitation of left ventricular volumes based on three-dimensional echocardiography. Eur J Echocardiogr 2010;11:359-68.

64. Manovel A, Dawson D, Smith B, Nihoyannopoulos P. Assessment of left ventricular function by different speckle-tracking software. Eur J Echocardiogr 2010;11:417-21.

65. Negishi K, Negishi T, Haluska BA, Hare JL, Plana JC, Marwick TH. Use of speckle strain to assess left ventricular responses to cardiotoxic chemotherapy and cardioprotection. Eur Heart J Cardiovasc Imaging 2013.

66. Ternacle J, Gallet R, Champagne S, Teiger E, Gellen B, Dubois Rande JL, et al. Changes in Three-Dimensional Speckle-Tracking-Derived Myocardial Strain during Percutaneous Coronary Intervention. J Am Soc Echocardiogr 2013;doi: 10.1016/j.echo.2013.09.004. [Epub ahead of print].

67. Tanaka H, Hara H, Saba S, Gorcsan J, 3rd. Usefulness of three-dimensional speckle tracking strain to quantify dyssynchrony and the site of latest mechanical activation. Am J Cardiol 2010;105:235-42.

68. Yu HK, Yu W, Cheuk DK, Wong SJ, Chan GC, Cheung YF. New three-dimensional speckle-tracking echocardiography identifies global impairment of left ventricular mechanics with a high sensitivity in childhood cancer survivors. J Am Soc Echocardiogr 2013;26:846-52.

69. Saltijeral A, Perez de Isla L, Veras K, Fernandez Mde J, Gorissen W, Rementeria J, et al. Myocardial strain characterization in different left ventricular adaptative responses to high

blood pressure: a study based on 3D-wall motion tracking analysis. Echocardiography 2010;27:1238-46.

70. Maffessanti F, Nesser HJ, Weinert L, Steringer-Mascherbauer R, Niel J, Gorissen W, et al. Quantitative evaluation of regional left ventricular function using three-dimensional speckle tracking echocardiography in patients with and without heart disease. Am J Cardiol 2009;104:1755-62.

71. Gayat E, Ahmad H, Weinert L, Lang RM, Mor-Avi V. Reproducibility and inter-vendor variability of left ventricular deformation measurements by three-dimensional speckle-tracking echocardiography. J Am Soc Echocardiogr 2011;24:878-85.

72. Marwick TH, Leano RL, Brown J, Sun JP, Hoffmann R, Lysyansky P, et al. Myocardial strain measurement with 2-dimensional speckle-tracking echocardiography: definition of normal range. JACC Cardiovasc Imaging 2009;2:80-4.

73. Muraru D, Badano LP, Peluso D, Dal Bianco L, Casablanca S, Kocabay G, et al. Comprehensive analysis of left ventricular geometry and function by three-dimensional echocardiography in healthy adults. J Am Soc Echocardiogr 2013;26:618-28.

74. Kawamura R, Seo Y, Ishizu T, Atsumi A, Yamamoto M, Machino-Ohtsuka T, et al. Feasibility of left ventricular volume measurements by three-dimensional speckle tracking echocardiography depends on image quality and degree of left ventricular enlargement: Validation study with cardiac magnetic resonance imaging. J Cardiol 2013;doi: 10.1016/j.jjcc.2013.08.010. [Epub ahead of print].

75. Macron L, Lairez O, Nahum J, Berry M, Deal L, Deux JF, et al. Impact of acoustic window on accuracy of longitudinal global strain: a comparison study to cardiac magnetic resonance. Eur J Echocardiogr 2011;12:394-9.

76. Xia JZ, Xia JY, Li G, Ma WY, Wang QQ. Left Ventricular Strain Examination of Different Aged Adults with 3D Speckle Tracking Echocardiography. Echocardiography 2013;doi: 10.1111/echo.12367. [Epub ahead of print].

77. Dalen H, Thorstensen A, Aase SA, Ingul CB, Torp H, Vatten LJ, et al. Segmental and global longitudinal strain and strain rate based on echocardiography of 1266 healthy individuals: the HUNT study in Norway. Eur J Echocardiogr 2010;11:176-83.

78. Yingchoncharoen T, Agarwal S, Popovic ZB, Marwick TH. Normal ranges of left ventricular strain: a meta-analysis. J Am Soc Echocardiogr 2013;26:185-91.

79. Cheng S, Larson MG, McCabe EL, Osypiuk E, Lehman BT, Stanchev P, et al. Age- and sex-based reference limits and clinical correlates of myocardial strain and synchrony: the framingham heart study. Circ Cardiovasc Imaging 2013;6:692-9.

80. Cheng S, Fernandes VR, Bluemke DA, McClelland RL, Kronmal RA, Lima JA. Age-related left ventricular remodeling and associated risk for cardiovascular outcomes: the Multi-Ethnic Study of Atherosclerosis. Circ Cardiovasc Imaging 2009;2:191-8.

81. Hurlburt HM, Aurigemma GP, Hill JC, Narayanan A, Gaasch WH, Vinch CS, et al. Direct ultrasound measurement of longitudinal, circumferential, and radial strain using 2-dimensional strain imaging in normal adults. Echocardiography 2007;24:723-31.

82. Galderisi M, Esposito R, Schiano-Lomoriello V, Santoro A, Ippolito R, Schiattarella P, et al. Correlates of global area strain in native hypertensive patients: a three-dimensional speckle-tracking echocardiography study. Eur Heart J Cardiovasc Imaging 2012;13:730-8.

83. Perez de Isla L, Balcones DV, Fernandez-Golfin C, Marcos-Alberca P, Almeria C, Rodrigo JL, et al. Three-dimensional-wall motion tracking: a new and faster tool for myocardial strain assessment: comparison with two-dimensional-wall motion tracking. J Am Soc Echocardiogr 2009;22:325-30.

84. Altman M, Bergerot C, Aussoleil A, Davidsen ES, Sibellas F, Ovize M, et al. Assessment of left ventricular systolic function by deformation imaging derived from speckle tracking: a comparison between 2D and 3D echo modalities. Eur Heart J Cardiovasc Imaging 2013;doi: 10.1093/ehjci/jet103. [Epub ahead of print].
85. Wu VC, Takeuchi M, Otani K, Haruki N, Yoshitani H, Tamura M, et al. Effect of Through-Plane and Twisting Motion on Left Ventricular Strain Calculation: Direct Comparison between Two-Dimensional and Three-Dimensional Speckle-Tracking Echocardiography. J Am Soc Echocardiogr 2013;doi: 10.1016/j.echo.2013.07.006. [Epub ahead of print].
86. Tatsumi K, Tanaka H, Matsumoto K, Hiraishi M, Miyoshi T, Tsuji T, et al. Mechanical left ventricular dyssynchrony in heart failure patients with narrow QRS duration as assessed by three-dimensional speckle area tracking strain. Am J Cardiol 2011;108:867-72.
87. Li CM, Li C, Bai WJ, Zhang XL, Tang H, Qing Z, et al. Value of Three-Dimensional Speckle-Tracking in Detecting Left Ventricular Dysfunction in Patients with Aortic Valvular Diseases. J Am Soc Echocardiogr 2013;doi:pii: S0894-7317(13)00586-5. 10.1016/j.echo.2013.07.018. [Epub ahead of print].
88. Matsumoto K, Tanaka H, Tatsumi K, Miyoshi T, Hiraishi M, Kaneko A, et al. Left ventricular dyssynchrony using three-dimensional speckle-tracking imaging as a determinant of torsional mechanics in patients with idiopathic dilated cardiomyopathy. Am J Cardiol 2012;109:1197-205.
89. Schueler R, Sinning JM, Momcilovic D, Weber M, Ghanem A, Werner N, et al. Three-dimensional speckle-tracking analysis of left ventricular function after transcatheter aortic valve implantation. J Am Soc Echocardiogr 2012;25:827-34.
90. Baccouche H, Maunz M, Beck T, Gaa E, Banzhaf M, Knayer U, et al. Differentiating cardiac amyloidosis and hypertrophic cardiomyopathy by use of three-dimensional speckle tracking echocardiography. Echocardiography 2012;29:668-77.

91. Tsang W, Kenny C, Adhya S, Kapetanakis S, Weinert L, Lang RM, et al. Interinstitutional Measurements of Left Ventricular Volumes, Speckle-Tracking Strain, and Dyssynchrony Using Three-Dimensional Echocardiography. J Am Soc Echocardiogr 2013;doi:pii: S0894-7317(13)00591-9. 10.1016/j.echo.2013.07.023. [Epub ahead of print].
92. Yusuf S, Hawken S, Ounpuu S, Dans T, Avezum A, Lanas F, et al. Effect of potentially modifiable risk factors associated with myocardial infarction in 52 countries (the INTERHEART study): case-control study. Lancet 2004;364:937-52.
93. Barker WH, Mullooly JP, Getchell W. Changing incidence and survival for heart failure in a well-defined older population, 1970-1974 and 1990-1994. Circulation 2006;113:799-805.
94. Steg PG, James SK, Atar D, Badano LP, Blomstrom-Lundqvist C, Borger MA, et al. ESC Guidelines for the management of acute myocardial infarction in patients presenting with ST-segment elevation. Eur Heart J 2012;33:2569-619.
95. Kim RJ, Albert TS, Wible JH, Elliott MD, Allen JC, Lee JC, et al. Performance of delayed-enhancement magnetic resonance imaging with gadoversetamide contrast for the detection and assessment of myocardial infarction: an international, multicenter, double-blinded, randomized trial. Circulation 2008;117:629-37.
96. Rehwald WG, Fieno DS, Chen EL, Kim RJ, Judd RM. Myocardial magnetic resonance imaging contrast agent concentrations after reversible and irreversible ischemic injury. Circulation 2002;105:224-9.
97. Mollema SA, Delgado V, Bertini M, Antoni ML, Boersma E, Holman ER, et al. Viability assessment with global left ventricular longitudinal strain predicts recovery of left ventricular function after acute myocardial infarction. Circ Cardiovasc Imaging 2010;3:15-23.
98. Chan J, Hanekom L, Wong C, Leano R, Cho GY, Marwick TH. Differentiation of subendocardial and transmural infarction using two-dimensional strain rate imaging to assess short-axis and long-axis myocardial function. J Am Coll Cardiol 2006;48:2026-33.

99. Lang RM, Bierig M, Devereux RB, Flachskampf FA, Foster E, Pellikka PA, et al. Recommendations for chamber quantification. Eur J Echocardiogr 2006;7:79-108.
100. Marra MP, Corbetti F, Cacciavillani L, Tarantini G, Ramondo AB, Napodano M, et al. Relationship between myocardial blush grades, staining, and severe microvascular damage after primary percutaneous coronary intervention: a study performed with contrast-enhanced magnetic resonance in a large consecutive series of patients. Am Heart J 2010;159:1124-32.
101. Muraru D, Beraldo M, Soldà E, Cucchini U, Peluso D, Tuveri MF, et al. Global 3D circumferential strain is related to infarct size and transmural extent of myocardial necrosis in patients with successfully reperfused STEMI [abstr]. Eur J Echocardiogr 2011;12:ii166.
102. Muraru D, Badano LP, Bellu R, Ermacora D, De Lazzari M, Marra MP, et al. Predictive value of 2D/3D deformation parameters and 3D wall motion score to identify transmural myocardial necrosis in STEMI patients: a comparative study against cardiac magnetic resonance [abstr]. Eur Heart J 2012;33:159.
103. Muraru D, Badano LP, Bellu R, De Lazzari M, Marra MP, Dal Bianco L, et al. Two-dimensional vs three-dimensional deformation parameters to estimate infarct size and global left ventricular function after STEMI: which parameter is better? [abstr]. Eur Heart J 2012;33:167-8.
104. Basso C, Rizzo S, Thiene G. The metamorphosis of myocardial infarction following coronary recanalization. Cardiovasc Pathol 2010;19:22-8.
105. Pasotti M, Prati F, Arbustini E. The pathology of myocardial infarction in the pre- and post-interventional era. Heart 2006;92:1552-6.
106. Thiene G, Basso C. Myocardial infarction: a paradigm of success in modern medicine. Cardiovasc Pathol 2010;19:1-5.

107. Cheong BY, Muthupillai R, Wilson JM, Sung A, Huber S, Amin S, et al. Prognostic significance of delayed-enhancement magnetic resonance imaging: survival of 857 patients with and without left ventricular dysfunction. Circulation 2009;120:2069-76.
108. Larose E, Rodes-Cabau J, Pibarot P, Rinfret S, Proulx G, Nguyen CM, et al. Predicting late myocardial recovery and outcomes in the early hours of ST-segment elevation myocardial infarction traditional measures compared with microvascular obstruction, salvaged myocardium, and necrosis characteristics by cardiovascular magnetic resonance. J Am Coll Cardiol 2010;55:2459-69.
109. Mahrholdt H, Wagner A, Parker M, Regenfus M, Fieno DS, Bonow RO, et al. Relationship of contractile function to transmural extent of infarction in patients with chronic coronary artery disease. J Am Coll Cardiol 2003;42:505-12.
110. Kim RJ, Chen EL, Lima JA, Judd RM. Myocardial Gd-DTPA kinetics determine MRI contrast enhancement and reflect the extent and severity of myocardial injury after acute reperfused infarction. Circulation 1996;94:3318-26.
111. Maron BJ. Hypertrophic cardiomyopathy: a systematic review. JAMA 2002;287:1308-20.
112. Cikes M, Sutherland GR, Anderson LJ, Bijnens BH. The role of echocardiographic deformation imaging in hypertrophic myopathies. Nat Rev Cardiol 2010;7:384-96.
113. Melacini P, Basso C, Angelini A, Calore C, Bobbo F, Tokajuk B, et al. Clinicopathological profiles of progressive heart failure in hypertrophic cardiomyopathy. Eur Heart J 2010;31:2111-23.
114. Corrado D, Basso C, Schiavon M, Thiene G. Screening for hypertrophic cardiomyopathy in young athletes. N Engl J Med 1998;339:364-9.
115. Gersh BJ, Maron BJ, Bonow RO, Dearani JA, Fifer MA, Link MS, et al. 2011 ACCF/AHA Guideline for the Diagnosis and Treatment of Hypertrophic Cardiomyopathy: a report of the American College of Cardiology Foundation/American Heart Association Task Force on

Practice Guidelines. Developed in collaboration with the American Association for Thoracic Surgery, American Society of Echocardiography, American Society of Nuclear Cardiology, Heart Failure Society of America, Heart Rhythm Society, Society for Cardiovascular Angiography and Interventions, and Society of Thoracic Surgeons. J Am Coll Cardiol 2011;58:e212-60.

116. Nagueh SF, Bierig SM, Budoff MJ, Desai M, Dilsizian V, Eidem B, et al. American Society of Echocardiography clinical recommendations for multimodality cardiovascular imaging of patients with hypertrophic cardiomyopathy: Endorsed by the American Society of Nuclear Cardiology, Society for Cardiovascular Magnetic Resonance, and Society of Cardiovascular Computed Tomography. J Am Soc Echocardiogr 2011;24:473-98.

117. Serri K, Reant P, Lafitte M, Berhouet M, Le Bouffos V, Roudaut R, et al. Global and regional myocardial function quantification by two-dimensional strain: application in hypertrophic cardiomyopathy. J Am Coll Cardiol 2006;47:1175-81.

118. Almaas VM, Haugaa KH, Strom EH, Scott H, Smith HJ, Dahl CP, et al. Noninvasive assessment of myocardial fibrosis in patients with obstructive hypertrophic cardiomyopathy. Heart 2013.

119. Funabashi N, Takaoka H, Horie S, Ozawa K, Takahashi M, Yajima R, et al. Risk stratification using myocardial peak longitudinal-strain on speckle-tracking transthoracic-echocardiogram to predict major adverse cardiac events in non ischemic hypertrophic-cardiomyopathy subjects confirmed by MDCT. Int J Cardiol 2013;168:4586-9.

120. Urbano-Moral JA, Rowin EJ, Maron MS, Crean A, Pandian NG. Investigation of Global and Regional Myocardial Mechanics with 3D Speckle Tracking Echocardiography and Relations to Hypertrophy and Fibrosis in Hypertrophic Cardiomyopathy. Circ Cardiovasc Imaging 2013.

List of Publications Related to PhD Project

Peer Review Papers

[P1] **Muraru D**, Cucchini U, Padayattil-Josè S, Mihăilă S, Miglioranza MH, Cecchetto A, Naso P, Peluso P, Iliceto S, Badano LP. Left ventricular myocardial strain by three-dimensional speckle-tracking echocardiography in healthy volunteers: a normative study. *J Am Soc Echocardiogr* 2014 (*accepted, under revision*).

[P2] Kocabay G, **Muraru D**, Peluso D, Cucchini U, Mihăilă S, Padayattil-Josè S, Denas G, Iliceto S, Vinereanu D, Badano LP. Normal left ventricular mechanics by two-dimensional speckle-tracking echocardiography: reference values in healthy adults. *Rev Esp Cardiol* 2014 (in press)

[P3] **Muraru D**, Badano LP, Peluso D, Dal Bianco L, Casablanca S, Kocabay G, Zoppellaro G, Iliceto S. Comprehensive analysis of left ventricular geometry and function by three-dimensional echocardiography in healthy adults. *J Am Soc Echocardiogr* 2013 Jun;26(6):618-28

[P4] Badano LP, Cucchini U, **Muraru D**, Al Nono O, Sarais C, Iliceto S. Use of three-dimensional speckle tracking to assess left ventricular myocardial function: intervendor consistency and reproducibility of strain measurements. *Eur Heart J Cardiovasc Imaging* 2013 Mar;14(3):285-93.

[P5] **Muraru D**, Badano LP, Ermacora D, Piccoli G, Iliceto S. Sources of variation and bias in assessing left ventricular volumes and dyssynchrony using three-dimensional echocardiography. *Int J Cardiovasc Imaging*. 2012 Aug;28(6):1357-68.

[P6] Badano LP, Boccalini F, **Muraru D**, Bianco LD, Peluso D, Bellu R, Zoppellaro G, Iliceto S. Current clinical applications of transthoracic three-dimensional echocardiography. *J Cardiovasc Ultrasound* 2012 Mar;20(1):1-22.

[P7] Mondillo S, Galderisi M, Mele D, Cameli M, Lomoriello VS, Ballo PC, D'Andrea A, **Muraru D**, Losi A, Agricola E, D'Errico A, Buralli S, Nistri S, Badano LP. Speckle tracking echocardiography: a new technology to assess myocardial function. *J Ultrasound Med* 2011;30:71-83.

Books

[B1] Badano LP, Galderisi M, **Muraru D**, Mondillo S. "Ecocardiografia multi planare e tridimensionale real-time", MB&Care, Livorno; 2011

[B2] Badano LP, Galderisi M, **Muraru D**, Mondillo S. "Speckle Tracking Echocardiography", MB&Care, Livorno; 2011

Conference Abstracts

[A1] Muraru D, Cucchini U, Padayattil-Jose S, Mihaila S, Miglioranza MH, Cecchetto A, Casablanca S, Iliceto S, Badano LP. Left ventricular myocardial strain by three-dimensional speckle-tracking echocardiography in healthy volunteers: a normative study. *J Am Coll Cardiol 2014 (in press)*

[A2] Muraru D, Mihaila S, Piasentini E, Casablanca S, Naso P, Puma L, Ermacora D, Zoppellaro G, Iliceto S, Badano LP. Do a vendor-specific and a vendor-independent software for 3D echocardiographic analysis provide similar values for left ventricular volumes and ejection fraction? *J Am Coll Cardiol 2014 (in press)*

[A3] Muraru D, Piasentini E, Mihaila S, Naso P, Casablanca S, Peluso D, Denas G, Ucci L, Iliceto S, Badano LP. Reference values for 3D echo parameters describing left ventricular mechanics obtained by vendor-independent software. *Eur Heart J Cardiovasc Imaging* 2013:14 (Suppl 2)

[A4] Muraru D, Piasentini E, Mihaila S, Padayattil-Jose' S, Peluso D, Ucci L, Naso P, Puma L, Casablanca S, Iliceto S. Reference ranges for left ventricular geometry and function by 3D echocardiography using a vendor-independent software for quantitative analysis. *Eur Heart J Cardiovasc Imaging* 2013:14 (Suppl 2)

[A5] Muraru D, Mihaila S, Piasentini E, Casablanca S, Naso P, Puma L, Ermacora D, Zoppellaro G, Iliceto S, Badano LP. Do a vendor-specific and a vendor-independent software for 3D echocardiographic analysis provide similar values for left ventricular volumes and ejection fraction? *Eur Heart J Cardiovasc Imaging* 2013:14 (Suppl 2)

[A6] Muraru D, Calore C, Badano LP, Melacini P, Mihaila S, Naso P, Casablanca S, Ortile A, Padayattil Jose' S, Iliceto S. Mitral valve abnormalities correlate with left ventricular remodelling and obstruction in hypertrophic cardiomyopathy: a quantitative 3D transthoracic echocardiographic study. *Eur Heart J Cardiovasc Imaging* 2013:14 (Suppl 2)

[A7] Muraru D, Calore C, Badano LP, Melacini P, Mihaila S, Peluso D, Puma L, Kocabay G, Rizzon G, Iliceto S. Left ventricular outflow tract planimetry by 3D echocardiography predicts obstruction and heart failure symptoms in hypertrophic cardiomyopathy. *Eur Heart J Cardiovasc Imaging* 2013:14 (Suppl 2)

[A8] Calore C, **Muraru D**, Badano LP, Melacini P, Mihaila S, Denas G, Naso P, Casablanca S, Santi F, Iliceto S. Relationship of 3D left ventricular mass with systolic and diastolic function indices in hypertrophic cardiomyopathy. *Eur Heart J Cardiovasc Imaging* 2013:14 (Suppl 2)

[A9] Calore C, **Muraru D**, Melacini P, Badano LP, Mihaila S, Puma L, Peluso D, Casablanca S, Ortile A, Iliceto S. Left atrial longitudinal strain correlates better than its emptying fraction with left ventricular impairment in hypertrophic cardiomyopathy. *Eur Heart J Cardiovasc Imaging* 2013:14 (Suppl 2)

[A10] Badano L, **Muraru D**, Zoppellaro G, Cucchini U, Ermacora D, De Lazzari M, Peluso D, Marra MP, Iliceto S. Predictive value of 2D and 3D deformation parameters and wall motion score to identify transmural myocardial necrosis in STEMI patients: a comparative study against CMR. *J Am Coll Cardiol.*2013;61(10_S): doi:10.1016/S0735-1097(13)61013-X.

[A11] **Muraru D**, Calore C, Badano LP, Melacini P, Mihaila S, Casablanca S, Cucchini U, Miglioranza MH, Polo A, Iliceto S. Radial function correlates with heart failure symptoms in hypertrophic cardiomyopathy with normal ejection fraction. *Eur Heart J* 2013; 34 (suppl 1): doi:10.1093/eurheartj/eht307.P622

[A12] **Muraru D**, Badano LP, Ermacora D, Bellu R, De Lazzari M, Marra MP, Dal Bianco L, Peluso D, Boccalini F, Iliceto S. Two-dimensional longitudinal strain is more accurate than three-dimensional longitudinal strain to identify infarcted LV segments in STEMI patients. *Eur Heart J* 2012; 33 (Abstract Supplement), 672-673

[A13] **Muraru D**, Badano LP, Bellu R, Ermacora D, De Lazzari M, Marra MP, Dal Bianco L, Peluso D, Cucchini U, Iliceto S. Predictive value of 2D/3D deformation parameters and 3D wall motion score to identify transmural myocardial necrosis in STEMI patients: a comparative study against cardiac magnetic resonance. *Eur Heart J* 2012; 33 (Abstract Supplement), 159

[A14] **Muraru D**, Badano LP, Ermacora D, Bellu R, De Lazzari M, Marra MP, Dal Bianco L, Peluso D, Cucchini U, Iliceto S. Two-dimensional vs three-dimensional deformation parameters to estimate infarct size and global left ventricular function after STEMI: which parameter is better? *Eur Heart J* 2012; 33 (Abstract Supplement), 167-168

[A15] Enache R, **Muraru D**, Piazza R, Popescu BA, Purcarea F, Calin A, Beladan CC, Rosca M, Nicolosi GL, Ginghina C. Left ventricular shape and mass impact apical rotation in patients with aortic regurgitation. A speckle-tracking echocardiography study. *Eur Heart J* 2012; 33 (Abstract Supplement), 31

[A16] **Muraru D**, Beraldo M, Solda' E, Cucchini U, Peluso D, Tuveri MF, Al Mamary A, Badano LP, Iliceto S. Global 3D circumferential strain is related to infarct size and transmural extent of myocardial necrosis in patients with successfully reperfused STEMI. *Eur J Echocardiogr* 2011;12(Suppl 2):ii21 (P283)

[A17] **Muraru D**, Dal Bianco L, Solda' E, Cucchini U, Peluso D, Tuveri MF, Al Mamary A, Badano LP, Iliceto S. Comprehensive assessment of left ventricular geometry and function in healthy subjects using three-dimensional echocardiography. *Eur J Echocardiogr* 2011;12(Suppl 2):ii36 (P344)

[A18] **Muraru D**, Beraldo M, Solda' E, Ermacora D, Cucchini U, Dal Bianco L, Peluso D, De Lazzari M, Badano LP, Iliceto S D. 3D echocardiography is a valuable clinical tool to identify global left ventricular remodeling and myocardial dysfunction early after STEMI. *Eur J Echocardiogr* 2011;12(Suppl 2):ii56 (P418)

[A19] Cucchini U, **Muraru D**, Badano LP, Solda' E, Tuveri MF, Al Nono O, Sarais C, Iliceto S. 3D strain parameters are highly accurate in identifying global left ventricular systolic dysfunction in ischemic heart disease. *Eur J Echocardiogr* 2011;12(Suppl 2):ii166 (P964)

[A20] **Muraru D**, Dal Bianco L, Beraldo M, Solda' E, Cucchini U, Peluso D, Tuveri MF, Al Mamary A, Badano LP, Iliceto S. Reference ranges for the various components of left ventricular myocardial deformation assessed by 3D speckle-tracking, and comparison with 2D speckle-tracking. *Eur J Echocardiogr* 2011;12(Suppl 2):ii 181 (P1020)

[A21] Enache R, **Muraru D,** Piazza R, Roman-Pognuz A, Popescu BA, Calin A, Beladan C, Purcarea F, Nicolosi GL, Ginghina C. Left ventricular mechanics in patients with aortic regurgitation. A speckle-tracking echocardiography study. *Eur J Echocardiogr* 2011;12(Suppl 2):ii59 (P427)

[A22] **Muraru D**, Cucchini U, Badano LP, Solda' E, Tuveri F, Al Nono O, Sarais C, Iliceto S. Inconsistency of 3D strain measurements between vendors. *Eur Heart J* 2011; 32(Abstr suppl): 205-6 (P1424)

[A23] **Muraru D**, Cucchini U, Badano LP, Solda' E, Tuveri F, Al Nono O, Sarais C, Iliceto S. Different vendors show comparably high reproducibility of 3D strain measurements except for radial strain. *Eur Heart J* 2011; 32(Abstr suppl): 205 (P1423)

[A24] **Muraru D**, Cucchini U, Badano LP, Solda' E, Tuveri F, Al Nono O, Sarais C, Iliceto S. Global area strain is a new and robust parameter to characterize left ventricular systolic function by three-dimensional speckle-tracking echocardiography. *Eur Heart J* 2011; 32(Abstr suppl): 207 (P1430)

[A25] Solda' E, **Muraru D**, Badano LP, Perazzolo Marra M, De Lazzari M, Cucchini U, Ermacora D, Sarais C, Iliceto S. 3D speckle tracking does not allow to characterize transmurality of myocardial necrosis in individual left ventricular segments. *Eur Heart J* 2011; 32(Abstr suppl): 1055 (P5634)

[A26] Enache R, Piazza R, **Muraru D**, Roman-Pognuz A, Calin A, Popescu BA, Purcarea F, Leiballi E, Ginghina C, Nicolosi GL. Assessment of left ventricular untwisting by speckle-tracking echocardiography in patients with aortic regurgitation. *Eur Heart J* 2011; 32(Abstr suppl): 203 (P1416)

[A27] Dal Bianco L, **Muraru D**, Badano LP, Ermacora D, Bellu R, De Lazzari M, Marra MP, Peluso D, Cucchini U, Kocabay G, Nour A, Iliceto S. Confronto tra i parametri di deformazione 2D e 3D nel stimare l'estensione dell'infarto miocardico e la funzione globale del ventricolo sinistro dopo STEMI: quale parametro è migliore? 73° CONGRESSO NAZIONALE della Società Italiana di Cardiologia Roma, 15 – 17 dicembre 2012

[A28] Dal Bianco L, **Muraru D**, Badano LP, Bellu R, Ermacora D, De Lazzari M, Marra MP, Peluso D, Cucchini U, Kocabay G, Nour A, Iliceto S. Valore predittivo dei parametri 2D/3D di deformazione miocardica e dell'indice di motilità 3D nell'identificare l'estensione della necrosi transmurale in

pazienti con STEMI: confronto con la RMC. 73° CONGRESSO NAZIONALE della Società Italiana di Cardiologia Roma, 15 – 17 dicembre 2012

[A29] Peluso D, **Muraru D**, Badano LP, Ermacora D, Bellu R, De Lazzari M, Marra MP, Dal Bianco L, Nour A, Sarais C, Cucchini U, Kocabay G, Iliceto S. Superiore accuratezza dello strain longitudinale 2D rispetto a quello 3D nell'identificare i segmenti coinvolti dalla necrosi nei pazienti con STEMI. 73° CONGRESSO NAZIONALE della Società Italiana di Cardiologia Roma, 15 – 17 dicembre 2012

[A30] Peluso D, **Muraru D**, Badano LP, Bellu R, Ermacora D, De Lazzari M, Marra MP, Dal Bianco L, Zoppellaro G, Kocabay G, Sarais C, Cucchini U, Nour A, Iliceto S. Lo strain longitudinale 2D e lo strain circonferenziale 3D risultano predittori accurati di necrosi transmurale alla risonanza magnetica dopo uno STEMI. 73° CONGRESSO NAZIONALE della Società Italiana di Cardiologia Roma, 15 – 17 dicembre 2012

[A31] Dal Bianco L, **Muraru D**, Beraldo M, Soldà E, Cucchini U, Peluso D, Tuveri F, Al Mamary A, Sambugaro F, Sarais C, Badano LP, Iliceto S. Valori di riferimento per le diverse componenti della deformazione miocardica valutate attraverso il 3D speckle tracking, e confronto con il 2D speckle tracking. 72° Congresso nazionale della Società Italiana di Cardiologia, Roma, 10-12 dicembre 2011

[A32] Dal Bianco L, **Muraru D**, Soldà E, Cucchini U, Peluso D, Tuveri F, Al Mamary A, Donolato T, Sarais C, Badano LP, Iliceto S. Valutazione integrata della geometria e della funzione del ventricolo sinistro in soggetti sani utilizzando l'ecocardiografia tridimensionale. 72° Congresso nazionale della Società Italiana di Cardiologia, Roma, 10-12 dicembre 2011.

[A33] Cucchini U, **Muraru D**, Badano LP, Soldà E, Tuveri MF, Al Nono O, Sarais C, Iliceto S. Valutazione della funzione ventricolare sinistra mediante *strain* tridimensionale (3D): accuratezza della metodica nella cardiopatia ischemica. 72° Congresso nazionale della Società Italiana di Cardiologia, Roma, 10-12 dicembre 2011.

[A34] Cucchini U, **Muraru D**, Badano LP, Soldà E, Tuveri MF, Al Nono O, Sarais C, Iliceto S. Confronto della riproducibilità dello *strain* tridimensionale misurato con metodica *speckle tracking* fra differenti piattaforme ecocardiografiche. 72° Congresso nazionale della Società Italiana di Cardiologia, Roma, 10-12 dicembre 2011.

[A35] Soldà E, **Muraru D**, Badano LP, Perazzolo Marra M, De Lazzari M, Cucchini U, Ermacora D, Sarais C, Iliceto S. Lo *strain* 3D nella valutazione della transmuralità dell'infarto miocardico; correlazione con l'estensione della necrosi valutata mediante risonanza magnetica cardiaca. 72° Congresso nazionale della Società Italiana di Cardiologia, Roma, 10-12 dicembre 2011.

[A36] Beraldo M, **Muraru D**, Soldà E, Ermacora D, Cucchini U, Dal Bianco L, Peluso D, De Lazzari M, Tuveri F, Badano LP, Iliceto S. 3D echocardiography is a valuable clinical tool to identify global LV remodeling and myocardial dysfunction early after STEMI. 72° Congresso nazionale della Società Italiana di Cardiologia, Roma, 10-12 dicembre 2011.

[A37] Beraldo M, **Muraru D**, Soldà E, Ermacora D, Cucchini U, Dal Bianco L, Peluso D, De Lazzari M, Badano LP, Iliceto S. Global 3D circumferential strain is related to infarct size and transmural extent of

myocardial necrosis in patients with successfully reperfused STEMI. 72° Congresso nazionale della Società Italiana di Cardiologia, Roma, 10-12 dicembre 2011.

[A38] **Muraru D**, Cucchini U, Badano LP, Soldà E, Tuveri MF, Al Nono O, Sarais C, Iliceto S. Inconsistency of 3D strain measurements between vendors. XV Congresso Nazionale della Società Italiana di Ecografia Cardiovascolare, Naples, 14-16 Aprile 2011; 05:8; ISBN 978-88-904308-1-7

[A39] Cucchini U, **Muraru D**, Badano LP, Soldà E, Tuveri MF, Al Nono O, Sarais C, Iliceto S. Confronto della riproducibilità dello strain tridimensionale misurato con metodica speckle-tracking fra differenti piattaforme ecocardiografiche. XV Congresso Nazionale della Società Italiana di Ecografia Cardiovascolare, Naples, 14-16 Aprile 2011;18:13; ISBN 978-88-904308-1-7.

[A40] Cucchini U, **Muraru D**, Badano LP, Soldà E, Tuveri MF, Al Nono O, Sarais C, Iliceto S. Valutazione della funzione ventricolare sinistra mediante strain tridimensionale (3D): accuratezza della metodica nella cardiopatia ischemica. XV Congresso Nazionale della Società Italiana di Ecografia Cardiovascolare, Naples, 14-16 Aprile 2011;21:14; ISBN 978-88-904308-1-7.

[A41] Soldà E, Cucchini U, Badano LP, Perazzolo-Marra M, De Lazzari M, **Muraru D**, Ermacora D, Sarais C, Iliceto S. Lo strain 3D nella valutazione della trasmuralità dell'infarto miocardico; correlazione con l'estensione della necrosi valutata mediante risonanza magnetica cardiaca. Valutazione della funzione ventricolare sinistra mediante strain tridimensionale (3D): accuratezza della metodica nella cardiopatia ischemica. XV Congresso Nazionale della Società Italiana di Ecografia Cardiovascolare, Napoli, 14-16 Aprile 2011;41:23; ISBN 978-88-904308-1-7

Additional Publications during PhD Fellowship (2011-2013)

Peer Review Papers

1. Mihăilă S, **Muraru D**, Piasentini E, Miglioranza MH, Peluso D, Cucchini U, Iliceto S, Vinereanu D, Badano LP. Quantitative analysis of the mitral annulus geometry and function in healthy volunteers using transthoracic three-dimensional echocardiography. *J Am Soc Echocardiogr* (*submitted*)
2. **Muraru D,** Maffessanti F, Kocabay G, Peluso D, Bianco LD, Piasentini E, Jose SP, Iliceto S, Badano LP. Ascending aorta diameters measured by echocardiography using both leading edge-to-leading edge and inner edge-to-inner edge conventions in healthy volunteers. *Eur Heart J Cardiovasc Imaging* 2013 Oct 4. [Epub ahead of print]
3. Maffessanti F, **Muraru D,** Esposito R, Gripari P, Ermacora D, Santoro C, Tamborini G, Galderisi M, Pepi M, Badano LP. Age-, body size-, and sex-specific reference values for right ventricular volumes and ejection fraction by three-dimensional echocardiography: a multicenter echocardiographic study in 507 healthy volunteers. *Circ Cardiovasc Imaging* 2013 Sep;6(5):700-10
4. Lancellotti P, Tribouilloy C, Hagendorff A, Popescu BA, Edvardsen T, Pierard LA, Badano L, Zamorano JL; Scientific Document Committee of the European Association of Cardiovascular Imaging. Collaborators: Edvardsen T, Nieman K, **Muraru D**, Bruder O, Cosyns B, Donal E, Dulgheru R, Galderisi M, Lancellotti P, Sicari R. Recommendations for the echocardiographic assessment of native valvular regurgitation: an executive summary from the European Association of Cardiovascular Imaging. *Eur Heart J Cardiovasc Imaging* 2013 Jul;14(7):611-44
5. Badano LP, **Muraru D**. The unbearable futility of deriving the left atrial size from a single-linear dimension. *Eur Heart J Cardiovasc Imaging* 2013 Jul;14(7):711-3. doi: 10.1093/ehjci/jet033. Epub 2013 Mar 28.
6. Badano LP, Nour A, **Muraru D**. Left atrium as a dynamic three-dimensional entity: implications for echocardiographic assessment. *Rev Esp Cardiol* 2013 Jan;66(1):1-4. doi: 10.1016/j.recesp.2012.07.020. Epub 2012 Oct 23.
7. Peluso D, Badano LP, **Muraru D**, Dal Bianco L, Cucchini U, Kocabay G, Kovàcs A, Casablanca S, Iliceto S. Right atrial size and function assessed with three-dimensional and speckle-tracking echocardiography in 200 healthy volunteers. *Eur Heart J Cardiovasc Imaging* 2013 Nov;14(11):1106-14. doi: 10.1093/ehjci/jet024. Epub 2013 Feb 19.
8. Gargani L, Pignone A, Agoston G, Moreo A, Capati E, Badano LP, Doveri M, Bazzichi L, Costantino MF, Pavellini A, Pieri F, Musca F, **Muraru D**, Epis O, Bruschi E, De Chiara B, Perfetto

F, Mori F, Parodi O, Sicari R, Bombardieri S, Varga A, Cerinic MM, Bossone E, Picano E. Clinical and echocardiographic correlations of exercise-induced pulmonary hypertension in systemic sclerosis: a multicenter study. *Am Heart J* 2013 Feb;165(2):200-7. doi: 10.1016/j.ahj.2012.10.020. Epub 2012 Nov 28.

9. Badano LP, **Muraru D**, Enriquez-Sarano M. Assessment of functional tricuspid regurgitation. *Eur Heart J* 2013 Jul;34(25):1875-85.
10. **Muraru D**, Cattarina M, Boccalini F, Dal Lin C, Peluso D, Zoppellaro G, Bellu R, Sarais C, Iliceto S, Badano LP. Mitral valve anatomy and function - new insights from three-dimensional echocardiography. *J Cardiovasc Med (Hagerstown)* 2013 Feb;14(2):91-9.
11. **Muraru D**, Badano LP, Vannan M, Iliceto S. Assessment of aortic valve complex by three-dimensional echocardiography: a framework for its effective application in clinical practice. *Eur Heart J Cardiovasc Imaging* 2012;13(7):541-55
12. **Muraru D**, Tuveri MF, Marra MP, Badano LP, Iliceto S. Carcinoid tricuspid valve disease: incremental value of three-dimensional echocardiography. *Eur Heart J Cardiovasc Imaging*. 2012 Apr;13(4):329.
13. Badano LP, **Muraru D**. Towards an integrated echocardiographic assessment of valvular mechanics by three-dimensional volumetric imaging. *J Am Soc Echocardiogr* 2012; 25(5):532-4
14. Kocabay G, Peluso D, **Muraru D**, Iliceto S, Badano LP. Diastolic Mitral Regurgitation in 2:1 Atrioventricular Block: Insight of the Diastolic Pressure. *Echocardiography* 2013 Feb;30(2):E51-2.
15. Kocabay G, **Muraru D**, Peluso D, Iliceto S, Badano LP. Three-Dimensional Transesophageal Echocardiography of Aortic Atherosclerosis. *Echocardiography*. 2012 Sep 7. doi: 10.1111/j.1540-8175.2012.01815.
16. Gargani L, **Muraru D**, Badano LP, Lancellotti P, Sicari R; European Association of Echocardiography. European Association of Echocardiography: Research Grant Programme. *Eur Heart J Cardiovasc Imaging*. 2012 Jan;13(1):47-50
17. **Muraru D**, Badano LP, Iliceto S. Evaluation of the tricuspid valve morphology and function by transthoracic three-dimensional echocardiography. *Curr Cardiol Rep* 2011;13(3):242-9
18. Badano LP, **Muraru D**, Onut R, Lestuzzi C, Toso F. Three-dimensional imaging of anomalous origin of the right coronary artery in a young athlete. *Eur Heart J Cardiovasc Img* 2011;12(6):481
19. Onut R, Badano LP, **Muraru D**, Toso F. A large penetrating atherosclerotic ulcer of the ascending aorta. *Eur Heart J Cardiovasc Img* 2011;12(6):481
20. **Muraru D**, Tuveri MF, Marra MP, Badano LP, Iliceto S. Carcinoid tricuspid valve disease: incremental value of three-dimensional echocardiography**.** *Eur Heart J Cardiovasc Img* in press

21. Popescu BA, **Muraru D**, Beladan CC, Lăcău IS, Ginghină C. Images in cardiology. Atrioventricular block in the elderly: does echocardiography hold the key? *J Am Coll Cardiol.* 2011;57(2):219.
22. Galderisi M, Nistri S, Mondillo S, Losi MA, Innelli P, Mele D, **Muraru D**, D'Andrea A, Ballo P, Sgalambro A, Esposito R, Marti G, Santoro A, Agricola E, Badano LP, Marchioli R, Filardi PP, Mercuro G and Marino PN on behalf of the Working Group of Echocardiography, Italian Society of Cardiology. Methodological Approach for the Assessment of Ultrasound Reproducibility of Cardiac Structure and Function: A proposal of the Study Group of Echocardiography of The Italian Society of Cardiology (Ultra Cardia SIC) Part I. *Cardiovascular Ultrasound* 2011 Sep 26;9:26.

Book chapters

1. **Muraru D**, Marra MP, Badano LP. Tricuspid and pulmonary valves. In Niemann K, Lancellotti P, Gaemperli O, Plein S eds. Advances in Cardiac Imaging 2014, in press
2. Rudski LG, **Muraru D**, Afilalo J, Lester S. Assessment of RV systolic and diastolic function. ASE's Dynamic echocardiography 2nd edition. Saunders Elsevier, St Louis, 2014 in press
3. Badano LP, Addetia K, **Muraru D**. Introduction, Etiology and Natural History of Tricuspid Regurgitation. In: Lang RM, Khandheria BK, Kronzon I, Mor-Avi, V, Goldstein SA. ASE's Dynamic echocardiography, 2nd edition. Saunders Elsevier, St Louis, 2014 in press
4. Badano LP, Addetia K, **Muraru D**. Quantification of Tricuspid Regurgitation. In: Lang RM, Khandheria BK, Kronzon I, Mor-Avi, V, Goldstein SA. ASE's Dynamic echocardiography, 2nd edition. Saunders Elsevier, St Louis, 2014 in press
5. Badano LP, **Muraru D**. Three-dimensional echocardiography. In: Lang RM, Khandheria BK, Kronzon I, Mor-Avi, V, Goldstein SA. ASE's Dynamic echocardiography, 2nd edition. Saunders Elsevier, St Louis, 2014 in press
6. **Muraru D**. Tricuspid regurgitation. EACVI Pocket Guide 2014, in press.
7. **Muraru D**. Pulmonary regurgitation. EACVI Pocket Guide 2014, in press.
8. Badano LP, **Muraru D**. Evaluation of tricuspid valve morphology and function by transthoracic three-dimensional echocardiography. In Shiota T: "3D echocardiography, 2nd edition" CRC Press, Los Angeles, 2014: in press
9. Badano LP, Cucchini U, **Muraru D**, Iliceto S. Il laboratorio digitale di ecocardiografia. In Nicolosi GL, Antonini Canterin F, Pavan D, Piazza R "Manuale di ecocardiografia clinica" 2° edizione, Piccin Editore, Padova, 2014, in press
10. Badano LP, **Muraru D**. Valvular prosteses. In Zamorano JL, Bax JJ, Knuuti J, Sechtem P, Lancellotti P, Badano LP: ESC textbook of cardiovascular imaging 2nd Edition. Oxford University Press, Oxford. 2014, in press

11. Badano LP, Mihaila S, **Muraru D**, Vinereanu D, Iliceto S. Functional classication of secondary mitral valve regurgitation. In: Lancellotti P, Fattouch K. Secondary mitral regurgitation at a glance. Springer Science + Business media, New York 2014, in press
12. Basso C, **Muraru D**, Badano L, Thiene G. Anatomy and pathology of right-sided atrio-ventricular and semilunar valves. In Rajamannan N. Cardiac Valvular Medicine. Springer-Verlag, London 2013: 211-222
13. Badano L, **Muraru D**. Natural history of tricuspid regurgitation and timing of intervention. in Rajamannan N. Cardiac Valvular Medicine. Springer-Verlag, London 2013: 223-248
14. Badano L, **Muraru D**, Iliceto S. Echocardiography of cardiac masses: from two- to three-dimensional imaging in Basso C, Valente M, Thiene G eds. Cardiac tumor pathology. Humana press, New York, 2013: 101-114
15. Badano L, **Muraru D**, Da Lin C, Iliceto S. Instrumentation and Data Acquisition in Shernan S, Lang R, Mor-Avi V and Shirali G. in Atlas of Three-Dimensional Echocardiography. Lippincott Williams & Wilkins 2012: 13-28
16. **Muraru D**, Enache R, Popescu BA, Ginghina C, Badano LP. The role of three-dimensional echocardiography in the assessment of valvular heart diseases. On behalf of Romanian Working Group of Echocardiography, in Progrese in Cardiologie 2012 (*Romanian*)
17. **Muraru D**, Sarais C. La valvola mitrale: La visione chirurgica fornita dall'ecocardiografia tridimensionale. in Badano LP, Galderisi M, Muraru D, Mondillo S. Ecocardiografia multiplanare e tridimensionale real-time. MB&Care Livorno 2011:59-70
18. **Muraru D**, Sarais C. La valvola aortica: Il valore aggiunto dell'ecocardiografia tridimensionale. in Badano LP, Galderisi M, Muraru D, Mondillo S. Ecocardiografia multiplanare e tridimensionale real-time. MB&Care Livorno 2011:71-84
19. **Muraru D**, Sarais C. Lo studio tridimensionale della struttura e della funzione del ventricolo destro: La riscoperta della camera dimenticata. in Badano LP, Galderisi M, Muraru D, Mondillo S. Ecocardiografia multiplanare e tridimensionale real-time. MB&Care Livorno 2011:41-50
20. **Muraru D**, Marra MP. Strain del ventricolo destro ed ipertensione arteriosa polmonare. in Badano LP, Galderisi M, Muraru D, Mondillo S. Speckle Tracking Echocardiography. MB&Care Livorno 2011:50-61
21. **Muraru D.** Doppler tissutale e metodologie derivate con tecnica Doppler nello studio della funzione miocardica. in Badano LP, Galderisi M, Muraru D, Mondillo S. Speckle Tracking Echocardiography. MB&Care Livorno 2011:5-18
22. Badano LP, **Muraru D**. Three-dimensional echocardiography in clinical practice. In Badano LP, Lang RM, Zamorano JL "Textbook Of Real-Time Three-Dimensional Echocardiography" Springer-Verlag London Ltd, London, 2011:33-44

23. **Muraru D**, Badano LP. Assessment of tricuspid valve morphology and function. In Badano P, Lang RM, Zamorano JL "Textbook Of Real-Time Three-Dimensional Echocardiography" Springer-Verlag London Ltd, London, 2011:173-182
24. Rigo F, Galderisi M, **Muraru D**, Badano LP. Role of three-dimensional echocardiography in drug trials. In Badano LP, Lang RM, Zamorano JL "Textbook Of Real-Time Three-Dimensional Echocardiography" Springer-Verlag London Ltd, London, 2011:183-192

Abstracts at international congresses

1. Miglioranza MH, **Muraru D**, Mihaila S, Peluso D, Cucchini U, Casablanca S, Iliceto S, Badano LP. Reference Values of Tricuspid Annulus Size and Dynamics by Two-Dimensional Transthoracic Echocardiography in 220 Healthy Volunteers. *J Am Coll Cardiol 2014 (in press)*
2. Mihaila S, **Muraru D**, Piasentini E, Peluso D, Casablanca S, Naso P, Puma L, Iliceto S, Vinereanu D, Badano LP. Static and dynamic analysis of the mitral valve annulus in normal subjects: a three-dimensional transthoracic echocardiography study. *J Am Coll Cardiol 2014 (in press)*
3. **Muraru D**, Addetia K, Veronesi F, Corsi C, Mor-Avi V, Yamat M, Weinert L, Lang RM, Badano LP. Dynamic Analysis of the Normal Tricuspid Annulus Using 3D Echocardiography. *Eur Heart J Cardiovasc Imaging* 2013:14 (Suppl 2)
4. **Muraru D**, Addetia K, Veronesi F, Corsi C, Mor-Avi V, Yamat M, Weinert L, Lang RM, Badano LP. Physiological determinants of tricuspid annulus size during the cardiac cycle: implications for tricuspid annulus sizing by three-dimensional echocardiography. *Eur Heart J Cardiovasc Imaging* 2013:14 (Suppl 2)
5. Veronesi F, **Muraru D**, Addetia K, Corsi C, Lamberti C, Lang RM, Mor-Avi V, Badano LP. A novel tool to semi-automatically characterize tricuspid valve function and shape using transthoracic echocardiography. *Eur Heart J Cardiovasc Imaging* 2013:14 (Suppl 2)
6. Miglioranza MH, **Muraru D**, Peluso D, Cucchini U, Mihaila S, Naso P, Puma L, Kocabay G, Badano LP. Two-dimensional assessment of tricuspid annulus dynamics and diameters: study for new reference values. *Eur Heart J Cardiovasc Imaging* 2013:14 (Suppl 2)
7. Peluso D, **Muraru D**, Cucchini U, Mihaila S, Casablanca S, Pigatto E, Cozzi F, Punzi L, Badano LP, Iliceto S. Right heart function by 3D-echocardiography and 2D-speckle tracking in scleroderma patients in absence of pulmonary hypertension. *Eur Heart J Cardiovasc Imaging* 2013:14 (Suppl 2)
8. Mihaila S, **Muraru D**, Piasentini E, Peluso D, Casablanca S, Naso P, Puma L, Iliceto S, Vinereanu D, Badano LP. Validation of a new, semiautomated software for quantitative assessment of the mitral annulus by three-dimensional echocardiography. *Eur Heart J Cardiovasc Imaging* 2013:14 (Suppl 2)

9. Mihaila S, **Muraru D**, Piasentini E, Peluso D, Casablanca S, Naso P, Puma L, Iliceto S, Vinereanu D, Badano LP. Static and dynamic analysis of the mitral valve annulus in normal subjects: a three-dimensional transthoracic echocardiography study. *Eur Heart J Cardiovasc Imaging* 2013:14 (Suppl 2).
10. Mihaila S, Piasentini E, **Muraru D**, Peluso D, Casablanca S, Naso P, Puma L, Iliceto S, Vinereanu D, Badano LP. Dynamic changes of mitral annular geometry during the cardiac cycle - a three-dimensional echo study in healthy volunteers. *Eur Heart J Cardiovasc Imaging* 2013:14 (Suppl 2).
11. Addetia K, **Muraru D**, Veronesi F, Corsi C, Mor-Avi V, Yamat M, Weinert L, Badano LP, RM. Lang. Dynamic Analysis of the Normal Tricuspid Annulus Using 3D Echocardiography. *Circulation* 2013; abstr suppl (P5214)
12. Badano L, Maffessanti F, **Muraru D**, Gripari P, Esposito R, Galderisi M, Tamborini G, Santoro C, Ermacora D, Pepi M. Reference values for right ventricular geometry and function by 3D echocardiography: a multicenter study of 533 healthy subjects. *J Am Coll Cardiol* 2013; 61 (10-S) doi:10.1016/S0735-1097(13)60893-1
13. Badano L, Peluso D, **Muraru D**, Dal Bianco L, Kovacs A, Iliceto S. Right atrial volumes and phasic functions by 3D echocardiography in healthy subjects. *J Am Coll Cardiol* 2013; 61 (10-S) doi:10.1016/S0735-1097(13)61101-8.
14. Maffessanti F, **Muraru D,** Esposito R, Tamborini G, Gripari P, Ermacora D, Santoro C, Galderisi M, Badano LP, Pepi M. Allometric normative equations for 3D right ventricular size and function: development and validation with equations derived using cardiac magnetic resonance. *Eur Heart J* 2013; 34 (Abstract Supplement), 685-686
15. Badano LP, **Muraru D**, Mihaila S, Miglioranza MH, Padayattil-Jose S, Ucci L, Dal Bianco L, Peluso D, Cucchini U, Iliceto S. Quantitative analysis of mitral valve geometry by transthoracic three-dimensional echocardiography: accuracy, feasibility, reproducibility and reference values. Eur Heart J 2013; 34 (suppl 1): doi:10.1093/eurheartj/eht311.5863
16. Ermacora D, Badano LP, **Muraru D**, Gentian D, Dal Bianco L, Casablanca S, Peluso D, Zoppellaro G, Cucchini U, Iliceto S. Reference values of right ventricular longitudinal strain by speckle tracking echocardiography in 219 healthy volunteers. *Eur Heart J* 2013; 34 (suppl 1): doi:10.1093/eurheartj/eht309.P3848
17. Kovacs A, Peluso D, **Muraru D**, Badano L, Casablanca S, Dal Bianco L, Zoppellaro G, Iliceto S. Shift in relative contribution of radial and longitudinal mechanics to right ventricular ejection fraction between normal subjects and patients with pulmonary hypertension. *Eur Heart J* 2013; 34 (suppl 1): doi:10.1093/eurheartj/eht307.P231
18. Peluso D, **Muraru D**, Cucchini U, Dal Bianco L, Pigatto E, Zanatta E, Punzi L, Cozzi F, Badano LP, Iliceto S. Right ventricular function by 3D-echocardiography and 2D-speckle tracking in

scleroderma patients in absence of pulmonary hypertension. *Eur Heart J* 2013; 34 (suppl 1):doi:10.1093/eurheartj/eht308.P1181

19. Mihaila S, **Muraru D**, Casablanca S, Peluso D, Cucchini U, Dal Bianco L, Vinereanu D, Iliceto S, Badano LP. Three-dimensional changes in mitral valve annulus geometry in organic and functional mitral regurgitation: insights for mitral valve repair. *Eur Heart J* 2013; 34 (suppl 1): doi:10.1093/eurheartj/eht310.P4751
20. Kovács A, Peluso D, **Muraru D**, Marra MP, Badano LP, Dal Bianco L, Zoppellaro G, Iliceto S. Right ventricular transverse displacement by speckle-tracking echocardiography: reference values in healthy subjects and clinical relevance in pulmonary hypertension. 5th World Symposium on Pulmonary Hypertension 2013
21. Kovács A, Peluso D, **Muraru D**, Marra MP, Badano LP, Dal Bianco L, Zoppellaro G, Iliceto S. Characterization of a novel parameter of right ventricular function by speckle tracking echocardiography in healthy subjects. 5th World Symposium on Pulmonary Hypertension 2013
22. Kovács A, Peluso D, **Muraru D**, Marra MP, Badano LP, Dal Bianco L, Zoppellaro G, Iliceto S. Paradoxical septal motion index strongly correlates with invasive hemodynamic parameters. 5th World Symposium on Pulmonary Hypertension 2013
23. Peluso D, Kovács A, **Muraru D**, Marra MP, Badano LP, Dal Bianco L, Zoppellaro G, Iliceto S. Impairment of right atrial function in pulmonary hypertension patients. 5th World Symposium on Pulmonary Hypertension 2013
24. **Muraru D**, Napodano M, Badano L, Tarantini G, Sarais C, Kocabay G, Isabella G, D'Onofrio A, Gerosa G, Iliceto S. Novel three-dimensional transoesophageal echocardiography platform allows a fast and accurate assessment of aortic annulus size and shape before transcatheter aortic valve implantation. *Eur Heart J Cardiovasc Imaging* 2012; 13(suppl 1):i38-i39
25. **Muraru D**, Cattarina M, Dal Bianco L, Peluso D, Zoppellaro G, Segafredo B, Calore C, Cucchini U, Iliceto S, Badano LP. Quantitative analysis of mitral valve geometry by transthoracic three-dimensional echocardiography: reference values, feasibility and reproducibility. *Eur Heart J Cardiovasc Imaging* 2012; 13(suppl 1)
26. **Muraru D**, Gripari P, Esposito R, Tamborini G, Galderisi M, Ermacora D, Maffessanti F, Santoro C, Pepi M, Badano L. Reference values for right ventricular geometry and function by three-dimensional echocardiography. A multicenter study of a large cohort of healthy subjects. *Eur Heart J Cardiovasc Imaging* 2012; 13(suppl 1)
27. Ippolito R, Gripari P, **Muraru D**, Esposito R, Kocabay G, Tamborini G, Galderisi M, Maffessanti F, Badano L, Pepi M. Age is an independent predictor of right ventricular geometry and function in males only. *Eur Heart J Cardiovasc Imaging* 2012; 13(suppl 1)
28. Kocabay GK, Dal Bianco L, **Muraru D**, Peluso D, Segafredo B, Iliceto S, Badano L. Reference values for aortic diameters obtained using both inner-edge-to-inner-edge and

leading-edge-to-leading-edge methods in 190 healthy subjects. *Eur Heart J Cardiovasc Imaging* 2012; 13(suppl 1)

29. **Muraru D**, Peluso D, Dal Bianco L, Beraldo M, Solda' E, Tuveri MF, Cucchini U, Al Mamary A, Badano LP, Iliceto S. Effect of ageing on left atrial geometry and function assessed by three-dimensional echocardiography. *Eur J Echocardiogr* 2011;12(Suppl 2):ii91 (P648)
30. **Muraru D**, Peluso D, Dal Bianco L, Beraldo M, Solda' E, Tuveri MF, Cucchini U, Al Mamary A, Badano LP, Iliceto S. Single-plane and biplane 2D algorithms and non-atrial specific 3D echo softwares underestimate left atrial volumes in comparison with specific 3D echo software tailored for left atrium. *Eur J Echocardiogr* 2011;12(Suppl 2):ii50 (P391)
31. Maffessanti F, Caiani E, **Muraru D**, Tuveri F, Dal Bianco L, Badano LP. Left atrial shape evaluation based on endocardial surfaces obtained by 3D echocardiography. *Eur J Echocardiogr* 2011;12(Suppl 2):ii15 (P260)
32. Peluso D, **Muraru D**, Dal Bianco L, Beraldo M, Solda' E, Tuveri MF, Cucchini U, Al Mamary A, Badano LP, Iliceto S. Comprehensive assessment of right atrial volume and function in healthy subjects using two-dimensional and speckle-tracking echocardiography. *Eur J Echocardiogr* 2011;12(Suppl 2):ii126 (P777)
33. Enache R, Piazza R, **Muraru D**, Roman-Pognuz A, Calin A, Popescu BA, Purcarea F, Leiballi E, Ginghina C, Nicolosi GL. Assessment of left ventricular untwisting by speckle-tracking echocardiography in patients with aortic regurgitation. *Eur Heart J* 2011; 32(Abstr suppl): 203 (P1416)

Acknowledgements

This research project was supported by GE Vingmed Ultrasound (Horten, Norway), as part of a formal agreement with the University of Padua which included the funding doctoral scholarship and the provision of research equipment for 3 years. Additional support is gratefully acknowledged from TomTec Imaging Systems and Toshiba Medical Systems for equipment grants.

This thesis would not have been possible without the valuable support and guidance from many people who have assisted me along the way.

I am indebted to my mentor, Professor Luigi P. Badano, who has taught me so much and to whom I owe my knowledge in 3D echocardiography and in conducting research, but also the commitment, the passion for "belle immagini" and the willingness to do every task without exception with both mind and heart. Thank you, Luigi, for your support and for guiding me every step of the way with endless optimism, kindness and no less patience!

I would like to thank to my principal supervisor, Professor Sabino Iliceto, for supporting and encouraging us to organize the new Echo Research lab, where the present project has been conducted. His generous support, advice and assistance in the organization have been instrumental for the successful collaboration with other sectors within the Department and for the timely completion of this research.

It is with gratitude I acknowledge also the generous support of Professor Gaetano Thiene, Professor Cristina Basso and Professor Annalisa Angelini, who guided me with insightful discussions during the doctoral fellowship and inspired me with their enthusiasm.

I also thank Assoc. Prof. Bogdan A. Popescu for the opportunity to learn clinical and research echocardiography at high standards and eventually become addicted to it.

I acknowledge the help of my colleagues and nurses from the Echo lab: your generous support and friendship meant a lot to me, it has been a pleasure to work with you and grow together day-by-day as a team.

Last, but not least, a special Thank you to my beloved family, for nourishing each day of my life with love, joy, humor and enthusiasm, as well as for their endless support to my decisions in life and career.